Hochschule
München (HM)
University of
Applied Sciences

Laboratory for
Mechatronic
and Renewable
Energy Systems
(LMRES)

A generic approach to modern electrical drives

Nonlinear Modelling, Dynamic Simulation, High-Performance Control and Optimal Operation

Christoph M. Hackl (with whole LMRES team)
christoph.hackl@hm.edu

30.09.2024 – IEEE-PEMC 2024 Tutorial, Pilsen, Czech Republic

ISES

Outline

Outline

Outline

Introduction: HM research environment

HM (www.hm.edu), ISES (ises.hm.edu) and LMRES (lmres.ee.hm.edu)

HM – Munich University of Applied Sciences

- 14 departmens
- >18.000 students
- ~480 professors
- 3 campuses

☞ **ISES is part of the Promotionszentrum "Energietechnik" with the right to award doctorates (since July 16th, 2024)!**

ISES – Institute for Sustainable Energy Systems

- 8 research labs (8 professors)
- 34 PhD candidates

LMRES – Laboratory for Mechatronic and Renewable Energy Systems

- International team
- 15 PhD candidates (status 2024)
- >150 publications / >8.3 Mio. € raised

Outline

Introduction: LMRES research activities

Research projects and research goals (funding: > 8.3 million €; e.g. DAAD, Bavaria, BMBF, BMWi, DFG, EU)

Intelligent components & systems
(efficient, functional, modular, fault-tolerant, reliable & robust, safe & secure)

Specification, design & (construction)
(generic, easy, fast, optimal, multi-criteria optimization)

Modelling
(nonlinear, switching, hybrid, dynamic, physics-based state space modelling)

System identification & self-commissioning
(real-time applicable, robust, fault-aware, self-learning)

Control
(linear, nonlinear, adaptive, fault-tolerant, self-learning, optimal, predictive)

Operation management
(intelligent, optimal, efficient self-learning)

Additional functionality
(e.g. active noise cancellation/suppression)

Generic development framework (tool chain) for:
- Power electronics
- Electrical machines
- Filters
- Mechatronics
- Renewables
- ...
- (Grids)
- (Digital twins of systems of systems)
- ...

Outline

Introduction: LMRES research interests

Interdisciplinary expertise & publications

System identification [9–26]

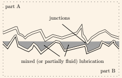

Fric-tion [27–29]

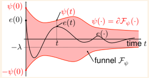

Non-identifier based adaptive control [14, 27, 30–46]

Paper coating machines [4–8]

Supervision & teaching (Award) [157–163]

Mechatronics & robotics [27, 28, 40, 46–58]

Mechatronic and renewable energy systems

Electro-active polymers [1–3]

Power electronics [19–21, 46, 58–88]

Wind energy, renewables & smart grid [13–15, 44, 46, 57, 58, 60, 61, 67, 68, 70–72, 74, 79, 85, 93–95, 98, 100, 107, 112, 120, 132, 136, 139–156]

Electrical machines & drives [13, 15, 17, 23–27, 30, 32, 33, 45, 46, 51, 55, 57, 69, 77, 78, 80, 89–138]

Outline

1. Introduction
   - HM research environment
   - LMRES research activities
   - LMRES research interests
   - LMRES selected research results

Introduction: LMRES selected research results

Electrical/industrial/traction drives (reliability) [115]

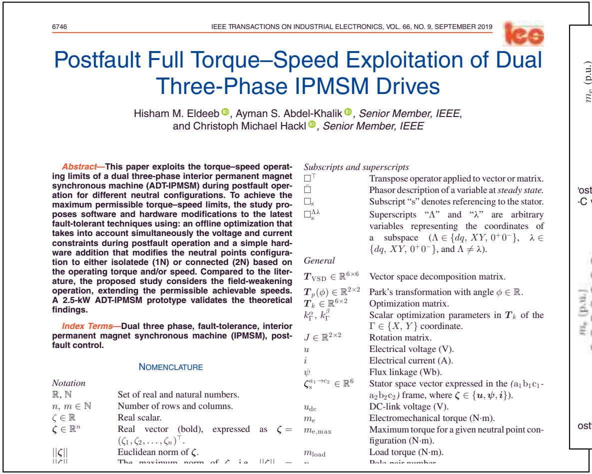

6746 IEEE TRANSACTIONS ON INDUSTRIAL ELECTRONICS, VOL. 66, NO. 9, SEPTEMBER 2019

Postfault Full Torque–Speed Exploitation of Dual Three-Phase IPMSM Drives

Hisham M. Eldeeb, Ayman S. Abdel-Khalik, *Senior Member, IEEE*, and Christoph Michael Hackl, *Senior Member, IEEE*

***Abstract*—This paper exploits the torque–speed operating limits of a dual three-phase interior permanent magnet synchronous machine (ADT-IPMSM) during postfault operation for different neutral configurations. To achieve the maximum permissible torque–speed limits, the study proposes software and hardware modifications to the latest fault-tolerant techniques using: an offline optimization that takes into account simultaneously the voltage and current constraints during postfault operation and a simple hardware addition that modifies the neutral points configuration to either isolatede (1N) or connected (2N) based on the operating torque and/or speed. Compared to the literature, the proposed study considers the field-weakening operation, extending the permissible achievable speeds. A 2.5-kW ADT-IPMSM prototype validates the theoretical findings.**

***Index Terms*—Dual three phase, fault-tolerance, interior permanent magnet synchronous machine (IPMSM), postfault control.**

Nomenclature

Notation

- $\mathbb{R}$, $\mathbb{N}$ — Set of real and natural numbers.
- $n,\ m \in \mathbb{N}$ — Number of rows and columns.
- $\zeta \in \mathbb{R}$ — Real scalar.
- $\boldsymbol{\zeta} \in \mathbb{R}^n$ — Real vector (bold), expressed as $\boldsymbol{\zeta} = (\zeta_1, \zeta_2, \ldots, \zeta_n)^\top$.
- $\|\boldsymbol{\zeta}\|$ — Euclidean norm of $\boldsymbol{\zeta}$.
- $\|\boldsymbol{\zeta}\|_\infty$ — The maximum norm of $\boldsymbol{\zeta}$, i.e., $\|\boldsymbol{\zeta}\|_\infty =$

Subscripts and superscripts

- $\square^\top$ — Transpose operator applied to vector or matrix.
- $\bar{\square}$ — Phasor description of a variable at *steady state*.
- $\square_s$ — Subscript "s" denotes referencing to the stator.
- $\square_s^{\Lambda\lambda}$ — Superscripts "Λ" and "λ" are arbitrary variables representing the coordinates of a subspace ($\Lambda \in \{dq,\ XY,\ 0^+0^-\}$, $\lambda \in \{dq,\ XY,\ 0^+0^-\}$, and $\Lambda \neq \lambda$).

General

- $\boldsymbol{T}_{\mathrm{VSD}} \in \mathbb{R}^{6\times6}$ — Vector space decomposition matrix.
- $\boldsymbol{T}_p(\phi) \in \mathbb{R}^{2\times2}$ — Park's transformation with angle $\phi \in \mathbb{R}$.
- $\boldsymbol{T}_k \in \mathbb{R}^{6\times2}$ — Optimization matrix.
- $k_\Gamma^\alpha,\ k_\Gamma^\beta$ — Scalar optimization parameters in $\boldsymbol{T}_k$ of the $\Gamma \in \{X,\ Y\}$ coordinate.
- $\boldsymbol{J} \in \mathbb{R}^{2\times2}$ — Rotation matrix.
- u — Electrical voltage (V).
- i — Electrical current (A).
- ψ — Flux linkage (Wb).
- $\boldsymbol{\zeta}_s^{a_1\to c_2} \in \mathbb{R}^6$ — Stator space vector expressed in the $(a_1b_1c_1$-$a_2b_2c_2)$ frame, where $\boldsymbol{\zeta} \in \{\boldsymbol{u}, \boldsymbol{\psi}, \boldsymbol{i}\}$.
- u_{dc} — DC-link voltage (V).
- m_{e} — Electromechanical torque (N·m).
- $m_{\mathrm{e,max}}$ — Maximum torque for a given neutral point configuration (N·m).
- m_{load} — Load torque (N·m).
- n_p — Pole pair number.

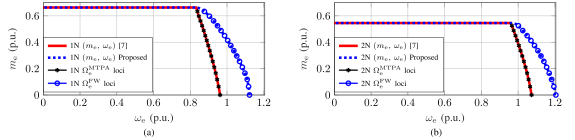

ostfault comparison of the permissible $(m_e,\ \omega_e)$ characteristics between the presented algorithm in [7] and proposed optim
-C with respect to the (a) 1N and (b) 2N neutral configurations, showing the enhancement in terms of extending the permissit

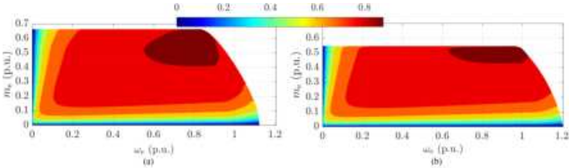

ostfault efficiency maps of (a) 1N and (b) 2N connections within the $(m_e,\ \omega_e)$ range of the proposed optimization in Section III-

Introduction: LMRES selected research results

Wind energy systems & power electronics (reliability; VDE Award) [78]

Modeling and Control of Permanent-Magnet Synchronous Generators Under Open-Switch Converter Faults

Christoph M. Hackl, *Senior Member, IEEE*, Urs Pecha, and Korbinian Schechner

***Abstract*—The mathematical modeling of open-switch faults in two-level machine-side converters and the fault-tolerant current control of isotropic permanent-magnet synchronous generators are discussed in this paper. The proposed converter model is generic for any open-switch fault and independent of the operation mode of the electrical machine. The proposed fault-tolerant current control system gives improved control performance and reduced torque ripple under open-switch faults by modifying the antiwindup strategy, adapting the space-vector modulation scheme, and by injecting additional reference currents. The theoretical derivations of model and control are validated by comparative simulation and measurement results.**

***Index Terms*—Antiwindup (AW), current control, *d*-current injection, fault tolerance, field-oriented control (FOC), flat-top modulation, open-switch fault, permanent-magnet synchronous generator (PMSG), wind turbine systems.**

Notation: $\mathbb{N}, \mathbb{R}$: natural and real numbers. $\boldsymbol{x} := (x_1, \ldots, x_n)^\top \in \mathbb{R}^n$: column vector, $n \in \mathbb{N}$ where "$^\top$" and ":=" mean "transposed" and "is defined as." $\boldsymbol{I}_n := \mathrm{diag}(1, \ldots, 1) \in \mathbb{R}^{n\times n}$: identity matrix. $\boldsymbol{O}_{n\times p} \in \mathbb{R}^{n\times p}$: zero matrix, $n, p \in \mathbb{N}$. $\boldsymbol{x} \in \mathbb{R}^n$ (in X)^n: physical quantity $\boldsymbol{x}$ where each of the n elements has SI unit X. $\bmod(x, y)$: remainder of the division x/y, $x \in \mathbb{R}$, $y \in \mathbb{R}\backslash\{0\}$. atan2: $\mathbb{R}^2 \to [-\pi, \pi)$, $(x, y) \to \mathrm{atan2}(y, x)$: extension of the inverse tangent function to whole circle. $\boldsymbol{T}_c := \frac{2}{3}\left[\begin{smallmatrix} 1 & -\frac{1}{2} & -\frac{1}{2} \\ \ldots \end{smallmatrix}\right]$ and $\boldsymbol{T}_c^{-1} :=$ $\boldsymbol{T}_\mathrm{p}(\phi) := \left[\begin{smallmatrix} \cos(\phi) & -\sin(\phi) \\ \sin(\phi) & \cos(\phi) \end{smallmatrix}\right] =: \boldsymbol{T}_\mathrm{p}(-\phi)^{-1}$: Park transformation matrix. $\boldsymbol{J} = \left[\begin{smallmatrix} 0 & -1 \\ 1 & 0 \end{smallmatrix}\right]$: rotation matrix.

I. Introduction

OPEN-SWITCH faults in converters for electric drives have gained increasing attention in the last years. An open-switch fault can be caused by thermic cycling, driver failures, or by a rupture of the insulated-gate bipolar transistor (IGBT) that is induced by a short-circuit fault [1]. Unlike a short-circuit fault, an open-switch fault does usually not trigger a system shutdown, but degrades the system performance and can cause—without proper counteractions—secondary faults in other components (see [2] and [3]). Open-switch faults are therefore a crucial kind of faults in converters and should be considered in the design of a robust and fault-tolerant (hence more reliable) electrical drive system.

This far, especially, the detection of faults in the converter and the identification of the faulty switch have been the focus of research. Various detection methods have already been presented [1]–[9]. Therefore, fault detection is *not* the topic of this paper.

The focus of this paper is on a fault-tolerant modification of the control system such that, even in the presence of an open-switch fault in the machine-side converter, a continuous

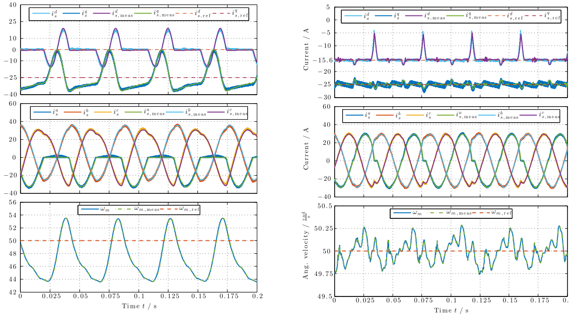

(a) (b)

13. Comparison of simulation and measurement results for standard control system and fault-tolerant control system with extended AW, modifi M (flat-top modulation), and optimally injected d-current. (a) Experiment (E_1): Comparison of simulation and measurement results for standard conti em: $\mathrm{THD}_{i_s^a} = 41.8\,\%$ (simulation) versus $\mathrm{THD}_{i_s^a,\mathrm{meas}} = 45.4\,\%$ (measurement). (b) Experiment (E_2): Comparison of simulation and measurement resu

Introduction: LMRES selected research results

Traction drives & power electronics (efficiency; Cooperation with BMW) [128]

3760 IEEE TRANSACTIONS ON INDUSTRIAL ELECTRONICS, VOL. 68, NO. 5, MAY 2021

Synchronous Optimal Pulsewidth Modulation for Synchronous Machines With Highly Operating Point Dependent Magnetic Anisotropy

Athina Birda, Joerg Reuss, and Christoph M. Hackl, *Senior Member, IEEE*

***Abstract*—The performance of synchronous optimal pulsewidth modulation is investigated for the control of an automotive low voltage electrical drive system, which consists of a two-level voltage source inverter and an interior permanent magnet synchronous motor. The machine magnetic anisotropy varies due to magnetic saturation and cross-saturation effects and depends on the motor operating point. The main objective of this article is to investigate the influence of the varying magnetic anisotropy on the optimized half-wave symmetric inverter pulse patterns. For this purpose, the optimized inverter switching angles are derived by minimizing the current harmonic distortion of an isotropic and anisotropic permanent magnet synchronous motor. Their performance is evaluated and compared by experimental results.**

***Index Terms*—Electric vehicle, magnetic anisotropy, permanent magnet synchronous motor (PMSM), synchronous optimal pulsewidth modulation (SOPWM).**

I. Introduction

As PART of the global effort to reduce the CO2 emissions, the interest of the automotive industry over the last years focused on the concept of electric mobility. Still, the limited operating range and increased price of electric vehicles remain the most important obstacles for their wide spread. The efficiency of the electrical drive system and, by that, the operating range of electric vehicles can be improved by optimizing the inverter compromising the motor current quality. To this end, the optimized inverter pulse patterns are determined, which minimize the harmonic distortion of the phase currents. The optimization procedure is conducted offline and the resulting optimized switching angles are stored in lookup tables (LUTs). Since the switching frequency f_{sw} is synchronized with the fundamental stator frequency f_r, the pulse number

$$q := f_{\mathrm{sw}}/f_r \tag{1}$$

is always an integer [1].

SOPWM is primarily employed in medium voltage high power induction motor drive applications, where the reduction of switching losses is of utmost importance [1], [2]. Moreover, it is a common modulation strategy for operating electric rail traction converters adopted by GE [3] and SIEMENS [4]. On the contrary, little research has been conducted when the SOPWM strategy is employed for the control of synchronous motor drives [5]–[13]. Especially, SOPWM has not yet been explored for automotive low-voltage interior permanent magnet synchronous motor (IPMSM) drives with highly operating point (OP) dependent magnetic anisotropy. This is the main motivation of this article.

In [5]–[7], the current harmonic content of an isotropic permanent magnet synchronous motor (PMSM) drive is min-

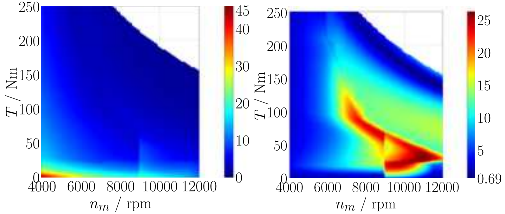

(a) (b)

Fig. 9. Numerical performance evaluation of the optimization results. (a) $I_{s,\mathrm{THD}}(\alpha_{\mathrm{aniso}})/\%$. (b) $I_{s,\mathrm{THD,dev}}/\%$.

Introduction: LMRES selected research results

Electrical machines (optimal feedforward torque control (OFTC); operation management) [105]

INTERNATIONAL JOURNAL OF CONTROL, 2017
https://doi.org/10.1080/00207179.2017.1338359

Taylor & Francis
Taylor & Francis Group

OPEN ACCESS Check for updates

A unified theory for optimal feedforward torque control of anisotropic synchronous machines

Hisham Eldeeb[a], Christoph M. Hackl[a,*], Lorenz Horlbeck[b] and Julian Kullick[a]

[a]Research Group 'Control of Renewable Energy Systems (CRES)', Munich School of Engineering (MSE), Technical University of Munich (TUM), Munich, Germany; [b]Institute of Automotive Technology (FTM), Technical University of Munich (TUM), Munich, Germany

ABSTRACT

A unified theory for optimal feedforward torque control of anisotropic synchronous machines with *non-negligible stator resistance* and *mutual inductance* is presented which allows to *analytically* compute (1) the optimal direct and quadrature reference currents for all operating strategies, such as maximum torque per current (MTPC), maximum current, field weakening, maximum torque per voltage (MTPV) or maximum torque per flux (MTPF), and (2) the transition points indicating when to switch between the operating strategies due to speed, voltage or current constraints. The analytical solutions allow for an (almost) instantaneous selection and computation of actual operation strategy and corresponding reference currents. Numerical methods (approximating these solutions only) are *no longer* required. The unified theory is based on one simple idea: all optimisation problems, their respective constraints and the computation of the intersection point(s) of voltage ellipse, current circle or torque, MTPC, MTPV, MTPF hyperbolas are reformulated implicitly as *quadrics* which allows to invoke the Lagrangian formalism and to find the roots of fourth-order polynomials analytically. The proposed theory is suitable for any anisotropic synchronous machine. Implementation and measurement results illustrate effectiveness and applicability of the theoretical findings in real world.

ARTICLE HISTORY
Received 18 March 2017
Accepted 31 May 2017

KEYWORDS
Maximum torque per ampere (MTPA); maximum torque per current (MTPC); maximum torque per voltage (MTPV); maximum torque per flux (MTPF); maximum current (MC); field weakening (FW); analytical solution; optimal feedforward torque control; efficiency; copper losses; anisotropy; synchronous machine; interior permanent-magnet synchronous machine; reluctance synchronous machine; permanent-magnet-assisted or enhanced synchronous

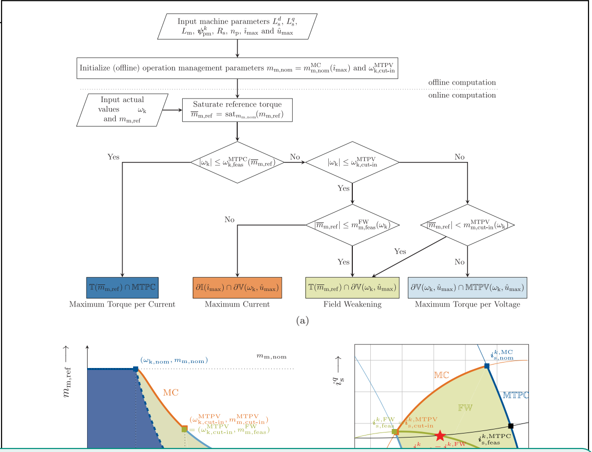

PEMC 2024 Session: TT01 - Power Electronics and Drives in Transportation
01 October 2024 @ 11:20-11:40 (PEMC24-000037)
N. Monzen and C.M. Hackl, "Optimal reference voltage saturation for nonlinear current control of synchronous machine drives"

$\mathbb{R}^n$: zero vector. $\boldsymbol{a}^\top\boldsymbol{b} := a_1b_1 + \cdots + a_nb_n$: scalar product of the vectors $\boldsymbol{a} := (a_1, \ldots, a_n)^\top$ and $\boldsymbol{b} := (b_1, \ldots, b_n)^\top$.

1. Introduction

Figure 5. Illustration of operation management: (a) Flow chart illustrating the decision tree for the selection of the optimal operation strategy, (b) machine map with threshold speed $\omega^{\mathrm{MTPC}}_{\mathrm{k,feas}}(m_{\mathrm{m,ref}})$ (see thick dashed line) for $\omega_{\mathrm{k}} = \omega^{\mathrm{MTPV}}_{\mathrm{k,cut\text{-}in}}$ and $m_{\mathrm{m,ref}} \le m^{\mathrm{FW}}_{\mathrm{m,feas}}$, and (c) current locus for $\omega_{\mathrm{k}} = \omega^{\mathrm{MTPV}}_{\mathrm{k,cut\text{-}in}}$ and $m_{\mathrm{m,ref}} \le m^{\mathrm{FW}}_{\mathrm{m,feas}}$.

Introduction: LMRES selected research results

Electrical drives & renewables (operation management; Geothermal Energy) [23]

IEEE TRANSACTIONS ON INDUSTRIAL ELECTRONICS, VOL. 70, NO. 1, JANUARY 2023 211

Nonlinear Modeling, Identification, and Optimal Feedforward Torque Control of Induction Machines Using Steady-State Machine Maps

Julian Kullick and Christoph M. Hackl, *Senior Member, IEEE*

***Abstract*—A novel but simple machine map-based modeling, identification, and optimal feedforward torque control (OFTC) approach for induction machines (IMs) is presented. It is based on, first, a generic, nonlinear transformer-like machine model considering nonlinear flux linkages (with magnetic saturation and cross coupling) and iron losses in the stator laminations in a novel, arbitrarily rotating but unique, robust, and reproducible (d, q)-reference frame; second, a holistic machine identification procedure, which evaluates steady-state measurements over a grid of (d, q) stator currents and produces temperature and frequency dependent machine maps, for example, flux linkages, torque, iron resistance, and efficiency; and third, a numerical offline optimization and extraction of different OFTC look-up tables (LUTs) for *optimal* current reference generation depending on reference torque and electrical frequency (and temperature). During the identification, stator winding temperature and electrical stator frequency of the IM are kept constant by an intelligent temperature and the speed control system. The presented measurement results for a squirrel-cage IM confirm that compared to constant flux operation or scalar V/Hz control, efficiency can be increased particularly in part-load operation by up to 7 % by Maximum Torque Per Losses minimizing copper *and* iron losses.**

***Index Terms*—Efficiency, flux linkages, induction machine (IM), iron resistance, machine identification, MTPA**

$\|\boldsymbol{x}\| := \sqrt{\boldsymbol{x}^\top \boldsymbol{x}} = \sqrt{x_1^2 + \dot{s} + x_n^2}$: Euclidean norm of $\boldsymbol{x}$; $\boldsymbol{X} \in \mathbb{R}^{n\times n}$: matrix ($n$ rows & columns); $\boldsymbol{X}^{-1}$, $\boldsymbol{X}^{-\top}$: inverse, inverse transpose of $\boldsymbol{X}$ (if exist), resp.; $\boldsymbol{I}_n := \mathrm{diag}(1,\dots,1) \in \mathbb{R}^{n\times n}$: identity matrix; $\boldsymbol{0}_n := (0, \dot{s}, 0)^\top \in \mathbb{R}^n$: zero vector; $\boldsymbol{x}^{dq} := (x^d, x^q)^\top \in \mathbb{R}^2$: stator or rotor (iron) current, voltage, flux linkage vectors, i.e., $\boldsymbol{x} \in \{\boldsymbol{i}^{dq}_{\mathrm{s/r(,Fe)}}, \boldsymbol{u}^{dq}_{\mathrm{s/r}}, \boldsymbol{\psi}^{dq}_{\mathrm{s/r}}, \dot{s}\}$; $\boldsymbol{X}^{dq} := \begin{bmatrix} X^d & X^{dq} \\ X^{qd} & X^q \end{bmatrix} \in \mathbb{R}^{2\times 2}$: stator/rotor (iron) resistance matrix, i.e., $\boldsymbol{R}_{\mathrm{s/r(,Fe)}}$; $\vartheta_{\mathrm{s/r}}$: stator/rotor temperature; x_{ref}: reference value of, e.g., temperature, electrical frequency, and currents, i.e., $x \in \{\vartheta_{\mathrm{s,ref}}, \omega_{\mathrm{p,ref}}, i^d_{\mathrm{s,ref}}, i^q_{\mathrm{s,ref}}, \dot{s}\}$; $T_{\mathrm{r/f}}$: rotor/filter time constant; n_{p}: pole pair number; $m_{\mathrm{m/l}}$: machine/load torque; Θ_{m}: machine inertia; ω_{m}: mechanical angular velocity; ϕ_{p} and $\omega_{\mathrm{p}} = \frac{\mathrm{d}}{\mathrm{d}t}\phi_{\mathrm{p}}$: Park transformation angle and angular velocity; $\boldsymbol{J} := \begin{bmatrix} 0 & -1 \\ 1 & 0 \end{bmatrix}$: rotation matrix (by $\frac{\pi}{2}$).

I. Motivation and Contributions

Maximum efficiency operation (or loss minimizing control) of induction machines has been subject to extensive research in

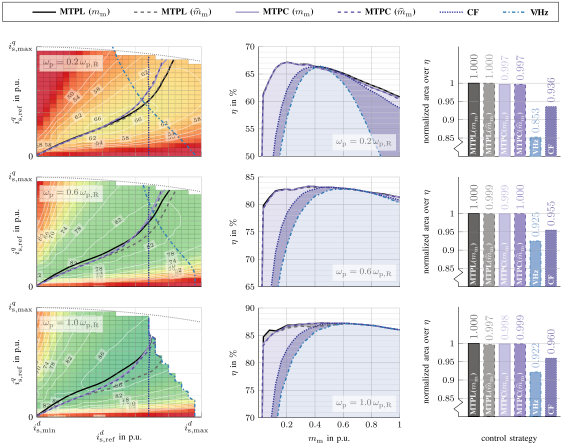

. 12. Efficiency comparison for $\omega_{\mathrm{p}} \in [0.2, 0.6, 1] \cdot \omega_{\mathrm{p,N}}$ (from top to bottom), with efficiency contour plots in current locus (left colum
ciency-over-torque plots (middle column) and overall performance bar plots (right column).

Introduction: LMRES selected research results

Electrical/industrial/traction drives (self-commissioning) [25]

Received 26 February 2022; revised 17 March 2022; accepted 22 March 2022. Date of publication 25 March 2022; date of current version 12 May 2022. The review of this paper was arranged by Associate Editor Haitham Abu-Rub.

Digital Object Identifier 10.1109/OJIES.2022.3162336

Analytical Prototype Functions for Flux Linkage Approximation in Synchronous Machines

SHIH-WEI SU [1], **CHRISTOPH M. HACKL** [2] **(Senior Member, IEEE), AND RALPH KENNEL** [1] **(Senior Member, IEEE)**

[1] Institute of Electrical Drive System and Power Electronics, Technical University of Munich, 80333 Munich, Germany
[2] Department of Electrical Engineering and Information Technology, Hochschule München University of Applied Sciences, 80335 Munich, Germany

CORRESPONDING AUTHOR: SHIH-WEI SU (e-mail: shihwei.su@tum.de).

ABSTRACT Physically motivated and analytical prototype functions are proposed to approximate the nonlinear flux linkages of nonlinear synchronous machines (SMs) in general; and reluctance synchronous machines (RSMs) and interior permanent magnet synchronous machines (IPMSMs) in particular. Such analytical functions obviate the need of huge lookup tables (LUTs) and are beneficial for optimal operation management and nonlinear control of such machines. The proposed flux linkage prototype functions are capable of mimicking the nonlinear self-axis and cross-coupling saturation effects of SMs. Moreover, the differentiable prototype functions allow to easily derive analytical expressions for the differential inductances by simple differentiation of the analytical flux linkage prototype functions. In total, two types of flux linkage prototype functions are developed. The first flux linkage approximation is rather simple and obeys the energy conservation rule for "symmetric" flux linkages of RSMs. With the gained knowledge, the second type of prototype functions is derived in order to achieve approximation flexibility necessary for SMs with permanent (or electrical) excitation with "unsymmetric" flux linkages due to the excitation offset. All proposed flux linkage prototype functions are continuously differentiable, obey the energy conservation rule and, as fitting results show, achieve a (very) high approximation accuracy over the whole operation range.

INDEX TERMS Analytical flux linkage prototype functions, interior permanent magnet synchronous ma-

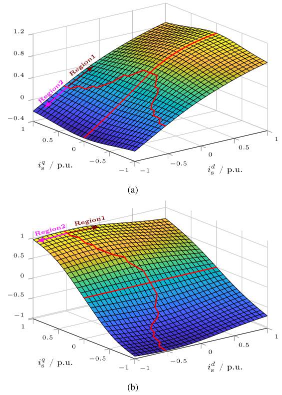

JRE 10. Approximation results of the proposed analytical flux linkage otype functions (40), (41), (46) and (47): (a) fitted d-axis flux linkages (b) fitted q-axis flux linkages $\hat{\psi}_s^q$; zero locus $\mathbb{L}_s^{dq}(L=0)$ [——] is

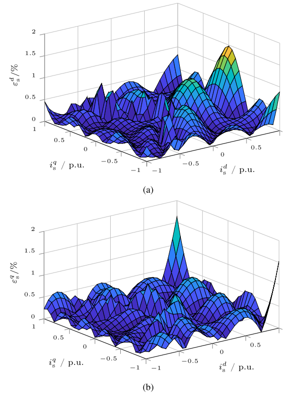

FIGURE 11. Approximation errors of the proposed analytical flux linkag prototype functions (40), (41), (46) and (47) compared to the real flux maps: (a) normalized d-axis error ε_s^d; (b) normalized q-axis error ε_s^q.

Introduction: LMRES selected research results

Electrical/industrial/traction drives (Artificial Neural Netwokrs; self-commissioning) [138]

IEEE TRANSACTIONS ON ENERGY CONVERSION, VOL. 38, NO. 3, SEPTEMBER 2023 1767

Simultaneous Identification of Inverter and Machine Nonlinearities for Self-Commissioning of Electrical Synchronous Machine Drives

Simon Wiedemann and Christoph Michael Hackl, *Senior Member, IEEE*

Abstract—**The proposed identification method allows for a simultaneous estimation of nonlinear output voltage deviations in voltage source inverters (VSIs) and nonlinear synchronous machine models. Based on the identified characteristics with the help of physically inspired structured artificial neural networks (ANNs), an efficient tuning of the current control system can be performed and the nonlinear voltage deviations caused by parasitic effects and dead-time distortions can be accurately compensated for. The identification is performed without position sensor while the rotor is mechanically locked by utilising measured phase currents and reference machine voltages only. Experiments for an interior permanent magnet synchronous machine (IPMSM) and a reluctance synchronous machine (RSM) show that the proposed method is capable of identifying the current dependent self-axis and cross-axis flux linkages, differential inductances and the nonlinear VSI voltage deviations as well as the phase resistance at the same time. The proposed method is fast and generic. Besides the rated machine current, voltage and frequency, no prior system knowledge is required making it applicable for the self-commissioning of any electrical synchronous machine drive.**

Index Terms—**Identification, self-commissioning, auto-tuning, synchronous machine, inverter dead-time, machine characterisation, flux linkage map, machine model, artifical neural network, encoderless.**

NOTATION

$\mathbb{N}, \mathbb{R}$: natural, real numbers; $\boldsymbol{x} := (x_1, \ldots, x_n)^\top \in \mathbb{R}[n]$: col-

I. INTRODUCTION

MODERN control methods and observer architectures of electrical machines rely mostly on accurate information of drive characteristics. Identified parameters of the linear machine model such as the phase resistances and inductances can be utilised to tune the current controllers [1], [2], [3] or observers and to compute the optimal reference currents for an energy efficient operation [2], [4]. This tuning can be further improved by the identification and utilisation of nonlinear flux linkage maps usually expressed in the synchronously rotating (d, q)-reference frame [2], [4], [5], [6], [7], [8] which allow to compute the differential inductances (in the following, the superscript d or q stands for the d- or q-axis, resp.). The automatic identification and tuning of the machine drive can be considered as self-commissioning/auto-tuning and is usually performed before machine operation via offline identification [1], [2], [9].

Self-commissioning algorithms heavily decrease the time required to characterise and tune an electrical machine drive compared to a manual process which, due to a lack of expertise and time of the control engineers, might lead to imprecise results and poor control dynamics [2] as well as an energy inefficient operation [9]. The importance of an automatic commissioning becomes obvious if one considers that around 53 % of the globally generated energy is consumed by electrical machines [10]. Despite several improvements on energy efficient

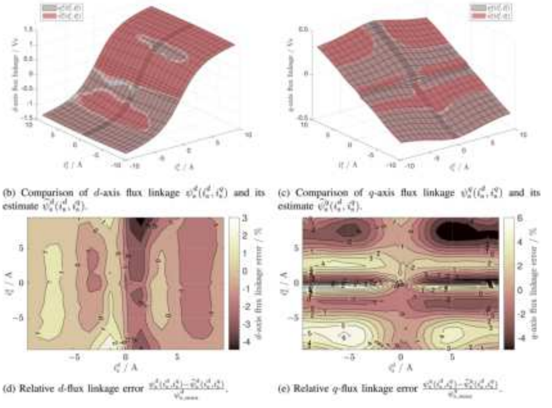

(b) Comparison of d-axis flux linkage $\psi_s^d(i_s^d, i_s^q)$ and its estimate $\widehat{\psi}_s^d(i_s^d, i_s^q)$.

(c) Comparison of q-axis flux linkage $\psi_s^q(i_s^d, i_s^q)$ and its estimate $\widehat{\psi}_s^q(i_s^d, i_s^q)$.

(d) Relative d-flux linkage error $\frac{\psi_s^d(i_s^d,i_s^q)-\widehat{\psi}_s^d(i_s^d,i_s^q)}{\psi_{s,\max}}$.

(e) Relative q-flux linkage error $\frac{\psi_s^q(i_s^d,i_s^q)-\widehat{\psi}_s^q(i_s^d,i_s^q)}{\psi_{s,\max}}$.

Fig. 9. **RSM identification results:** (a) Time series; (b) & (c) flux linkages; (e) & (f) relative flux linkage errors.

significantly increased model complexity as for which it is often omitted (such as in [16]). The bias $b^{q,\mathrm{self}}$ as shown in

-4% to 3% for $\widehat{\psi}_s^d(i_s^d, i_s^q)$ and -4% to 6% for $\widehat{\psi}_s^q(i_s^d, i_s^q)$. Fig. 1

Introduction: LMRES selected research results

Smart grid/renewables/power systems (grid synchronisation) [22]

3298 IEEE TRANSACTIONS ON POWER ELECTRONICS, VOL. 35, NO. 3, MARCH 2020

Modified Second-Order Generalized Integrators With Modified Frequency Locked Loop for Fast Harmonics Estimation of Distorted Single-Phase Signals

Christoph M. Hackl, *Senior Member, IEEE*, and Markus Landerer

***Abstract*—This article proposes *modified second-order generalized integrators* (mSOGIs) for a fast estimation of all harmonic components of arbitrarily distorted single-phase signals, such as voltages or currents in power systems. The estimation is based on the internal model principle leading to an overall observer consisting of parallelized mSOGIs. The observer is tuned by pole placement. For a constant fundamental frequency, the observer is capable of estimating all harmonic components with prescribed settling time by choosing the observer poles appropriately. For time-varying fundamental frequencies, the harmonic estimation is combined with a *modified frequency locked loop* (mFLL) with gain normalization, sign-correct antiwindup, and rate limitation. The estimation performances of the proposed parallelized mSOGIs with and without mFLL are illustrated and validated by measurement results. The results are compared to standard approaches such as parallelized standard SOGIs (sSOGIs) and adaptive notch filters (ANFs).**

***Index Terms*—Amplitude estimation, frequency estimation, frequency-locked loop (FLL), phase estimation, second-order generalized integrator (SOGI).**

Notation

$\mathbb{N}, \mathbb{R}, \mathbb{C}, \mathbb{Q}$: natural, real, complex and rational numbers. For the following, let $n, m \in \mathbb{N}$. $\boldsymbol{x} := (x_1, \ldots, x_n)^\top \in \mathbb{R}^n$: column vector (where $:=$ means "is defined as" and $^\top$ means "transposed"). $\boldsymbol{0}_n := (0, 0, \ldots, 0)^\top \in \mathbb{R}^n$: zero vector. $\|\boldsymbol{x}\| := \sqrt{\boldsymbol{x}^\top \boldsymbol{x}}$: Euclidean norm of $\boldsymbol{x}$. $\boldsymbol{A} \in \mathbb{R}^{n \times m}$: real (non-square) matrix. $\mathrm{diag}(\boldsymbol{a}) \in \mathbb{R}^{n \times n}$: diagonal matrix with

I. Introduction

A. Motivation and Literature Review

IN VIEW of the increasing number of decentralized generation units with power electronics-based grid connection and the decreasing number of large-scale generators, the overall inertia in the grid is diminishing. This results in faster and more abrupt frequency fluctuations and significant harmonic distortion of physical quantities (such as currents or voltages) of the power system [1]. Fast frequency fluctuations endanger stability of the power grid. Significant harmonic distortions of voltages and currents can degrade power quality and lead to damage or even destruction of grid components. To be capable of taking appropriate countermeasures such as 1) improving system stability and power quality and 2) compensating for such deteriorated operation conditions, it is crucial to detect and estimate fundamental and higher harmonic components of the considered quantities in real time as fast and accurate as possible. Modern power electronic devices (e.g., flexible ac transmission systems or grid-connected converters of decentralized renewable energy systems) can then be used to implement such countermeasures. That is why, grid state estimation became of particular interest to the research community in the past years and has been studied extensively (see e.g., [2]–[24] to name a few).

It is well known that a signal with significant harmonic

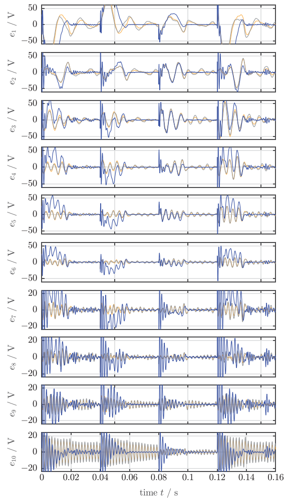

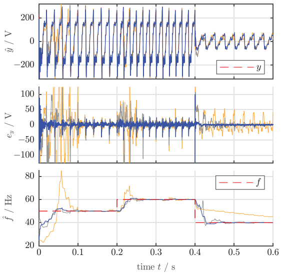

Fig. 11. Measurement results for Scenario (S_4): Comparison of the estimation performances of *parallelized* mSOGIs (——), sSOGIs (——), and ANFs (——) *without* FLL. Signals shown from top to bottom are: Harmonic signals y_1 to y_{10} (- - -) and their estimates $\widehat{y}_1$ to $\widehat{y}_{10}$ and harmonic estimation errors $e_1 = y_1 - \widehat{y}_1$ to $e_{10} = y_{10} - \widehat{y}_{10}$.

frequency are identical for this scenario. Therefore, the estimation performances purely can be compared according to the respective observer tunings only. The fundamental signal $y = y_1$ undergoes step-like changes in amplitude, phase and amplitude and phase as described above.

The estimation performances of fundamental mSOGI (——), fundamental sSOGI (——), and fundamental ANF (——) are shown in Fig. 7. The first and second subplots show input signal $y = y_1$ (- - -) and its estimates $\widehat{y} = \widehat{y}_1$ and the estimation errors $e_y = y_1 - \widehat{y}_1$, respectively. All three observers are capable of estimating the input signal y. All estimation errors $e_y \to 0$ tend to

Outline

Outline

Motivation

Emerging applications of electrical drives: Electrical drives are **the** mechatronic actuators of the future

(a) Full-electric vehicles (e-mobility).

(b) Mobile (industrial) robots.

(c) Autonomous, full-electric tractor (farming).

(d) Full-electric aircraft.

Outline

2 Motivation

Motivation

Electrical machines — widely-used, compact and efficient actuators


www.miele.de


www.farmwood.co.uk


www.abb.com (from video)


www.siemens.com


www.bmw.de


www.siemens.com


www.siemens.com


www.lilium.com

- household and buildings (e.g. wasching machines, air conditioning or fans)
- industrial applications (e.g. pumps, milling, grinding)
- traction drives (e.g. electric vehicles, trains, etc.)
- power generation (e.g. conventional power plants or wind turbine systems)
- (more) electric aircrafts
- ...

Outline

2 Motivation

- Emerging applications of electrical drives
- Electrical machines — widely-used, compact and efficient actuators
- Core components of mechatronic system
- Motion control via mechatronic actuators
- Block diagram of mechatronic actuator
- Overall control system

Motivation

Core components of mechatronic system

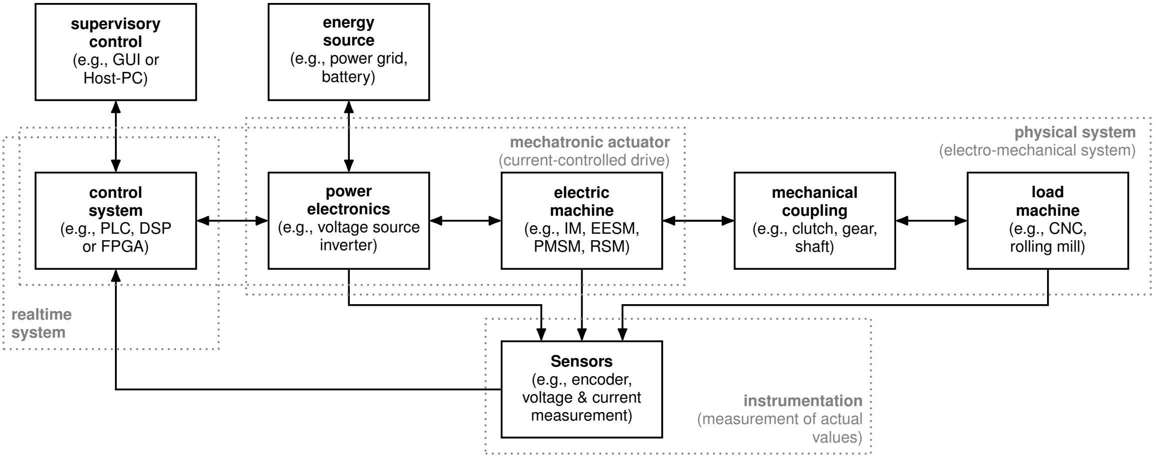

Outline

Motivation

Motion control via mechatronic actuators

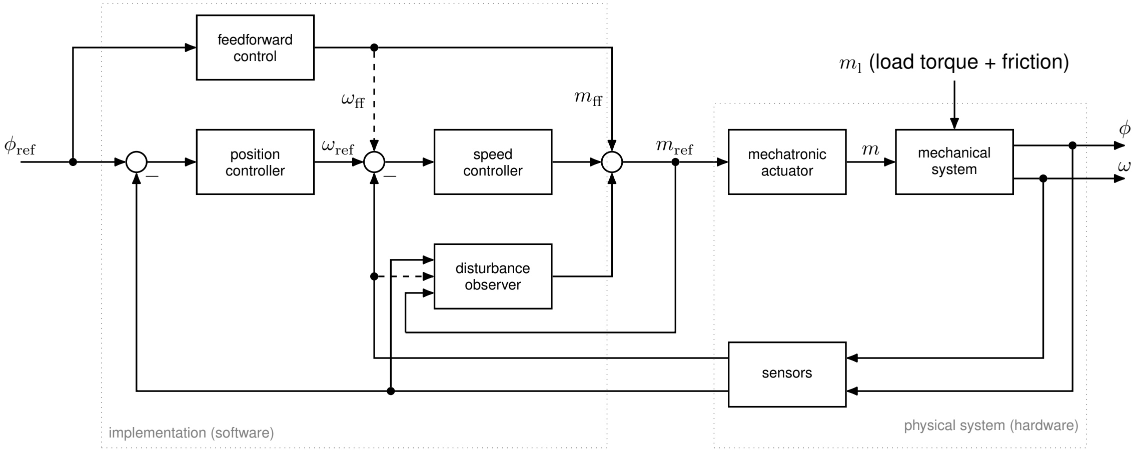

Outline

2 Motivation

Motivation

Block diagram of mechatronic actuator (e.g., with electrical three-phase machine)

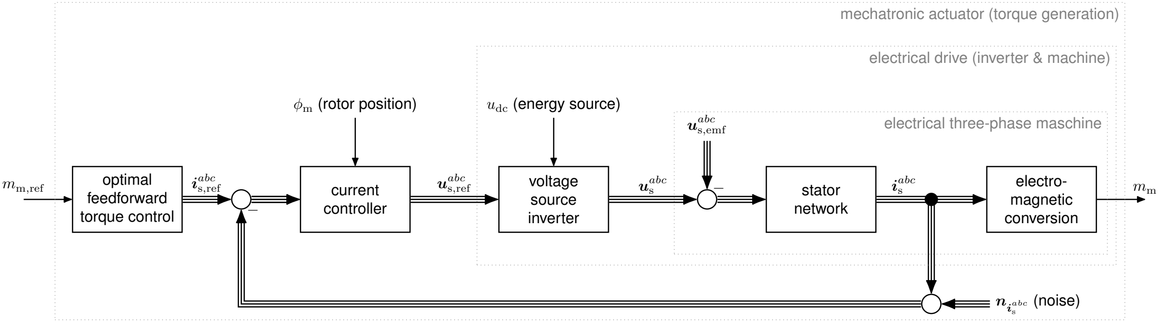

Outline

2 Motivation

- Emerging applications of electrical drives
- Electrical machines — widely-used, compact and efficient actuators
- Core components of mechatronic system
- Motion control via mechatronic actuators
- Block diagram of mechatronic actuator
- Overall control system

Motivation

Overall control system (e.g., for Reluctance Synchronous Machine (RSM))

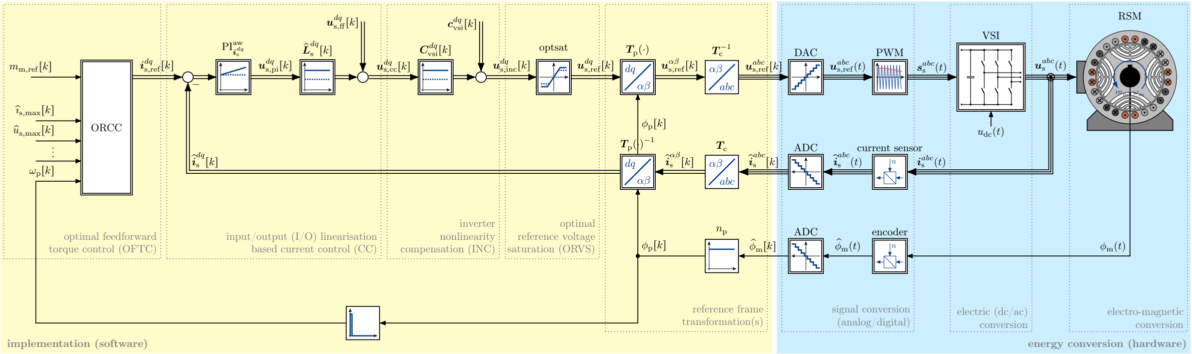

Outline

Outline

Preliminaries

Single-phase alternating current (AC) systems

Definition (Phase signal ($x \in \{u, i\}$))

$$x\colon \mathbb{R}_{\geqslant 0} \to \mathbb{R}, \quad t \mapsto x(t) := \hat{x}(t)\,\cos(\phi_x(t))$$

with *amplitude* $\hat{x}(\cdot) \in \mathcal{L}^{\infty}(\mathbb{R}_{\geqslant 0}; \mathbb{R})$ and *phase angle* $\phi_x(\cdot) \in \mathcal{C}^{\mathrm{abs}}(\mathbb{R}_{\geqslant 0}; \mathbb{R})$.

Definition (Sliding average, rectified value, root mean square [sinusoidal signals with $\hat{x}, T > 0$ and $\phi_x = \frac{2\pi}{T} t$])

- *Sliding average*: $\forall\, t \geqslant T > 0\colon\ \overline{X}(t) := \frac{1}{T}\int_{t-T}^{t} x(\tau)\,\mathrm{d}\tau\ \ [= 0]$
- *Rectified value*: $\forall t \geqslant T > 0\colon\ \overline{X}_{\mathrm{dc}}(t) := \frac{1}{T}\int_{t-T}^{t} |x(\tau)|\,\mathrm{d}\tau\ \ [= \frac{2\hat{x}}{\pi}]$
- *Root mean square (RMS)*: $\forall t \geqslant T > 0\colon\ X_{\mathrm{rms}}(t) := \sqrt{\frac{1}{T}\int_{t-T}^{t} x(\tau)^2\,\mathrm{d}\tau}\ \ [= \frac{\hat{x}}{\sqrt{2}}]$

Outline

Preliminaries

Three-phase alternating current (AC) systems

Definition (Phase signals in vector notation ($x \in \{u, i, \psi, \ldots\}$))

$$\boldsymbol{x}^{abc}\colon \mathbb{R}_{\geqslant 0} \to \mathbb{R}^3, \quad t \mapsto \boldsymbol{x}^{abc}(t) := \begin{pmatrix} x^a(t) \\ x^b(t) \\ x^c(t) \end{pmatrix} := \begin{pmatrix} \hat{x}^a(t)\, \cos(\phi_x^a(t)) \\ \hat{x}^b(t)\, \cos(\phi_x^b(t)) \\ \hat{x}^c(t)\, \cos(\phi_x^c(t)) \end{pmatrix}$$

with *amplitudes* $\hat{x}^a(\cdot), \hat{x}^b(\cdot), \hat{x}^c(\cdot) \in \mathcal{L}^\infty(\mathbb{R}_{\geqslant 0}; \mathbb{R})$ and *phase angles* $\phi_x^a(\cdot), \phi_x^b(\cdot), \phi_x^c(\cdot) \in \mathcal{C}^{\mathrm{abs}}(\mathbb{R}_{\geqslant 0}; \mathbb{R})$ (differentiable a.e.).

Fact (Line-to-line signals)

$$\boldsymbol{x}^{a\text{-}b\text{-}c}(t) := \begin{pmatrix} x^{a\text{-}b}(t) \\ x^{b\text{-}c}(t) \\ x^{c\text{-}a}(t) \end{pmatrix} := \begin{pmatrix} x^a(t) - x^b(t) \\ x^b(t) - x^c(t) \\ x^c(t) - x^a(t) \end{pmatrix} = \underbrace{\begin{bmatrix} 1 & -1 & 0 \\ 0 & 1 & -1 \\ -1 & 0 & 1 \end{bmatrix}}_{=:\, \boldsymbol{T}_{\mathrm{v}}^{\star}, \quad {\color{red}\det(\boldsymbol{T}_{\mathrm{v}}^{\star})=0}} \boldsymbol{x}^{abc}(t)$$

Outline

Preliminaries

Interconnection of three-phase (AC) systems

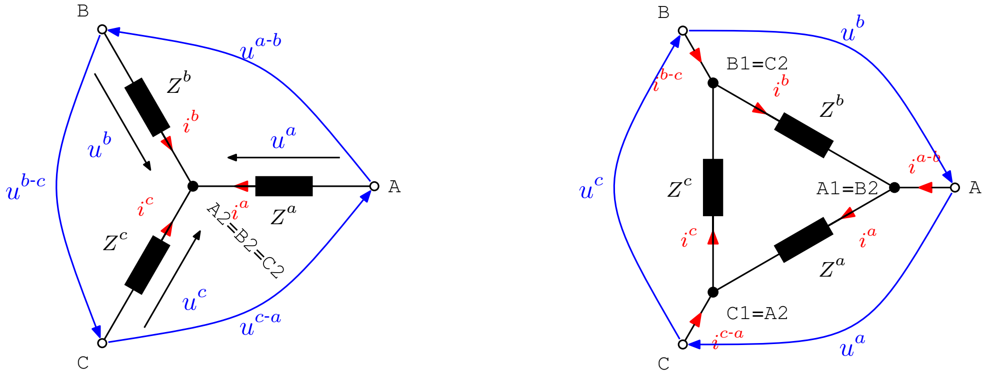

Fact (Star or Y connection)

- $i^a + i^b + i^c = 0$
- $u^{a\text{-}b} + u^{b\text{-}c} + u^{c\text{-}a} = 0$
- $(u^a + u^b + u^c \neq 0)$

Fact (Delta or △ connection)

- $i^{a\text{-}b} + i^{b\text{-}c} + i^{c\text{-}a} = 0$
- $u^a + u^b + u^c = 0$
- $(i^a + i^b + i^c \neq 0)$

Preliminaries

Interconnection of three-phase (AC) systems (terminal box)

Star connection (symbol ⅄)

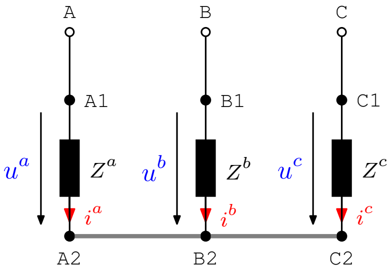

Delta connection (symbol △)

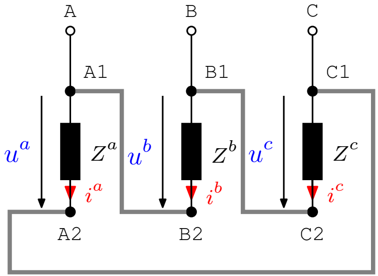

Outline

Preliminaries

Balanced three-phase (AC) systems

$$\boldsymbol{x}^{abc}\colon \mathbb{R}_{\geqslant 0} \to \mathbb{R}^3, \quad t \mapsto \boldsymbol{x}^{abc}(t) := \begin{pmatrix} x^a(t) \\ x^b(t) \\ x^c(t) \end{pmatrix} := \begin{pmatrix} \hat{x}^a(t)\,\cos(\phi_x^a(t)) \\ \hat{x}^b(t)\,\cos(\phi_x^b(t)) \\ \hat{x}^c(t)\,\cos(\phi_x^c(t)) \end{pmatrix}$$

Assumption 1 (Identical phase amplitudes)

$$\forall\, t \geqslant 0\colon \qquad \hat{x}(t) := \hat{x}^a(t) = \hat{x}^b(t) = \hat{x}^c(t)$$

Assumption 2 (Phase shift between phases of $-\frac{2}{3}\pi$)

$$\forall\, t \geqslant 0\colon \quad \phi_x(t) = \phi_x^a(t) = \phi_x^b(t) + \tfrac{2}{3}\pi = \phi_x^c(t) + \tfrac{4}{3}\pi, \quad \phi_x(\cdot) \in \mathcal{C}^{\mathrm{abs}}(\mathbb{R}_{\geqslant 0}; \mathbb{R}).$$

Fact (Gamma (zero) component cancels out for balanced systems)

$$\forall\, t \geqslant 0\colon \qquad x^\gamma(t) := x^a(t) + x^b(t) + x^c(t) \overset{\text{(A.1), (A.2)}}{=} 0$$

Preliminaries

Balanced three-phase (AC) systems: Examples

Examples

Balanced phase voltages:

$$\forall\, t \geqslant 0\colon \quad \boldsymbol{u}^{abc}(t) := \begin{pmatrix} u^a(t) \\ u^b(t) \\ u^c(t) \end{pmatrix} = \widehat{u}(t) \begin{pmatrix} \cos(\phi_u(t)) \\ \cos\left(\phi_u(t) - \frac{2}{3}\pi\right) \\ \cos\left(\phi_u(t) - \frac{4}{3}\pi\right) \end{pmatrix}$$

Balanced phase currents:

$$\forall\, t \geqslant 0\colon \quad \boldsymbol{i}^{abc}(t) := \begin{pmatrix} i^a(t) \\ i^b(t) \\ i^c(t) \end{pmatrix} = \widehat{\imath}(t) \begin{pmatrix} \cos(\phi_i(t)) \\ \cos\left(\phi_i(t) - \frac{2}{3}\pi\right) \\ \cos\left(\phi_i(t) - \frac{4}{3}\pi\right) \end{pmatrix}$$

Definition (Phase difference or phase shift)

$$\forall\, t \geqslant 0\colon \qquad \varphi(t) := \phi_u(t) - \phi_i(t)$$

Outline

Preliminaries

for electrical machines

Induction machine (IM)

http://www.automation.siemens.com/bilddb/

Synchronous machine (SM)

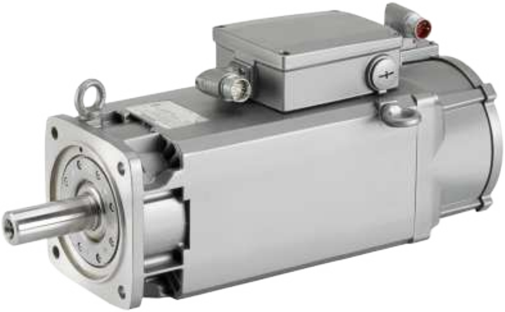

http://www.automation.siemens.com/bilddb/

Preliminaries

Space vector theory: Sectional view of induction machine

www.siemens.com

Preliminaries

Space vector theory: Illustration for induction machine (IM)

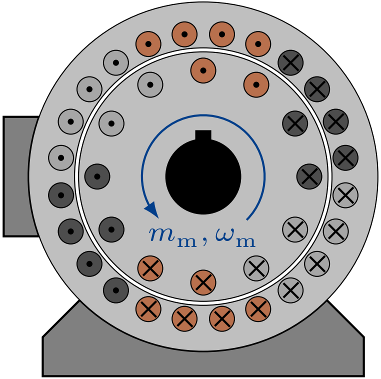

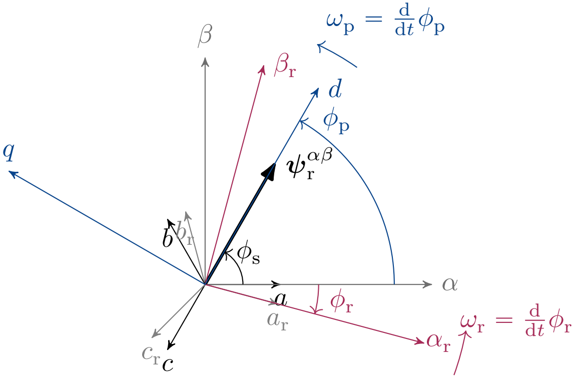

(α, β)-reference frame

$(\alpha_{\mathrm{r}}, \beta_{\mathrm{r}})$-reference frame

(d, q)-reference frame

Preliminaries

Space vector theory: Illustration for permenant-magnet synchronous machine (PMSM)

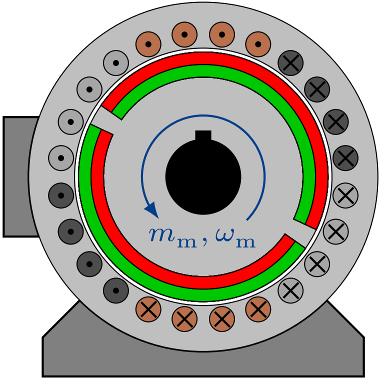

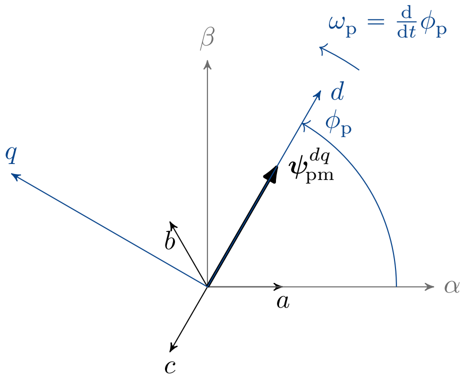

(α, β)-reference frame

(d, q)-reference frame

Preliminaries

Space vector theory: Clarke transformation $(a, b, c) \to (\alpha, \beta, \gamma)$

Definition (Clarke transformation with $\kappa \in \{2/3, \sqrt{2/3}\}$)

$$\boldsymbol{f}_{\mathrm{c}}^{\star}\colon \mathbb{R}^3 \to \mathbb{R}^3,\ \underbrace{\begin{pmatrix} x^a \\ x^b \\ x^c \end{pmatrix}}_{=:\boldsymbol{x}^{abc}} \mapsto \underbrace{\begin{pmatrix} x^\alpha \\ x^\beta \\ x^\gamma \end{pmatrix}}_{=:\boldsymbol{x}^{\alpha\beta\gamma}} := \boldsymbol{f}_{\mathrm{c}}(\boldsymbol{x}^{abc}) := \underbrace{\kappa \begin{bmatrix} 1 & -\frac{1}{2} & -\frac{1}{2} \\ 0 & \frac{\sqrt{3}}{2} & -\frac{\sqrt{3}}{2} \\ \frac{1}{\sqrt{2}} & \frac{1}{\sqrt{2}} & \frac{1}{\sqrt{2}} \end{bmatrix}}_{=:\boldsymbol{T}_{\mathrm{c}}^{\star} \in \mathbb{R}^{3\times 3},\ \forall\, \kappa \neq 0:\ \det(\boldsymbol{T}_{\mathrm{c}}^{\star}) \neq 0} \begin{pmatrix} x^a \\ x^b \\ x^c \end{pmatrix}$$

$$(\boldsymbol{T}_{\mathrm{c}}^{\star})^{-1} = \frac{1}{\kappa} \begin{bmatrix} \frac{2}{3} & 0 & \frac{\sqrt{2}}{3} \\ -\frac{1}{3} & \frac{1}{\sqrt{3}} & \frac{\sqrt{2}}{3} \\ -\frac{1}{3} & -\frac{1}{\sqrt{3}} & \frac{\sqrt{2}}{3} \end{bmatrix}, \quad \text{hence: } \boldsymbol{x}^{abc} = (\boldsymbol{f}_{\mathrm{c}}^{\star})^{-1}(\boldsymbol{x}^{\alpha\beta\gamma}) = (\boldsymbol{T}_{\mathrm{c}}^{\star})^{-1}\boldsymbol{x}^{\alpha\beta\gamma}.$$

Remark (Choice of κ)

$\kappa = \frac{2}{3} \implies$ amplituden-invariant transformation, i.e. $|x^a| = |x^\alpha|$.

$\kappa = \sqrt{\frac{2}{3}} \implies$ power-invariant transformation, i.e. $(\boldsymbol{u}^{abc})^\top \boldsymbol{i}^{abc} = (\boldsymbol{u}^{\alpha\beta\gamma})^\top \boldsymbol{i}^{\alpha\beta\gamma}$.

Preliminaries

Space vector theory: Simplified Clarke transformation $(a, b, c) \to (\alpha, \beta)$

For **balanced systems**, i.e. $\boxed{x^a(t) + x^b(t) + x^c(t) = 0}$ for all $t \geqslant 0$, we have :

$$\boldsymbol{f}_{\mathrm{c}} : \mathbb{R}^3 \to \mathbb{R}^2, \underbrace{\begin{pmatrix} x^a \\ x^b \\ x^c \end{pmatrix}}_{=:\boldsymbol{x}^{abc}} \mapsto \underbrace{\begin{pmatrix} x^\alpha \\ x^\beta \end{pmatrix}}_{=:\boldsymbol{x}^{\alpha\beta}} := \boldsymbol{f}_{\mathrm{c}}(\boldsymbol{x}^{abc}) = \kappa \underbrace{\begin{bmatrix} 1 & -\frac{1}{2} & -\frac{1}{2} \\ 0 & \frac{\sqrt{3}}{2} & -\frac{\sqrt{3}}{2} \end{bmatrix}}_{=:\boldsymbol{T}_{\mathrm{c}} \in \mathbb{R}^{2\times 3}} \begin{pmatrix} x^a \\ x^b \\ x^c \end{pmatrix}$$

where

$$(\boldsymbol{T}_{\mathrm{c}})^{-1} := \frac{1}{\kappa} \begin{bmatrix} \frac{2}{3} & 0 \\ -\frac{1}{3} & \frac{1}{\sqrt{3}} \\ -\frac{1}{3} & -\frac{1}{\sqrt{3}} \end{bmatrix}, \quad \text{somit gilt} \quad \boldsymbol{x}^{abc} = (\boldsymbol{T}_{\mathrm{c}})^{-1} \boldsymbol{x}^{\alpha\beta}.$$

Preliminaries

Space vector theory: Park transformation $(\alpha, \beta) \to (d, q)$

Definition (Park transformation (simplified))

$$\boldsymbol{f}_{\mathrm{p}} \colon \mathbb{R}^2 \times \mathbb{R} \to \mathbb{R}^2, \qquad \Big(\underbrace{\begin{pmatrix} x^{\alpha} \\ x^{\beta} \end{pmatrix}}_{=:\boldsymbol{x}^{\alpha\beta}}, \phi\Big) \mapsto \underbrace{\begin{pmatrix} x^{d} \\ x^{q} \end{pmatrix}}_{=:\boldsymbol{x}^{dq}} := \boldsymbol{f}_{\mathrm{p}}(\boldsymbol{x}^{\alpha\beta}, \phi) = \underbrace{\begin{bmatrix} \cos(\phi) & \sin(\phi) \\ -\sin(\phi) & \cos(\phi) \end{bmatrix}}_{=:\boldsymbol{T}_{\mathrm{p}}(\phi)^{-1} \in \mathbb{R}^{2\times 2}, \forall\, \phi \in \mathbb{R}:\ \det(\boldsymbol{T}_{\mathrm{p}}) \neq 0} \begin{pmatrix} x^{\alpha} \\ x^{\beta} \end{pmatrix}$$

Properties

- $\forall\, \phi_1, \phi_2 \in \mathbb{R}\colon \quad \boldsymbol{T}_{\mathrm{p}}(\phi_1 + \phi_2) = \boldsymbol{T}_{\mathrm{p}}(\phi_1) \cdot \boldsymbol{T}_{\mathrm{p}}(\phi_2)$
- $\forall\, \phi \in \mathbb{R}\colon \quad \boldsymbol{T}_{\mathrm{p}}(\phi) = \begin{bmatrix} \cos(\phi) & -\sin(\phi) \\ \sin(\phi) & \cos(\phi) \end{bmatrix} = \boldsymbol{T}_{\mathrm{p}}(-\phi)^{-1} = \boldsymbol{T}_{\mathrm{p}}(-\phi)^{\top}$
- $\boldsymbol{J} := \boldsymbol{T}_{\mathrm{p}}(\tfrac{\pi}{2}) = \begin{bmatrix} 0 & -1 \\ 1 & 0 \end{bmatrix}$ and $\forall \phi \in \mathbb{R}\colon\ \boldsymbol{J}\boldsymbol{T}_{\mathrm{p}}(\phi) = \boldsymbol{T}_{\mathrm{p}}(\phi)\boldsymbol{J}$
- $\forall\, \phi(\cdot) \in \mathcal{C}^{\mathrm{abs}}(\mathbb{R}_{\geqslant 0}; \mathbb{R})\colon \quad \omega(\cdot) := \frac{\mathrm{d}}{\mathrm{d}t}\phi(\cdot) \ \wedge\ \frac{\mathrm{d}}{\mathrm{d}t}\boldsymbol{T}_{\mathrm{p}}(\phi(t)) = \omega(t)\boldsymbol{J}\boldsymbol{T}_{\mathrm{p}}(\phi(t))$

Outline

Preliminaries

Power definitions: Classical power definitions (sinusoidal signals)

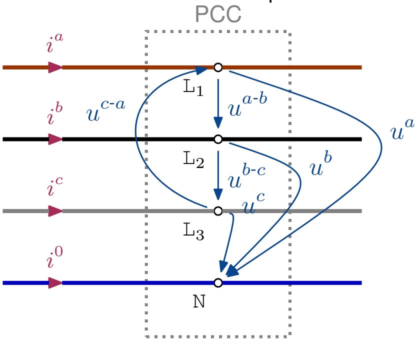

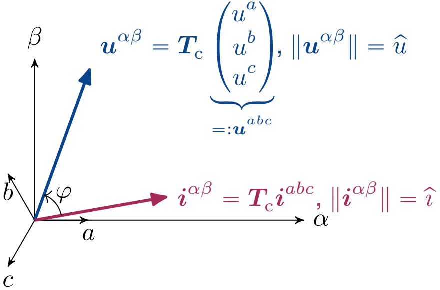

Definition (Average active power [for $T, \widehat{u}, \widehat{\imath}, \varphi > 0$])

$$\forall\, t \geqslant T := \frac{2\pi}{\omega}: \qquad P_{3\sim}(t) := \frac{1}{T}\int_{t-T}^{t} \boldsymbol{u}^{abc}(\tau)^\top \boldsymbol{i}^{abc}(\tau)\,\mathrm{d}\tau \ \left[= \tfrac{3}{2}\widehat{u}\,\widehat{\imath}\cos(\varphi)\right]$$

Definition (Average reactive power [for $T, \widehat{u}, \widehat{\imath}, \varphi > 0$])

$$\forall\, t \geqslant T := \frac{2\pi}{\omega}: \qquad Q_{3\sim}(t) := \frac{1}{T}\int_{t-T}^{t} \boldsymbol{u}^{abc}(\tau)^\top \boldsymbol{i}^{abc}\!\left(\tau - \tfrac{T}{4}\right)\mathrm{d}\tau \ \left[= \tfrac{3}{2}\widehat{u}\,\widehat{\imath}\sin(\varphi)\right]$$

Preliminaries

Power definitions: Instantaenous power theory

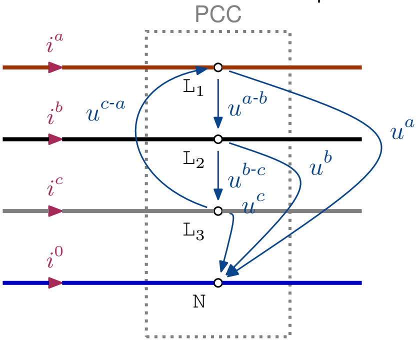

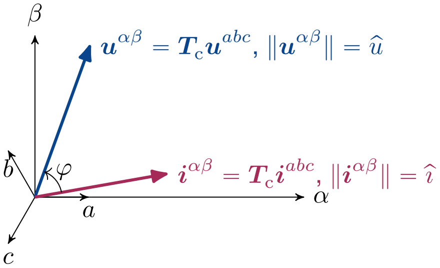

Definition (Instantaenous active power)

$$\forall\, t \geqslant 0: \quad p_{3\sim}(t) := \frac{2}{3\kappa^2} \boldsymbol{u}^{\alpha\beta}(t)^\top \boldsymbol{i}^{\alpha\beta}(t) = \frac{2}{3\kappa^2} \boldsymbol{u}^{dq}(t)^\top \boldsymbol{i}^{dq}(t) \left[= \tfrac{3}{2} \widehat{u}(t) \widehat{\imath}(t) \cos(\varphi(t))\right]$$

Definition (Instantaenous reactive power)

$$\forall\, t \geqslant 0: \quad q_{3\sim}(t) := \frac{2}{3\kappa^2} \boldsymbol{u}^{\alpha\beta}(t)^\top \boldsymbol{J} \boldsymbol{i}^{\alpha\beta}(t) = \frac{2}{3\kappa^2} \boldsymbol{u}^{dq}(t)^\top \boldsymbol{J} \boldsymbol{i}^{dq}(t) \left[= \tfrac{3}{2} \widehat{u}(t) \widehat{\imath}(t) \sin(\varphi(t))\right]$$

Outline

Outline

Nonlinear modelling: Motivation

Output of DeepAI Figure Generator (prompted with “Electric vehicle with motor, power electronics & battery”)

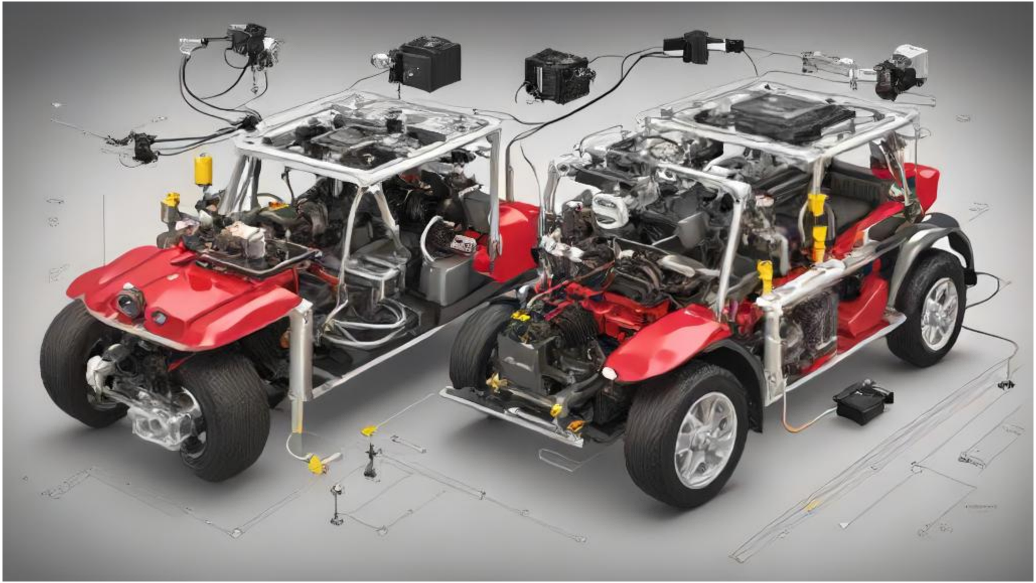

Outline

Outline

Nonlinear modelling: Two-level voltage source inverter (2L-VSI)

Electrical circuit with rectifier

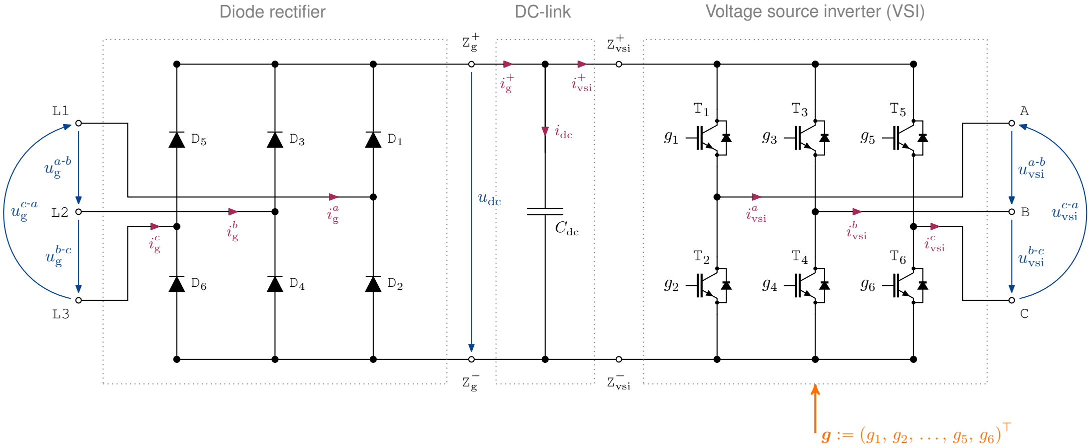

Nonlinear modelling: Two-level voltage source inverter (2L-VSI)

Electrical circuit with rectifier (ideal semi-conductors)

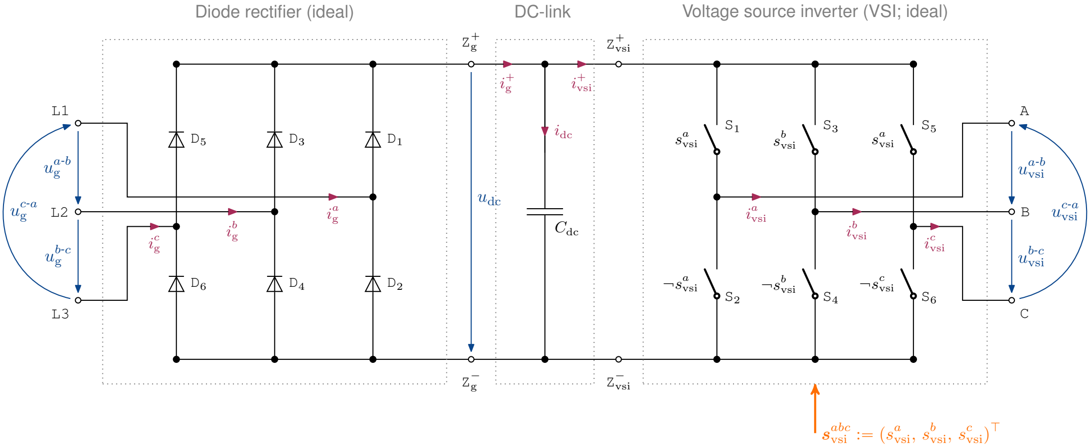

Nonlinear modelling: Two-level voltage source inverter (2L-VSI)

Electrical circuit with split dc-link and mid-point voltages (ideal switches)

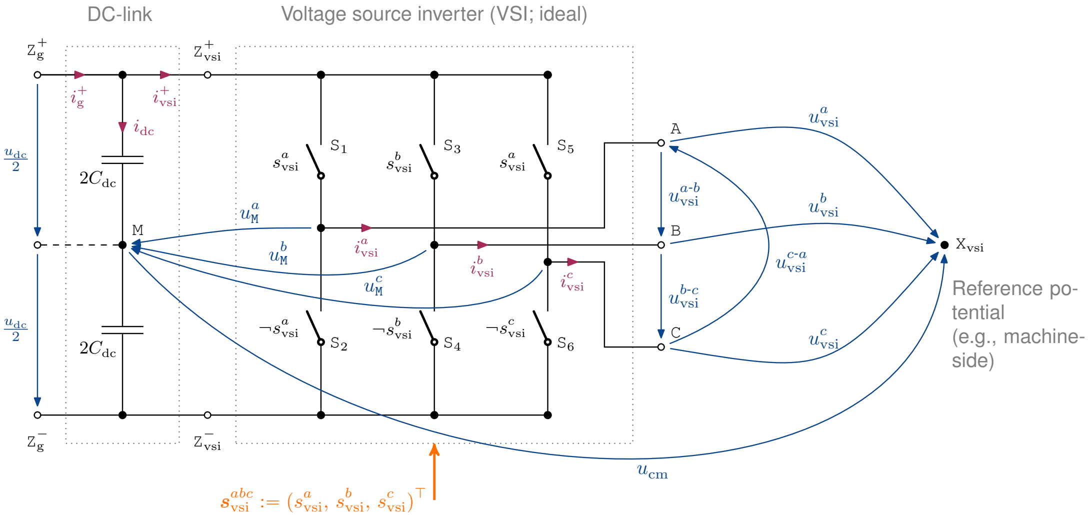

Outline

Nonlinear modelling: Two-level voltage source inverter (2L-VSI)

Switching model (as matrix-vector product)

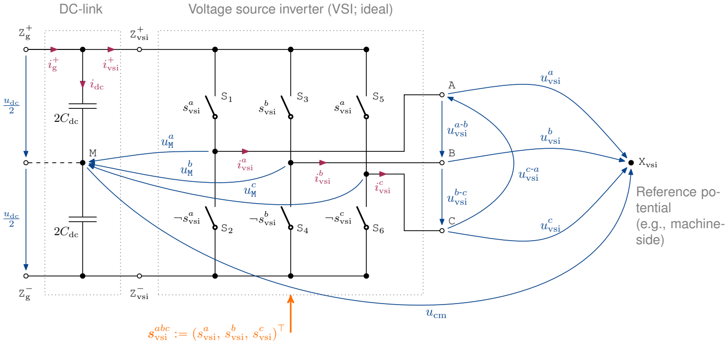

☞ **This model can easily and modularly be extended to include conduction and switching losses as well [164].**

$$u_{vsi}^{a\text{-}b\text{-}c} = \begin{pmatrix} u_{vsi}^{a\text{-}b} \\ u_{vsi}^{b\text{-}c} \\ u_{vsi}^{c\text{-}a} \end{pmatrix} = u_{dc} \begin{bmatrix} 1 & -1 & 0 \\ 0 & 1 & -1 \\ -1 & 0 & 1 \end{bmatrix} \boldsymbol{s}_{vsi}^{abc}$$

$$u_{vsi}^a + u_{vsi}^b + u_{vsi}^c = 0 \implies \boldsymbol{u}_{vsi}^{abc} = \frac{u_{dc}}{3} \begin{bmatrix} 2 & -1 & -1 \\ -1 & 2 & -1 \\ -1 & -1 & 2 \end{bmatrix} \boldsymbol{s}_{vsi}^{abc} = \underbrace{u_{dc}\left(\boldsymbol{s}_{vsi}^{abc} - \tfrac{1}{2}\mathbf{1}_3\right)}_{=:\boldsymbol{u}_M^{abc}} + \mathbf{1}_3 u_{cm}$$

Outline

Nonlinear modelling: Two-level voltage source inverter (2L-VSI)

Modulation: Voltage hexagon

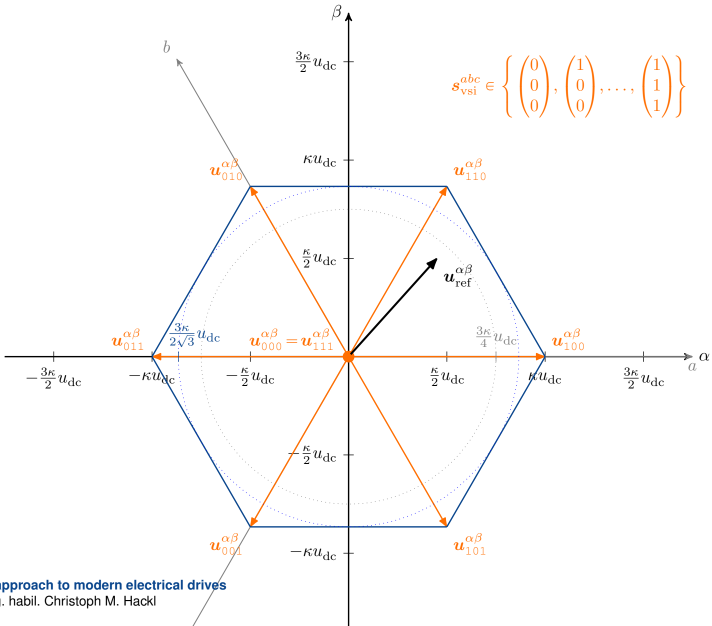

Nonlinear modelling: Two-level voltage source inverter (2L-VSI)

Modulation: Pulse Width Modulation (PWM) and Space Vector Modulation (SVM)

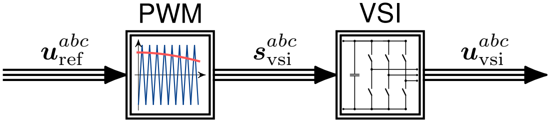

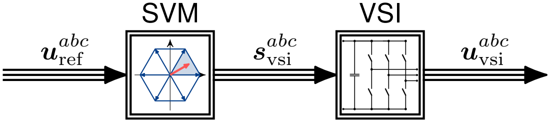

Switching signal vector

$$\boldsymbol{s}_{\text{vsi}}^{abc} = \begin{pmatrix} s_{\text{vsi}}^{a} \\ s_{\text{vsi}}^{b} \\ s_{\text{vsi}}^{c} \end{pmatrix} = \begin{pmatrix} \sigma\left(\frac{u_{\text{ref}}^{a}}{u_{\text{dc}}/2} - u_{\text{car}}\right) \\ \sigma\left(\frac{u_{\text{ref}}^{b}}{u_{\text{dc}}/2} - u_{\text{car}}\right) \\ \sigma\left(\frac{u_{\text{ref}}^{c}}{u_{\text{dc}}/2} - u_{\text{car}}\right) \end{pmatrix}$$

with Heaviside function

$$\sigma(x) := \begin{cases} 1 & , \quad x \geqslant 0 \\ 0 & , \quad x < 0 \end{cases}$$

Switching signal vector

$$\boldsymbol{s}_{\text{vsi}}^{abc} = \begin{pmatrix} \sigma\left(\frac{u_{\text{ref,svm}}^{a}}{u_{\text{dc}}/2} - u_{\text{car}}\right) \\ \sigma\left(\frac{u_{\text{ref,svm}}^{b}}{u_{\text{dc}}/2} - u_{\text{car}}\right) \\ \sigma\left(\frac{u_{\text{ref,svm}}^{c}}{u_{\text{dc}}/2} - u_{\text{car}}\right) \end{pmatrix}$$

with extended reference voltages

$$\boldsymbol{u}_{\text{ref,svm}}^{abc} := \boldsymbol{u}_{\text{ref}}^{abc} - \begin{pmatrix} \frac{\max(\boldsymbol{u}_{\text{ref}}^{abc})+\min(\boldsymbol{u}_{\text{ref}}^{abc})}{2} \\ \frac{\max(\boldsymbol{u}_{\text{ref}}^{abc})+\min(\boldsymbol{u}_{\text{ref}}^{abc})}{2} \\ \frac{\max(\boldsymbol{u}_{\text{ref}}^{abc})+\min(\boldsymbol{u}_{\text{ref}}^{abc})}{2} \end{pmatrix}$$

Nonlinear modelling: Two-level voltage source inverter (2L-VSI)

Modulation (example): Symmetrical PWM and averaged delay

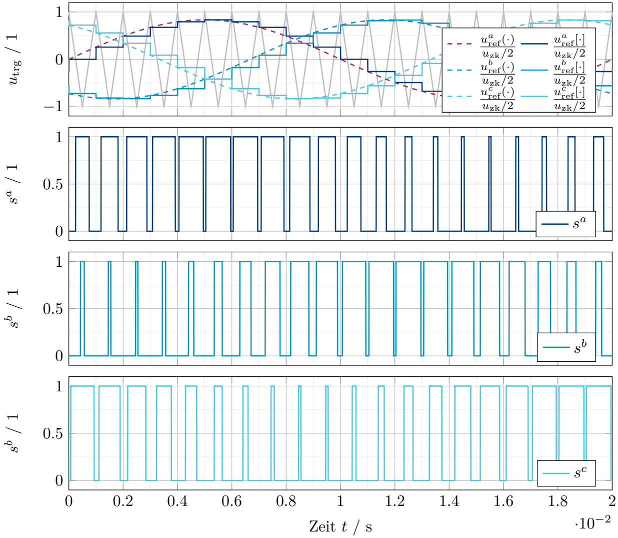

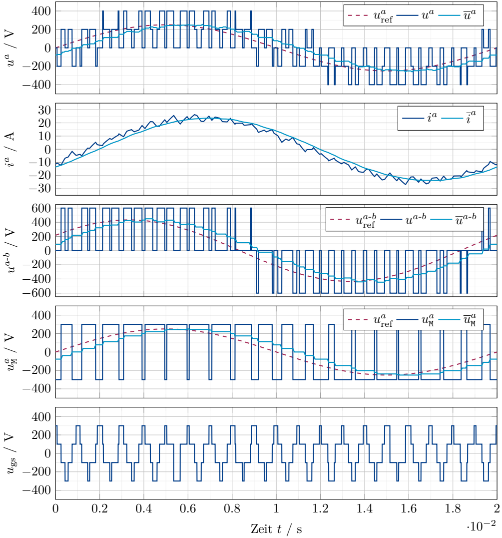

Outline

Nonlinear modelling: Two-level voltage source inverter (2L-VSI)

Dynamics and its approximation

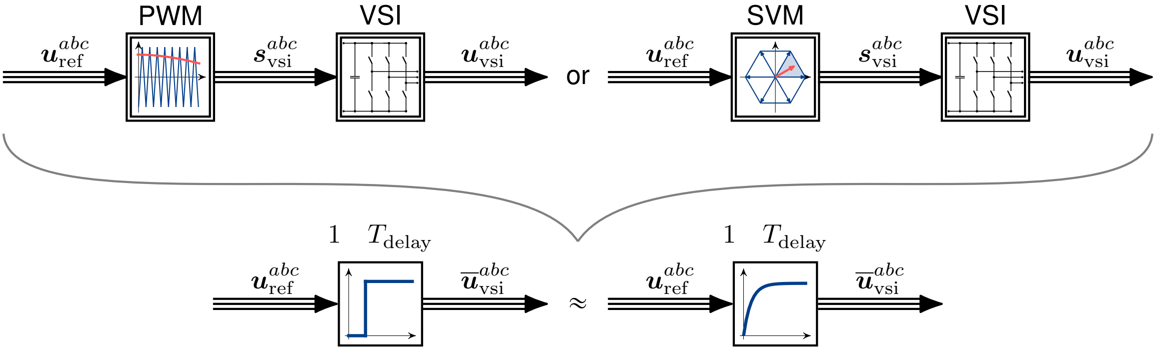

Delay depends on switching frequency $\frac{1}{T_{\mathrm{sw}}}$ and implementation of PWM or SVM:

$$T_{\mathrm{delay}} \propto T_{\mathrm{sw}} \quad \Longrightarrow \quad F_{\mathrm{vsi}}(s) := \frac{\overline{\boldsymbol{u}}_{\mathrm{vsi}}^{abc}(s)}{\boldsymbol{u}_{\mathrm{ref}}^{abc}(s)} = e^{-sT_{\mathrm{delay}}} \approx \frac{1}{1 + sT_{\mathrm{delay}}}$$

Outline

Nonlinear modelling: Electrical machine

Exemplary 2D-FEM design of Electrically-Excited Synchronous Machine (**EESM**) with damper windings

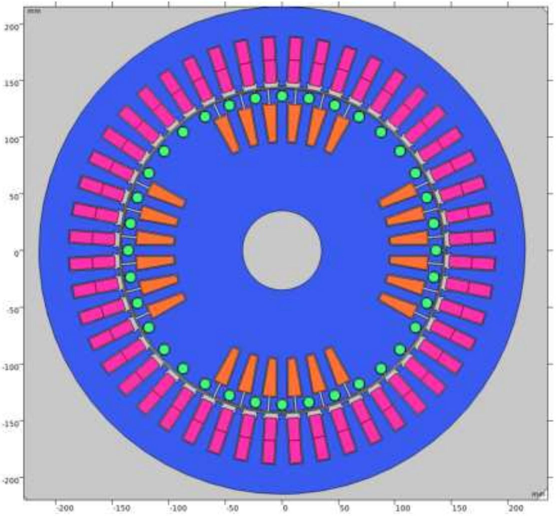

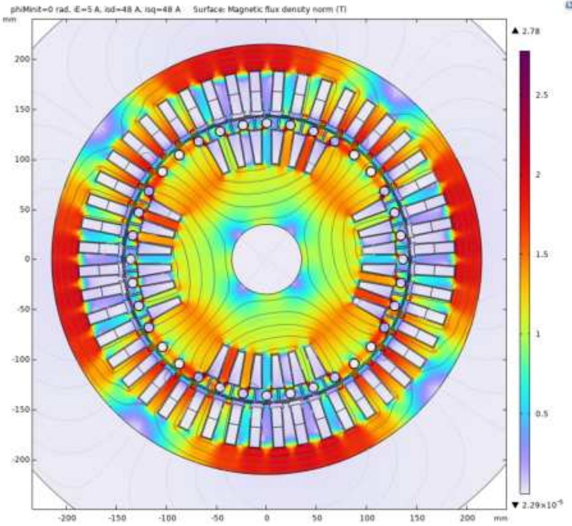

Outline

Nonlinear modelling: Electrical machine

Key equations: Dependencies for each winding of an electric machine (holds for transformer or rotatory machine)

Kirchhoff's voltage equation:

- single-phase: $u = R\,i + \frac{\mathrm{d}}{\mathrm{d}t}\psi \quad \iff \quad \frac{\mathrm{d}}{\mathrm{d}t}\psi = u - R\,i$
- three-phase: $\boldsymbol{u}_{\mathrm{z}}^{abc} = \boldsymbol{R}_{\mathrm{z}}^{abc}\boldsymbol{i}_{\mathrm{z}}^{abc} + \frac{\mathrm{d}}{\mathrm{d}t}\boldsymbol{\psi}_{\mathrm{z}}^{abc} \quad \iff \quad \frac{\mathrm{d}}{\mathrm{d}t}\boldsymbol{\psi}_{\mathrm{z}}^{abc} = \boldsymbol{u}_{\mathrm{z}}^{abc} - \boldsymbol{R}_{\mathrm{z}}^{abc}\boldsymbol{i}_{\mathrm{z}}^{abc}, \quad \mathrm{z} \in \{\mathrm{s}, \mathrm{Fe}, \mathrm{r}, \mathrm{e}, \dots\}$

where

- applied winding voltage u (arbitrary shape) or $\boldsymbol{u}_{\mathrm{z}}^{abc} := (u_{\mathrm{z}}^{a}, u_{\mathrm{z}}^{b}, u_{\mathrm{z}}^{c})^\top \in \mathbb{R}^3$
- winding current i (arbitrary shape) or $\boldsymbol{i}_{\mathrm{z}}^{abc} := (i_{\mathrm{z}}^{a}, i_{\mathrm{z}}^{b}, i_{\mathrm{z}}^{c})^\top \in \mathbb{R}^3$
- winding resistance $R := R(i, \phi, \omega, \vartheta, \dots)$ or $\boldsymbol{R}_{\mathrm{z}}^{abc} := \boldsymbol{R}_{\mathrm{z}}^{abc}(\boldsymbol{i}_{\mathrm{z}}^{abc}, \phi, \omega, \boldsymbol{\vartheta}_{\mathrm{z}}^{abc}, \dots) \in \mathbb{R}^{3\times 3}$
- flux linkage $\psi := \psi(i, \phi, \omega, \vartheta, \dots)$ or $\boldsymbol{\psi}_{\mathrm{z}}^{abc} := (\psi_{\mathrm{z}}^{a}, \psi_{\mathrm{z}}^{b}, \psi_{\mathrm{z}}^{c})^\top = \boldsymbol{\psi}_{\mathrm{z}}^{abc}(\boldsymbol{i}_{\mathrm{z}}^{abc}, \phi, \omega, \boldsymbol{\vartheta}_{\mathrm{z}}^{abc}, \dots) \in \mathbb{R}^3$

***Remark**: Resistance R and flux linkage ψ may depend on states $\boldsymbol{x} := (i, \phi, \omega, \vartheta, \dots)^\top \in \mathbb{R}^{N_{\boldsymbol{x}}}$ such as e.g. current(s) i, angle ϕ, angular frequency ω and temperature(s) ϑ to cover iron losses, magnetic saturation & cross-coupling, anisotropy, harmonics, proximity & skin effect, slip rings or winding asymmetries, etc.*

Outline

Nonlinear modelling: Electrical machine

Reference frames (considering of γ-component might be crucial [165])

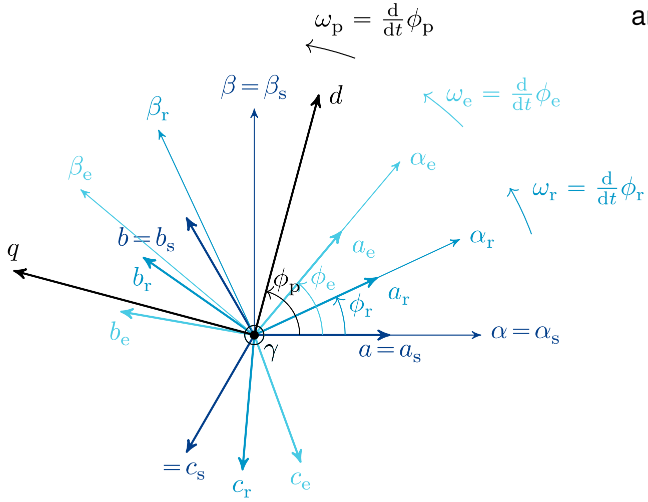

arbitrarily rotating (d, q, γ)-reference frame

excitor-fixed $(\alpha_e, \beta_e, \gamma)$-reference frame

rotor-fixed $(\alpha_r, \beta_r, \gamma)$-reference frame

stator-fixed (α, β, γ)-reference frame

Outline

4 Nonlinear modelling
- Motivation
- Two-level voltage source inverter (2L-VSI)
- Electrical machine
  - Key equations
  - Reference frames
  - Generic machine dynamics
  - Equivalent circuit

Nonlinear modelling: Electrical machine

Generic machine dynamics: Three-phase machine model (cross-sectional view; without iron losses)

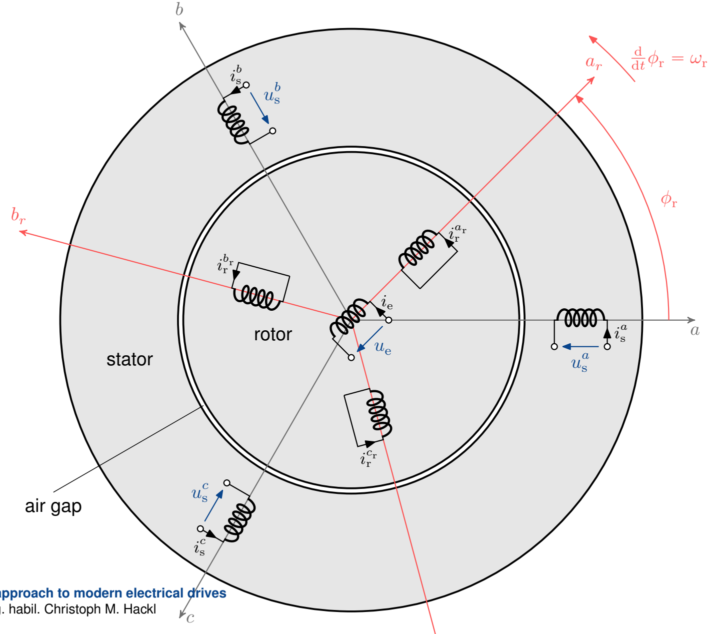

Nonlinear modelling: Electrical machine

Generic machine dynamics: Three-phase machine model in (a, b, c)-reference frame

$$
\left.
\begin{array}{llcl}
\text{Stator:} & \frac{\mathrm{d}}{\mathrm{d}t}\boldsymbol{\psi}_{\mathrm{s}}^{a_\mathrm{s}b_\mathrm{s}c_\mathrm{s}} & = & \boldsymbol{u}_{\mathrm{s}}^{a_\mathrm{s}b_\mathrm{s}c_\mathrm{s}} - \boldsymbol{R}_{\mathrm{s}}^{a_\mathrm{s}b_\mathrm{s}c_\mathrm{s}} \boldsymbol{i}_{\mathrm{s}}^{a_\mathrm{s}b_\mathrm{s}c_\mathrm{s}}, \\
\text{Stator iron:} & \frac{\mathrm{d}}{\mathrm{d}t}\boldsymbol{\psi}_{\mathrm{s,Fe}}^{a_\mathrm{s}b_\mathrm{s}c_\mathrm{s}} & = & - \boldsymbol{R}_{\mathrm{s,Fe}}^{a_\mathrm{s}b_\mathrm{s}c_\mathrm{s}} \boldsymbol{i}_{\mathrm{s,Fe}}^{a_\mathrm{s}b_\mathrm{s}c_\mathrm{s}}, \\
\text{Rotor:} & \frac{\mathrm{d}}{\mathrm{d}t}\boldsymbol{\psi}_{\mathrm{r}}^{a_\mathrm{r}b_\mathrm{r}c_\mathrm{r}} & = & \boldsymbol{u}_{\mathrm{r}}^{a_\mathrm{r}b_\mathrm{r}c_\mathrm{r}} - \boldsymbol{R}_{\mathrm{r}}^{a_\mathrm{r}b_\mathrm{r}c_\mathrm{r}} \boldsymbol{i}_{\mathrm{r}}^{a_\mathrm{r}b_\mathrm{r}c_\mathrm{r}}, \\
\text{Rotor iron:} & \frac{\mathrm{d}}{\mathrm{d}t}\boldsymbol{\psi}_{\mathrm{r,Fe}}^{a_\mathrm{r}b_\mathrm{r}c_\mathrm{r}} & = & - \boldsymbol{R}_{\mathrm{r,Fe}}^{a_\mathrm{r}b_\mathrm{r}c_\mathrm{r}} \boldsymbol{i}_{\mathrm{r}}^{a_\mathrm{r}b_\mathrm{r}c_\mathrm{r}}, \\
\text{Excitor:} & \frac{\mathrm{d}}{\mathrm{d}t}\boldsymbol{\psi}_{\mathrm{e}}^{a_\mathrm{e}b_\mathrm{e}c_\mathrm{e}} & = & \boldsymbol{u}_{\mathrm{e}}^{a_\mathrm{e}b_\mathrm{e}c_\mathrm{e}} - \boldsymbol{R}_{\mathrm{e}}^{a_\mathrm{e}b_\mathrm{e}c_\mathrm{e}} \boldsymbol{i}_{\mathrm{e}}^{a_\mathrm{e}b_\mathrm{e}c_\mathrm{e}}, \\
\text{Mechanical subsystem:} & \frac{\mathrm{d}}{\mathrm{d}t}\omega_{\mathrm{m}} & = & \frac{1}{\Theta_{\mathrm{m}}}\Big(m_{\mathrm{m}} - \mathfrak{F}\omega_{\mathrm{m}} + m_{\mathrm{l}}\Big) \\
 & \frac{\mathrm{d}}{\mathrm{d}t}\phi_{\mathrm{m}} & = & \omega_{\mathrm{m}}
\end{array}
\right\} \quad (1)
$$

with machine torque $m_{\mathrm{m}}(\boldsymbol{i}_{\mathrm{s}}^{a_\mathrm{s}b_\mathrm{s}c_\mathrm{s}}, \boldsymbol{i}_{\mathrm{s,Fe}}^{a_\mathrm{s}b_\mathrm{s}c_\mathrm{s}}, \boldsymbol{i}_{\mathrm{r}}^{a_\mathrm{r}b_\mathrm{r}c_\mathrm{r}}, \boldsymbol{i}_{\mathrm{r}}^{a_\mathrm{r}b_\mathrm{r}c_\mathrm{r}}, \boldsymbol{i}_{\mathrm{e}}^{a_\mathrm{e}b_\mathrm{e}c_\mathrm{e}}, \boldsymbol{\psi}_{\mathrm{pm}}^{a_\mathrm{r}b_\mathrm{r}c_\mathrm{r}}, \phi_{\mathrm{m}}, \dots)$.

Nonlinear modelling: Electrical machine

Generic machine dynamics: Three-phase machine model in (α, β, γ)-reference frame [after Clarke and (selected) Park transformations]

$$
\left.
\begin{array}{lrcll}
\text{Stator:} & \frac{\mathrm{d}}{\mathrm{d}t}\boldsymbol{\psi}_{\mathrm{s}}^{\alpha\beta\gamma} & = & \boldsymbol{u}_{\mathrm{s}}^{\alpha\beta\gamma} - \boldsymbol{R}_{\mathrm{s}}^{\alpha\beta\gamma}\boldsymbol{i}_{\mathrm{s}}^{\alpha\beta\gamma} & , \\
\text{Stator iron:} & \frac{\mathrm{d}}{\mathrm{d}t}\boldsymbol{\psi}_{\mathrm{s,Fe}}^{\alpha\beta\gamma} & = & - \boldsymbol{R}_{\mathrm{s,Fe}}^{\alpha\beta\gamma}\boldsymbol{i}_{\mathrm{s,Fe}}^{\alpha\beta\gamma} & , \\
\text{Rotor:} & \frac{\mathrm{d}}{\mathrm{d}t}\boldsymbol{\psi}_{\mathrm{r}}^{\alpha\beta\gamma} & = & \boldsymbol{u}_{\mathrm{r}}^{\alpha\beta\gamma} - \boldsymbol{R}_{\mathrm{r}}^{\alpha\beta\gamma}\boldsymbol{i}_{\mathrm{r}}^{\alpha\beta\gamma} & +\omega_{\mathrm{r}}\boldsymbol{J}_0\boldsymbol{\psi}_{\mathrm{r}}^{\alpha\beta\gamma}, \\
\text{Rotor iron:} & \frac{\mathrm{d}}{\mathrm{d}t}\boldsymbol{\psi}_{\mathrm{r,Fe}}^{\alpha\beta\gamma} & = & - \boldsymbol{R}_{\mathrm{r,Fe}}^{\alpha\beta\gamma}\boldsymbol{i}_{\mathrm{r,Fe}}^{\alpha\beta\gamma} & +\omega_{\mathrm{r}}\boldsymbol{J}_0\boldsymbol{\psi}_{\mathrm{r,Fe}}^{\alpha\beta\gamma}, \\
\text{Excitor:} & \frac{\mathrm{d}}{\mathrm{d}t}\boldsymbol{\psi}_{\mathrm{e}}^{\alpha\beta\gamma} & = & \boldsymbol{u}_{\mathrm{e}}^{\alpha\beta\gamma} - \boldsymbol{R}_{\mathrm{e}}^{\alpha\beta\gamma}\boldsymbol{i}_{\mathrm{e}}^{dq\gamma} & +\omega_{\mathrm{r}}\boldsymbol{J}_0\boldsymbol{\psi}_{\mathrm{e}}^{\alpha\beta\gamma}, \\
\text{Mechanical subsystem:} & \frac{\mathrm{d}}{\mathrm{d}t}\omega_{\mathrm{m}} & = & \frac{1}{\Theta_{\mathrm{m}}}\Big(m_{\mathrm{m}} - \mathfrak{F}\omega_{\mathrm{m}} + m_{\mathrm{l}}\Big) & \\
 & \frac{\mathrm{d}}{\mathrm{d}t}\phi_{\mathrm{m}} & = & \omega_{\mathrm{m}} &
\end{array}
\right\} \qquad (2)
$$

with machine torque $m_{\mathrm{m}}(\boldsymbol{i}_{\mathrm{s}}^{\alpha\beta\gamma}, \boldsymbol{i}_{\mathrm{s,Fe}}^{\alpha\beta\gamma}, \boldsymbol{i}_{\mathrm{r}}^{\alpha\beta\gamma}, \boldsymbol{i}_{\mathrm{r,Fe}}^{\alpha\beta\gamma}, \boldsymbol{i}_{\mathrm{e}}^{\alpha\beta\gamma}, \boldsymbol{\psi}_{\mathrm{pm}}^{\alpha\beta\gamma}, \phi_{\mathrm{m}}, \dots)$ and rotation matrix (by $\pi/2$)

$$
\boldsymbol{J}_0 := \begin{bmatrix} 0 & -1 & 0 \\ 1 & 0 & 0 \\ 0 & 0 & 0 \end{bmatrix}
$$

***Remark**: Please note that consideration of γ-component might be crucial to allow for e.g. currents including third-order harmonics as possibly present in delta-connected or grounded star-point configurations [165].*

Nonlinear modelling: Electrical machine

Generic machine dynamics: Three-phase machine model in (d,q,γ)-reference frame [after Clarke and (arbitrary) Park transformation]

$$
\left.
\begin{array}{lrcll}
\text{Stator:} & \frac{\mathrm{d}}{\mathrm{d}t}\boldsymbol{\psi}_{\mathrm{s}}^{dq\gamma} & = & \boldsymbol{u}_{\mathrm{s}}^{dq\gamma} - \boldsymbol{R}_{\mathrm{s}}^{dq\gamma}\boldsymbol{i}_{\mathrm{s}}^{dq\gamma} & -\omega_{\mathrm{p}}\boldsymbol{J}_0\boldsymbol{\psi}_{\mathrm{s}}^{dq\gamma}, \\
\text{Stator iron:} & \frac{\mathrm{d}}{\mathrm{d}t}\boldsymbol{\psi}_{\mathrm{s,Fe}}^{dq\gamma} & = & - \boldsymbol{R}_{\mathrm{s,Fe}}^{dq\gamma}\boldsymbol{i}_{\mathrm{s,Fe}}^{dq\gamma} & -\omega_{\mathrm{p}}\boldsymbol{J}_0\boldsymbol{\psi}_{\mathrm{s,Fe}}^{dq\gamma}, \\
\text{Rotor:} & \frac{\mathrm{d}}{\mathrm{d}t}\boldsymbol{\psi}_{\mathrm{r}}^{dq\gamma} & = & \boldsymbol{u}_{\mathrm{r}}^{dq\gamma} - \boldsymbol{R}_{\mathrm{r}}^{dq\gamma}\boldsymbol{i}_{\mathrm{r}}^{dq\gamma} & -(\omega_{\mathrm{p}}-\omega_{\mathrm{r}})\boldsymbol{J}_0\boldsymbol{\psi}_{\mathrm{r}}^{dq\gamma}, \\
\text{Rotor iron:} & \frac{\mathrm{d}}{\mathrm{d}t}\boldsymbol{\psi}_{\mathrm{r,Fe}}^{dq\gamma} & = & - \boldsymbol{R}_{\mathrm{r,Fe}}^{dq\gamma}\boldsymbol{i}_{\mathrm{r,Fe}}^{dq\gamma} & -(\omega_{\mathrm{p}}-\omega_{\mathrm{r}})\boldsymbol{J}_0\boldsymbol{\psi}_{\mathrm{r,Fe}}^{dq\gamma}, \\
\text{Excitor:} & \frac{\mathrm{d}}{\mathrm{d}t}\boldsymbol{\psi}_{\mathrm{e}}^{dq\gamma} & = & \boldsymbol{u}_{\mathrm{e}}^{dq\gamma} - \boldsymbol{R}_{\mathrm{e}}^{dq\gamma}\boldsymbol{i}_{\mathrm{e}}^{dq\gamma} & -(\omega_{\mathrm{p}}-\omega_{\mathrm{e}})\boldsymbol{J}_0\boldsymbol{\psi}_{\mathrm{e}}^{dq\gamma}, \\
\text{Mechanical subsystem:} & \frac{\mathrm{d}}{\mathrm{d}t}\omega_{\mathrm{m}} & = & \frac{1}{\Theta_{\mathrm{m}}}\Big(m_{\mathrm{m}} - \mathfrak{F}\omega_{\mathrm{m}} + m_{\mathrm{l}}\Big) & \\
 & \frac{\mathrm{d}}{\mathrm{d}t}\phi_{\mathrm{m}} & = & \omega_{\mathrm{m}} &
\end{array}
\right\} \tag{3}
$$

with machine torque $m_{\mathrm{m}}(\boldsymbol{i}_{\mathrm{s}}^{dq\gamma}, \boldsymbol{i}_{\mathrm{s,Fe}}^{dq\gamma}, \boldsymbol{i}_{\mathrm{r}}^{dq\gamma}, \boldsymbol{i}_{\mathrm{r,Fe}}^{dq\gamma}, \boldsymbol{i}_{\mathrm{e}}^{dq\gamma}, \boldsymbol{\psi}_{\mathrm{pm}}^{dq\gamma}, \phi_{\mathrm{m}}, \dots)$ and rotation matrix (by $\pi/2$)

$$\boldsymbol{J}_0 := \begin{bmatrix} 0 & -1 & 0 \\ 1 & 0 & 0 \\ 0 & 0 & 0 \end{bmatrix}$$

***Remark**: Please note that consideration of γ-component might be crucial to allow for e.g. currents including third-order harmonics as possibly present in delta-connected or grounded star-point configurations [165].*

Outline

Nonlinear modelling: Electrical machine

Equivalent circuit of generic three-phase machine model in (d, q, γ)-reference frame

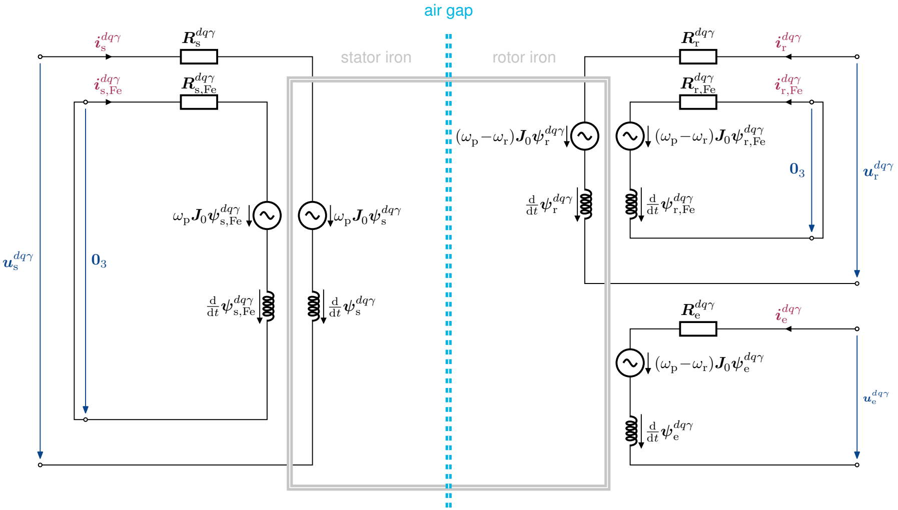

Outline

Outline

Dynamic simulation: Electrical machine dynamics

Possible implementations of electrical dynamics in (d, q, γ)-reference frame [for simplicity: only considering stator currents]

- Flux linkage dynamics with inverse interpolation $\boldsymbol{i}_{\mathrm{s}}^{dq\gamma} = \boldsymbol{f}_{\psi}^{-1}(\boldsymbol{\psi}_{\mathrm{s}}^{dq\gamma}, \ldots)$

$$\frac{\mathrm{d}}{\mathrm{d}t}\boldsymbol{\psi}_{\mathrm{s}}^{dq\gamma} = \boldsymbol{u}_{\mathrm{s}}^{dq\gamma} - \boldsymbol{R}_{\mathrm{s}}^{dq\gamma}\boldsymbol{i}_{\mathrm{s}}^{dq\gamma} - \omega_{\mathrm{p}}\boldsymbol{J}_0\boldsymbol{\psi}_{\mathrm{s}}^{dq\gamma} \tag{4}$$

- Current dynamics with differential inductances and flux linkages

$$\frac{\mathrm{d}}{\mathrm{d}t}\boldsymbol{i}_{\mathrm{s}}^{dq\gamma} = (\boldsymbol{L}_{\mathrm{s}}^{dq\gamma})^{-1}\Big(\boldsymbol{u}_{\mathrm{s}}^{dq\gamma} - \boldsymbol{R}_{\mathrm{s}}^{dq\gamma}\boldsymbol{i}_{\mathrm{s}}^{dq\gamma} - \omega_{\mathrm{p}}\boldsymbol{J}_0\boldsymbol{\psi}_{\mathrm{s}}^{dq\gamma} + \underbrace{\frac{\partial\boldsymbol{\psi}_{\mathrm{s}}^{dq\gamma}}{\partial\phi_{\mathrm{m}}}\omega_{\mathrm{m}} + \frac{\partial\boldsymbol{\psi}_{\mathrm{s}}^{dq\gamma}}{\partial\vartheta}\frac{\mathrm{d}}{\mathrm{d}t}\vartheta + \ldots}_{=:\boldsymbol{\delta}_{\mathrm{s}}^{dq\gamma}}\Big) \tag{5}$$

- Current dynamics with differential and apparent inductances and permanent-magnet flux linkages

$$\frac{\mathrm{d}}{\mathrm{d}t}\boldsymbol{i}_{\mathrm{s}}^{dq\gamma} = (\boldsymbol{L}_{\mathrm{s}}^{dq\gamma})^{-1}\Big(\boldsymbol{u}_{\mathrm{s}}^{dq\gamma} - \boldsymbol{R}_{\mathrm{s}}^{dq\gamma}\boldsymbol{i}_{\mathrm{s}}^{dq\gamma} - \omega_{\mathrm{p}}\boldsymbol{J}_0(\boldsymbol{L}_{\mathrm{s,app}}^{dq\gamma}\boldsymbol{i}_{\mathrm{s}}^{dq\gamma} + \boldsymbol{\psi}_{\mathrm{pm}}^{dq\gamma}) + \boldsymbol{\delta}_{\mathrm{s}}^{dq\gamma}\Big) \tag{6}$$

Remark: *Important to note that* $\boldsymbol{L}_{\mathrm{s}}^{dq\gamma} := \frac{\mathrm{d}\boldsymbol{\psi}_{\mathrm{s}}^{dq\gamma}}{\mathrm{d}\boldsymbol{i}_{\mathrm{s}}^{dq\gamma}} \neq \boldsymbol{L}_{\mathrm{s,app}}^{dq\gamma} := \frac{\boldsymbol{\psi}_{\mathrm{s}}^{dq\gamma}(\boldsymbol{i}_{\mathrm{s}}^{dq\gamma},\ldots) - \boldsymbol{\psi}_{\mathrm{s}}^{dq\gamma}(\boldsymbol{0}_3,\ldots)}{\boldsymbol{i}_{\mathrm{s}}^{dq\gamma}}$

Dynamic simulation: Electrical machine dynamics

Crucial distinction: Illustration of differential inductance L (tangent) and apparent inductance L_{app} (secant)

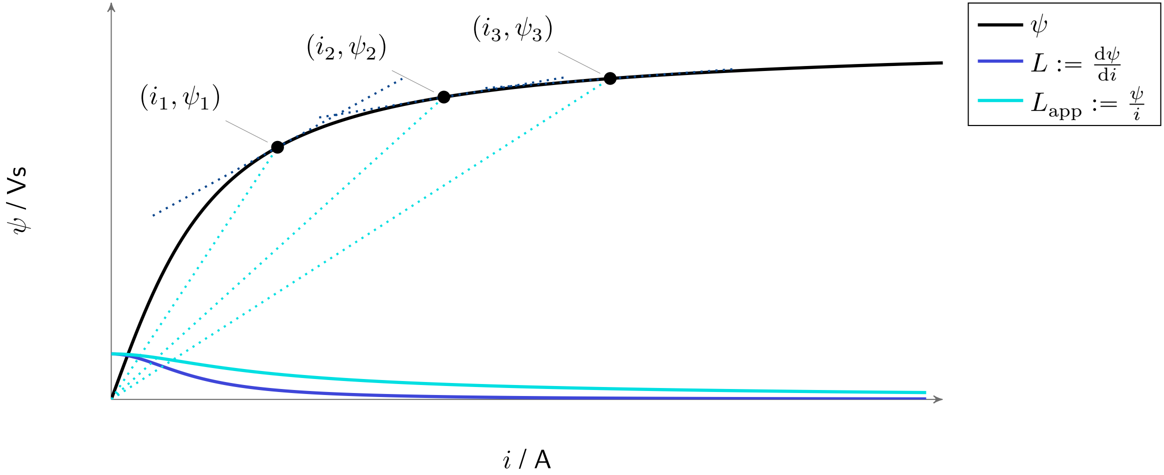

Outline

5 Dynamic simulation
- Electrical machine dynamics
- Block diagrams
- Required system knowledge
- Exemplary implementation results

Dynamic simulation: Block diagrams

Flux Linkage Dynamics with Inverse Interpolation (**FLD+II**)

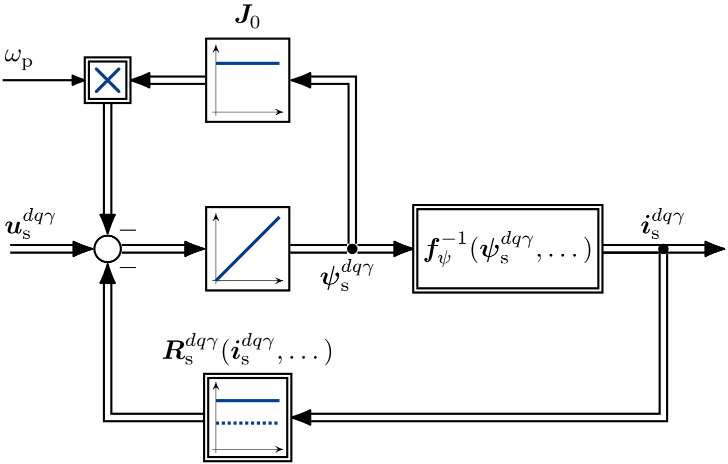

Dynamic simulation: Block diagrams

Current Dynamics with Differential Inductances and Flux Linkages (**CD+DI&FL**)

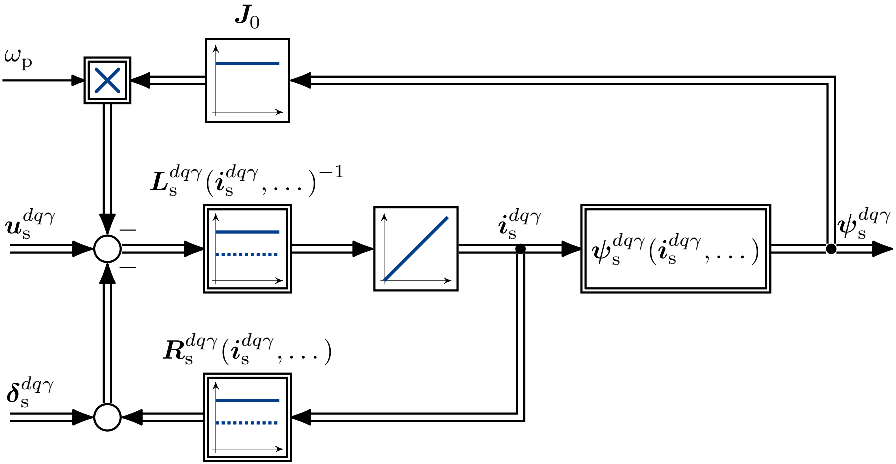

Dynamic simulation: Block diagrams

Current Dynamics with Differential/Apparent Inductances & Permanent-Magnet Flux Linkages (**CD+DAI&PMFL**)

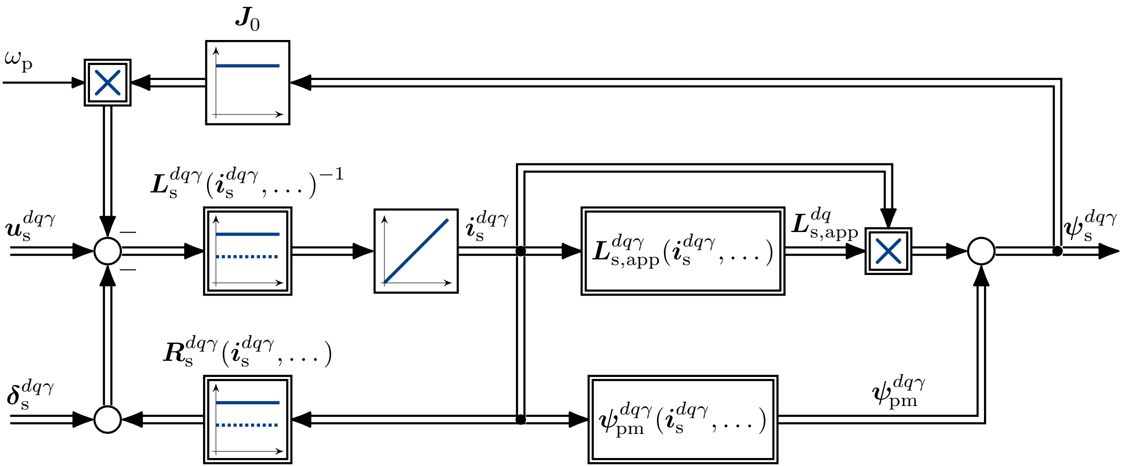

Outline

Dynamic simulation: Required system knowledge

Required system data and execution times for high-fidelity simulation of different dynamics implementations

	FLD+II	CD+DI&FL	CD+DAI&PMFL
$\boldsymbol{R}_{\mathrm{s}}^{dq(\gamma)}(\boldsymbol{x})$	$3\ (+0) \times N_{\boldsymbol{x}}$-D–LUTs	$3\ (+0) \times N_{\boldsymbol{x}}$-D–LUTs	$3\ (+0) \times N_{\boldsymbol{x}}$-D–LUTs
$\boldsymbol{L}_{\mathrm{s}}^{dq(\gamma)}(\boldsymbol{x})$	–	$3\ (+3) \times N_{\boldsymbol{x}}$-D–LUTs	$3\ (+3) \times N_{\boldsymbol{x}}$-D–LUTs
$\boldsymbol{L}_{\mathrm{s,app}}^{dq(\gamma)}(\boldsymbol{x})$	–	–	$2\ (+1) \times N_{\boldsymbol{x}}$-D–LUTs
$\boldsymbol{\psi}_{\mathrm{pm}}^{dq(\gamma)}(\boldsymbol{x})$	–	–	$2\ (+1) \times N_{\boldsymbol{x}}$-D–LUTs
$\boldsymbol{\psi}_{\mathrm{s}}^{dq(\gamma)}$	$2\ (+1) \times N_{\boldsymbol{x}}$-D–LUTs	$2\ (+1) \times N_{\boldsymbol{x}}$-D–LUTs	–
$\boldsymbol{f}_{\psi}(\cdot)^{-1}$	yes	no	no
t_{exec} (in p.u.)	$1.00^{\star}$ / $1.07^{\dagger}$ / $2.55^{\ddagger}$	1.55	1.83

***Remark**: The states $\boldsymbol{x} := (\boldsymbol{i}_{\mathrm{x}}^{abc}, \phi_{\mathrm{m}}, \phi_{\mathrm{p}}, \omega_{\mathrm{m}}, \omega_{\mathrm{p}}, \boldsymbol{\vartheta}_{\mathrm{x}}^{abc}, \dots)^{\top} \in \mathbb{R}^{N_{\boldsymbol{x}}}$ comprise currents, machine and/or transformation angles, machine and/or transformation angular frequencies and temperatures to allow for proper simulation/emulation of iron losses, magnetic saturation and cross-coupling, anisotropy, proximity and/or skin effect, slip rings or winding asymmetries, etc.; $N_{\boldsymbol{x}}$ represents the dimension of the considered states. *: Bilinear Inversion (reference as fastest), †: pre-processed LUTs for inverse interpolation of flux*

☞ **LMRES (HM) is working with several academic/industrial partners on fast, accurate and overall machine identification approaches in order to allow for even more sophisticated machine simulation and/or emulation.**

Dynamic simulation: Required system knowledge

Examples of identified stator/permanent-magnet flux linkages, differential/apparent inductances and back-emf harmonics

	$\psi_s^{dq}(i_s^{dq})$	$L_s^{dq}(i_s^{dq})$	$\psi_{pm}^{dq}(i_s^{dq})$	$L_{s,app}^{dq}(i_s^{dq})$	$\delta_s^{dq\gamma} = \frac{\partial \psi_s^{dq\gamma}}{\partial \phi_m}\omega_m$
d	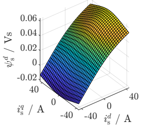	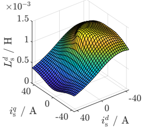	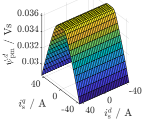	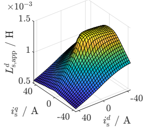	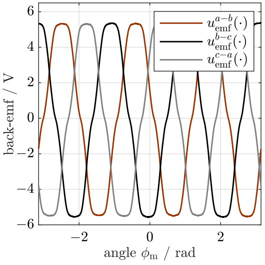
q	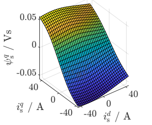	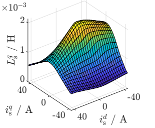	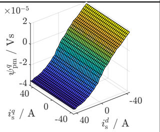	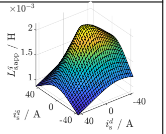	
dq/qd	–	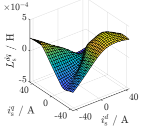	–	–	

Remark: *For simplicity, only the dependencies on* $i_s^{dq} := (i_s^d, i_s^q)^\top$ *are shown, i.e.* $x := (i_s^d, i_s^q)^\top$ *with* $N_x = 2$.

Outline

Dynamic simulation: Exemplary implementation results

Open-loop current responses for diff. dynamics implementations (3.8 kW IPMSM @ $\omega_{\mathrm{m,R}} = 576\ \frac{\text{rad}}{\text{s}}$):

[——] FLD+II (bil. Inv.), [——] CD+DI&FL, [——] CD+DAI&FL, [——] CD+DAI&FL ($\boldsymbol{L}_{\mathrm{s}}^{dq} = \boldsymbol{L}_{\mathrm{s,app}}^{dq}$; wrong implement.!)

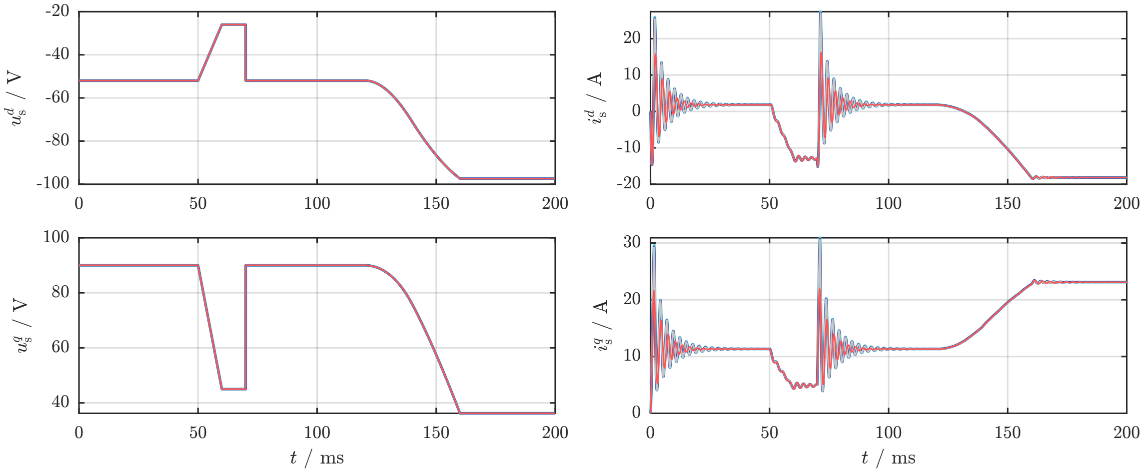

Dynamic simulation: Exemplary implementation results

Comparison of closed-loop nonlinear electrical drive system ($4.0\,$kW RSM @ $\omega_{\mathrm{m}} \approx 80\,\frac{\mathrm{rad}}{\mathrm{s}}$):
[——] simulation (CD+DI&FL), [——] measurement

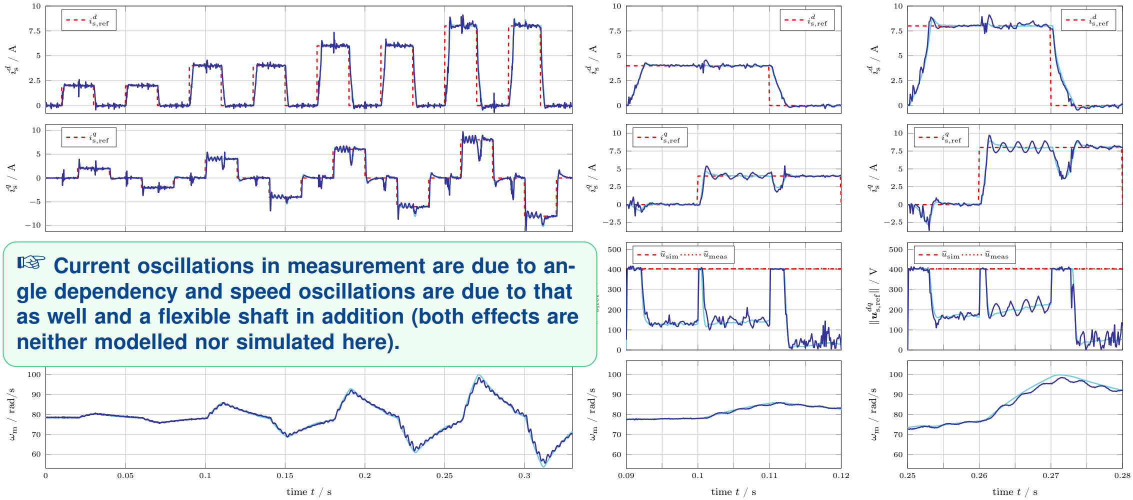

☞ **Current oscillations in measurement are due to angle dependency and speed oscillations are due to that as well and a flexible shaft in addition (both effects are neither modelled nor simulated here).**

Dynamic simulation: Exemplary implementation results

Flux Linkage Prototype Functions (**FLPFs**) [25] – Analytic functions for flux linkage representation

$\psi_{\mathrm{s}}^{d/q}$ of typ. RSM

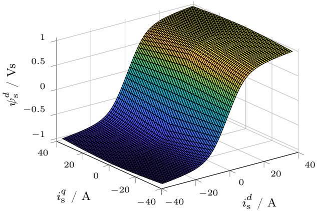

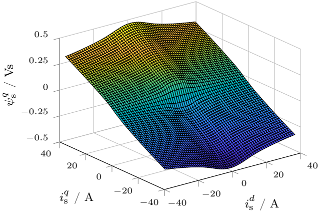

$\psi_{\mathrm{s}}^{d/q}$ of typ. IPMSM

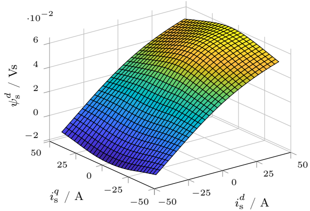

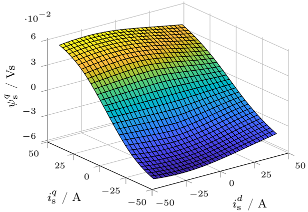

General FLPF idea

$$\widehat{\psi}_{\mathrm{s}}^{d}(i_{\mathrm{s}}^{d}, i_{\mathrm{s}}^{q}) = \widehat{\psi}_{\mathrm{s,self}}^{d}(i_{\mathrm{s}}^{d}) - \widehat{\psi}_{\mathrm{s,cross}}^{d}(i_{\mathrm{s}}^{d}, i_{\mathrm{s}}^{q})$$

$$\widehat{\psi}_{\mathrm{s}}^{q}(i_{\mathrm{s}}^{d}, i_{\mathrm{s}}^{q}) = \widehat{\psi}_{\mathrm{s,self}}^{q}(i_{\mathrm{s}}^{d}) - \widehat{\psi}_{\mathrm{s,cross}}^{q}(i_{\mathrm{s}}^{d}, i_{\mathrm{s}}^{q})$$

Dynamic simulation: Exemplary implementation results

Flux Linkage Prototype Functions (**FLPFs**) [25] – Observation for self-axis effects ($9.6\,$kW RSM)

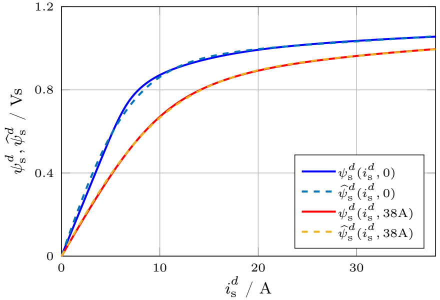

(a) d-axis flux linkage ψ_s^d v.s. d-axis current i_s^d

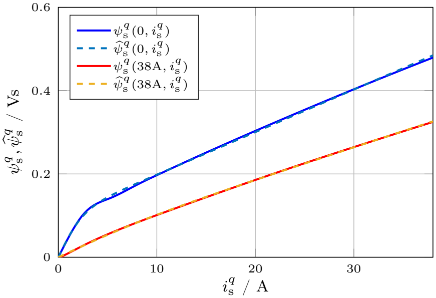

(b) q-axis flux linkage ψ_s^q v.s. q-axis current i_s^q

e.g., $\widehat{\psi}_{s,\text{self}}^{d,q}(i_s^d) \propto \tanh(i_s^{d/q}) + i_s^{d/q}$

Dynamic simulation: Exemplary implementation results

Flux Linkage Prototype Functions (**FLPFs**) [25] – Observation for cross-coupling effects ($9.6\,$kW RSM)

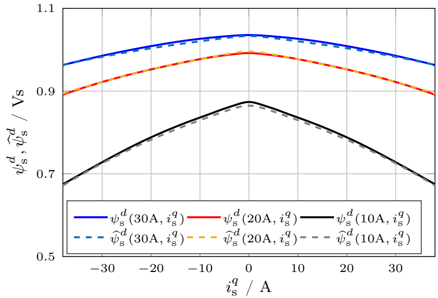

(a) d-axis flux linkage ψ_s^d v.s. q-axis current i_s^q

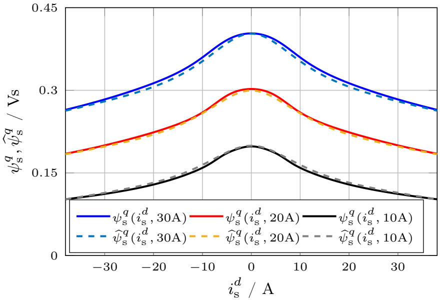

(b) q-axis flux linkage ψ_s^q v.s. d-axis current i_s^d

e.g., $\widehat{\psi}^{d/q}_{s,\mathrm{cross}} \propto -\ln\big(\cosh(i_s^{d/q})\big)$ or $\widehat{\psi}^{d/q}_{s,\mathrm{cross}} \propto \exp\big(-(i_s^{d/q})^2\big)$

Dynamic simulation: Exemplary implementation results

Flux Linkage Prototype Functions (**FLPFs**) [25] – Estimation accuracy & properties ($9.6\,$kW RSM)

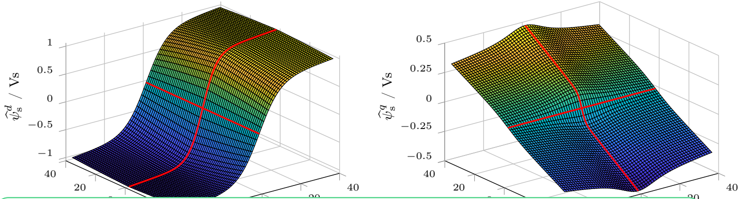

☞ **Flux linkage prototype functions (FLPFs) can also be used for self-commissioning [166] or in the framework of Artificial Neuronal Networks (ANNs) to identify inverter and machine simultaneously [138].**

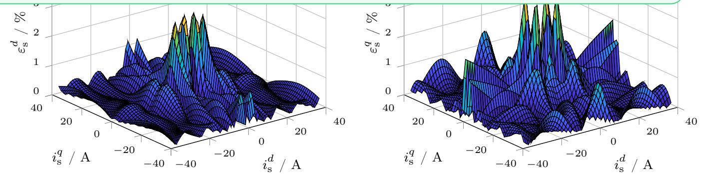

- **Flux linkages** approximated by FLPFs $\widehat{\psi}_{\mathrm{s}}^{d}(i_{\mathrm{s}}^{d}, i_{\mathrm{s}}^{q})$ & $\widehat{\psi}_{\mathrm{s}}^{q}(i_{\mathrm{s}}^{d}, i_{\mathrm{s}}^{q})$ with high accuracy (usually $\geqslant 95\%$)
- **Energy conservation** assured, i.e. $\frac{\partial \widehat{\psi}_{\mathrm{s}}^{d}(i_{\mathrm{s}}^{d}, i_{\mathrm{s}}^{q})}{\partial i_{\mathrm{s}}^{q}} = \frac{\partial \widehat{\psi}_{\mathrm{s}}^{q}(i_{\mathrm{s}}^{d}, i_{\mathrm{s}}^{q})}{\partial i_{\mathrm{s}}^{d}}$ (reciprocity)
- **Few parameters** to be fitted (only $10 \sim 20$ parameters needed)
- **Differentiability** allows to derive differential inductances analytically
- **Inter-/extrapolation capability** due to analytical function evaluation (no numerical inaccuracies or oscillations)
- **Extensibility** ensures applicability to different SMs (e.g., RSMs, IPMSMs or even EESMs)

Dynamic simulation: Exemplary implementation results

Active Harmonics Suppression (**AHS**) in $2.6\,$kW BLDC machine (compensating for $\boldsymbol{\delta}_{\mathrm{s}}^{dq\gamma} = \frac{\partial \boldsymbol{\psi}_{\mathrm{s}}^{dq\gamma}}{\partial \phi_{\mathrm{m}}} \omega_{\mathrm{m}}$)

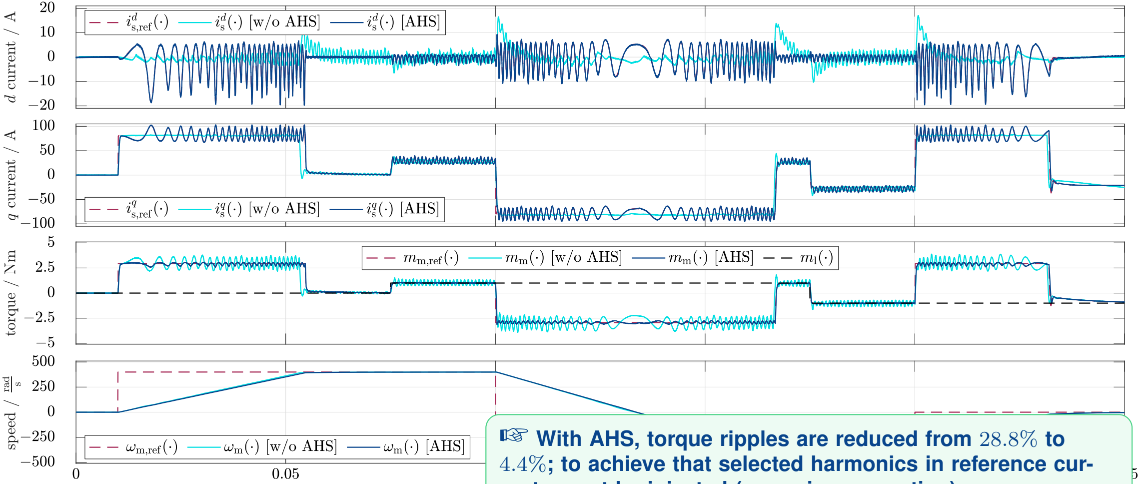

☞ **With AHS, torque ripples are reduced from 28.8% to 4.4%; to achieve that selected harmonics in reference currents must be injected (paper in preparation).**

Outline

Outline

High-performance control

Overview

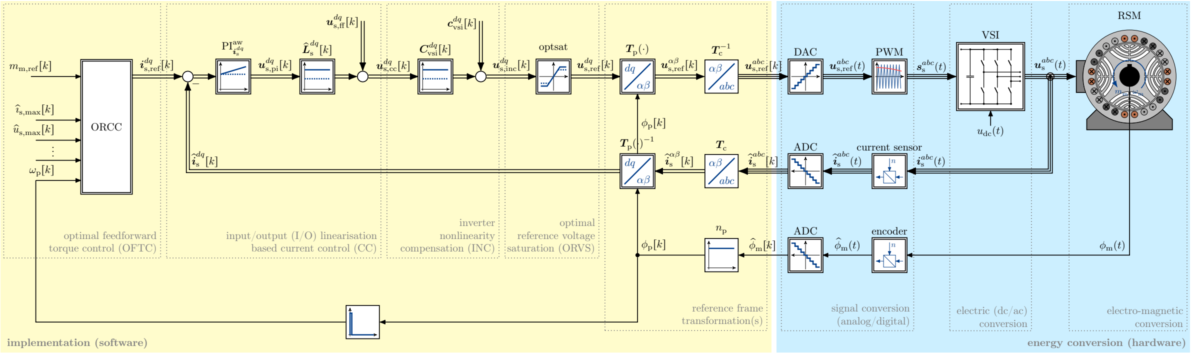

Outline

Outline

High-performance control: Nonlinear current control

Controller structure of input/output (I/O) linearization based nonlinear current control system

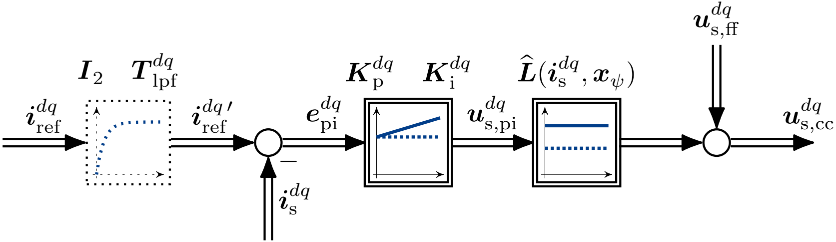

Nonlinear (vector-valued) PI controller

$$
\begin{aligned}
\boldsymbol{u}_{\mathrm{s,cc}}^{dq} &= \overbrace{\boldsymbol{K}_{\mathrm{p}}^{dq}\boldsymbol{e}_{\mathrm{pi}}^{dq} + \boldsymbol{K}_{\mathrm{i}}^{dq}\boldsymbol{x}_{\mathrm{i}}^{dq}}^{=:\boldsymbol{u}_{\mathrm{s,pi}}^{dq}} + \overbrace{\widehat{\boldsymbol{R}}_{\mathrm{s}}^{dq}\boldsymbol{i}_{\mathrm{s}}^{dq} + \omega_{\mathrm{p}}\boldsymbol{J}\widehat{\boldsymbol{\psi}}_{\mathrm{s}}^{dq} + \widehat{\boldsymbol{\delta}}_{\mathrm{s}}^{dq}}^{=:\boldsymbol{u}_{\mathrm{s,ff}}^{dq}}, \\
\frac{\mathrm{d}}{\mathrm{d}t}\boldsymbol{x}_{\mathrm{i}}^{dq} &= f_{\mathrm{aw}}\left(\widehat{u}_{\mathrm{s,max}}, \boldsymbol{u}_{\mathrm{s,ref}}^{dq}\right)\boldsymbol{e}_{\mathrm{pi}}^{dq}
\end{aligned}
$$

with feedforward term $\boldsymbol{u}_{\mathrm{s,ff}}^{dq}$ and integral state $\boldsymbol{x}_{\mathrm{i}}^{dq}$, gain matrices $\boldsymbol{K}_{\mathrm{p}}^{dq} := \mathrm{diag}(k_{\mathrm{p}}^{d}, k_{\mathrm{p}}^{q})$ and $\boldsymbol{K}_{\mathrm{i}}^{dq} := \mathrm{diag}(k_{\mathrm{i}}^{d}, k_{\mathrm{i}}^{q})$ and anti-windup (“conditional integration”) with

$$
f_{\mathrm{aw}}\left(\widehat{u}_{\mathrm{s,max}}, \boldsymbol{u}_{\mathrm{s,ref}}^{dq}\right) = \begin{cases} 0, & \text{if } \|\boldsymbol{u}_{\mathrm{s,ref}}^{dq}\| > \widehat{u}_{\mathrm{s,max}}, \\ 1, & \text{else.} \end{cases}
$$

Outline

High-performance control: Nonlinear current control

Principle idea of I/O linearization (ideal conditions, i.e., $\boldsymbol{u}_{\mathrm{s,cc}}^{dq} = \boldsymbol{u}_{\mathrm{s}}^{dq}$, $\widehat{\boldsymbol{R}}_{\mathrm{s}}^{dq} = \boldsymbol{R}_{\mathrm{s}}^{dq}$, $\widehat{\boldsymbol{L}}_{\mathrm{s}}^{dq} = \boldsymbol{L}_{\mathrm{s}}^{dq}$ and $\widehat{\boldsymbol{\delta}}_{\mathrm{s}}^{dq} = \boldsymbol{\delta}_{\mathrm{s}}^{dq}$)

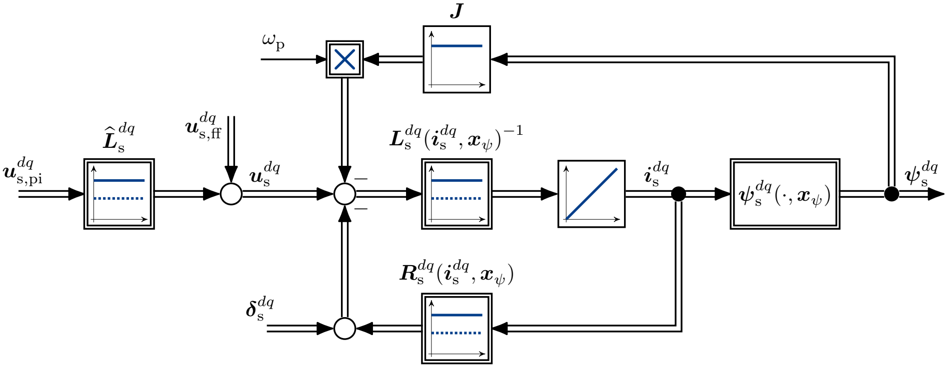

$$\frac{\mathrm{d}}{\mathrm{d}t}\boldsymbol{i}_{\mathrm{s}}^{dq} = (\boldsymbol{L}_{\mathrm{s}}^{dq})^{-1}\Big[\underbrace{\widehat{\boldsymbol{L}}_{\mathrm{s}}^{dq}\boldsymbol{u}_{\mathrm{s,pi}}^{dq} + \overbrace{\boldsymbol{R}_{\mathrm{s}}^{dq}\boldsymbol{i}_{\mathrm{s}}^{dq} + \omega_{\mathrm{p}}\boldsymbol{J}\boldsymbol{\psi}_{\mathrm{s}}^{dq} + \boldsymbol{\delta}_{\mathrm{s}}^{dq}}^{=:\boldsymbol{u}_{\mathrm{s,ff}}^{dq}}}_{\boldsymbol{u}_{\mathrm{s,cc}}^{dq} \approx \boldsymbol{u}_{\mathrm{s}}^{dq}} - \boldsymbol{R}_{\mathrm{s}}^{dq}\boldsymbol{i}_{\mathrm{s}}^{dq} - \omega_{\mathrm{p}}\boldsymbol{J}\boldsymbol{\psi}_{\mathrm{s}}^{dq} - \boldsymbol{\delta}_{\mathrm{s}}^{dq}\Big] = \boldsymbol{u}_{\mathrm{s,pi}}^{dq}$$

Outline

High-performance control: Nonlinear current control

Closed-loop system with reference current filter (after ideal I/O-linearization and without anti-windup)

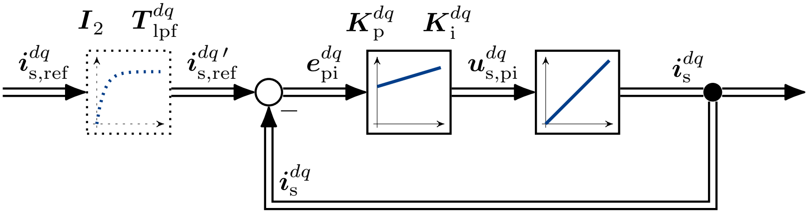

Reference current filter (optional; set $\boldsymbol{T}_{\mathrm{lpf}}^{dq} = \mathrm{diag}(T_{\mathrm{lpf}}^{d}, T_{\mathrm{lpf}}^{q}) = \boldsymbol{O}_{2\times 2}$ if not used)

$$F_{\mathrm{lpf}}(s) = \frac{i_{\mathrm{s,ref}}^{d/q\,\prime}}{i_{\mathrm{s,ref}}^{d/q}} = \frac{1}{1 + s\,T_{\mathrm{lpf}}^{d/q}} \quad \text{with} \quad T_{\mathrm{lpf}}^{d/q} := \frac{k_{\mathrm{p}}^{d/q}}{k_{\mathrm{i}}^{d/q}}$$

Current closed-loop system (neglecting anti-windup)

$$F_{\mathrm{cl}}(s) = \frac{i_{\mathrm{s}}^{d/q}}{i_{\mathrm{s,ref}}^{d/q}} = \frac{k_{\mathrm{p}}^{d/q}\,s + k_{\mathrm{q}}^{d/q}}{s^2 + k_{\mathrm{p}}^{d/q}\,s + k_{\mathrm{q}}^{d/q}} = \frac{1 + \frac{k_{\mathrm{p}}^{d/q}}{k_{\mathrm{i}}^{d/q}}\,s}{1 + \frac{k_{\mathrm{p}}^{d/q}}{k_{\mathrm{i}}^{d/q}}\,s + \frac{1}{k_{\mathrm{i}}^{d/q}}\,s^2}$$

Outline

High-performance control: Nonlinear current control

Controller tuning via pole placement

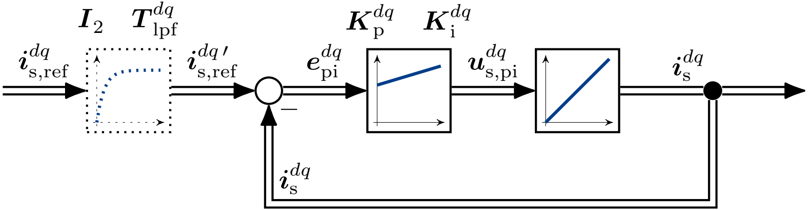

Pole placement by comparing coefficients (separately for d & q possible!)

$$\chi_{\mathrm{ref}}^{d/q}(s) := s^2 + 2D^{d/q}\omega_0^{d/q}\, s + 1 \stackrel{!}{=} s^2 + k_{\mathrm{p}}^{d/q}\, s + k_{\mathrm{q}}^{d/q} =: \chi_{\mathrm{cl}}^{d/q}(s)$$

Obtained controller parameters (for given bandwidth $\omega_0^{d/q}$ and damping D^{dq})

$$\Longrightarrow \quad k_{\mathrm{p}}^{d/q} = 2D^{d/q}\omega_0^{d/q} \quad \text{and} \quad k_{\mathrm{i}}^{d/q} = \left(\omega_0^{d/q}\right)^2$$

Outline

High-performance control: Nonlinear current control

Vector-valued PI controller with anti-windup (conditional integration)

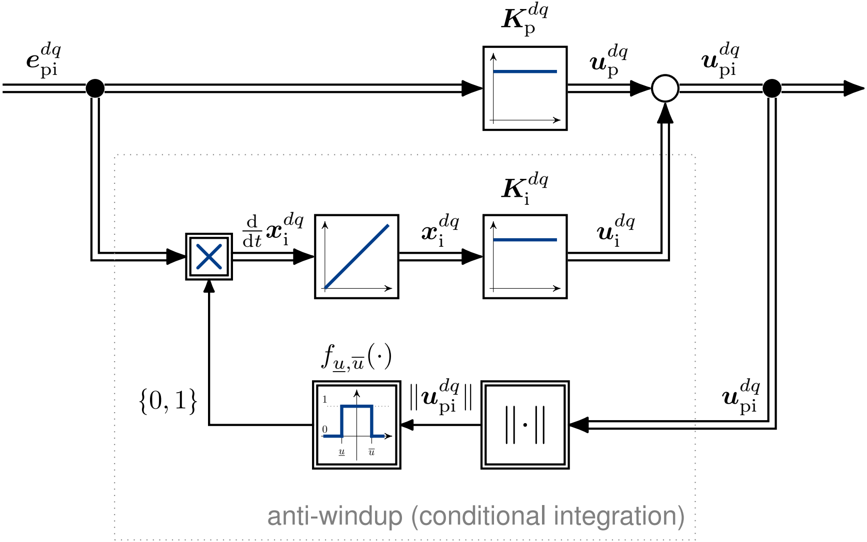

Outline

6 High-performance control

Outline

6 High-performance control

- Overview
- Nonlinear current control
- Inverter nonlinearity compensation
  - Problem statement
  - Nonlinear voltage drops
  - Average model
  - Dead-time effects
  - Transformation to (d, q)-reference frame
  - Validation
- Optimal reference voltage saturation

High-performance control

Inverter nonlinearity compensation: Overview

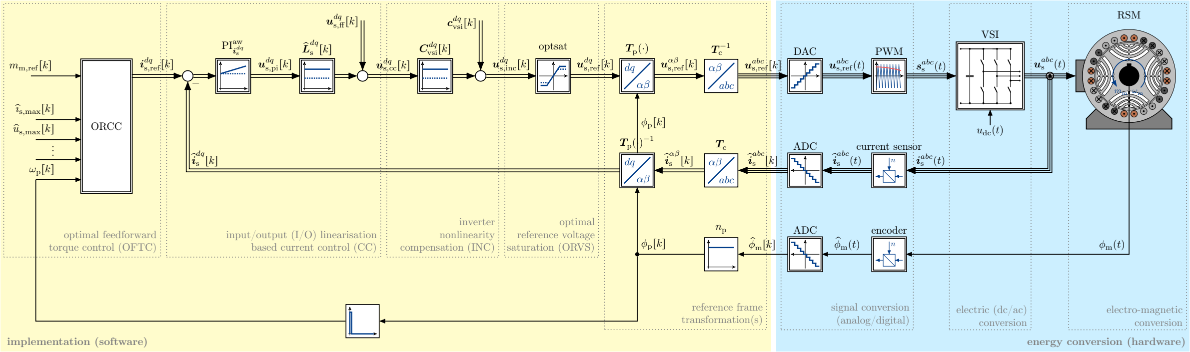

High-performance control: Inverter nonlinearity compensation

Problem statement: Drawbacks of voltage source inverters

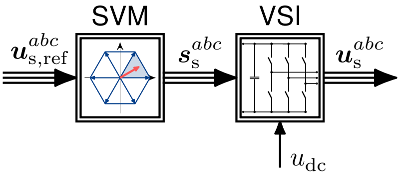

Any voltage source inverter (VSI) suffers from *four* inevitable drawbacks (D$_i$):

(D$_1$) voltage deterioration due to nonlinear current-dependent voltage drops over semiconductors [167],

(D$_2$) voltage ripples due to the switching behavior of the power electronic devices [168],

(D$_3$) delayed voltage response due to modulation [169], and

(D$_4$) output voltage constraints due to a limited dc-link voltage.

$\Longrightarrow$ Here we will discuss and solve the first and third problem! For each drawback, several improvements or compensation strategies exist. This subsection focuses on the first and third drawback and its impact, in particular, on the output voltage by the inverter nonlinearity which leads to a deteriorates from the desired VSI voltage. The second drawback can be tackled by optimal pulse pattern and/or increased switching frequency [117, 128, 129].

Outline

High-performance control: Inverter nonlinearity compensation

Nonlinear voltage drops in a half-bridge

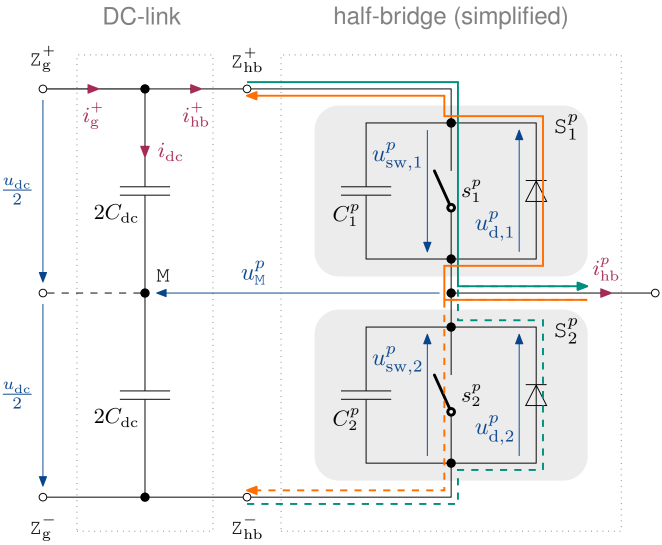

Mid-point voltage varies with switching state and current direction (this holds for any phase $p \in \{a, b, c\}$)

$$u_M^p = \begin{cases} \frac{u_{dc}}{2} - u_{sw,1}^p & , s_1^p = 1 \wedge i_{hb}^p \geqslant 0 \\ \frac{u_{dc}}{2} + u_{d,1}^p & , s_1^p = 1 \wedge i_{hb}^p < 0 \\ -\frac{u_{dc}}{2} - u_{d,2}^p & , s_1^p = 0 \wedge i_{hb}^p \geqslant 0 \\ -\frac{u_{dc}}{2} + u_{sw,2}^p & , s_1^p = 0 \wedge i_{hb}^p < 0 \end{cases}$$

***Remark**: Important to note that voltage drops $u_{sw,1/2}^p$ and $u_{d,1/2}^p$ over power switch and power diodes, respectively, usually depend on currents and temperatures. Moreover, they may be different for each upper and/or lower branch (index 1 & 2) and each phase $p \in \{a, b, c\}$.*

High-performance control: Inverter nonlinearity compensation

Nonlinear voltage drops in a three-phase VSI

Assuming $u_{\mathrm{sw}}^p := u_{\mathrm{sw},1}^p = u_{\mathrm{sw},2}^p$ and $u_{\mathrm{d}}^p := u_{\mathrm{d},1}^p = u_{\mathrm{d},2}^p$, one obtains (for all $p \in \{a,b,c\}$)

$$u_{\mathrm{M}}^p = \big(u_{\mathrm{dc}} - u_{\mathrm{sw}}^p + u_{\mathrm{d}}^p\big)\big(s_1^p - \tfrac{1}{2}\big) - \tfrac{1}{2}\,\mathrm{sgn}(i_{\mathrm{hb}}^p)\big(u_{\mathrm{sw}}^p + u_{\mathrm{d}}^p\big),$$

where

$$\mathrm{sgn}(x) := \begin{cases} 1 & \text{, if } x \geqslant 1 \\ -1 & \text{, if } x < 1. \end{cases}$$

For a 2L-VSI, we have three phases $p \in \{a,b,c\}$, switching vector $\boldsymbol{s}_{\mathrm{vsi}}^{abc} = (s_1^a, s_1^b, s_1^c)^\top$ and current vector $\boldsymbol{i}_{\mathrm{vsi}}^{abc} = (i_{\mathrm{hb}}^a, i_{\mathrm{hb}}^b, i_{\mathrm{hb}}^c)^\top$, which yields the mid-point voltage vector

$$\boldsymbol{u}_{\mathtt{M}}^{abc} = \mathrm{diag}\left[u_{\mathrm{dc}}\mathbf{1}_3 - \boldsymbol{u}_{\mathrm{sw}}^{abc} + \boldsymbol{u}_{\mathrm{d}}^{abc}\right]\big(\boldsymbol{s}_{\mathrm{vsi}}^{abc} - \tfrac{1}{2}\mathbf{1}_3\big) - \tfrac{1}{2}\,\mathrm{diag}\left[\mathrm{sgn}(\boldsymbol{i}_{\mathrm{vsi}}^{abc})\right]\big(\boldsymbol{u}_{\mathrm{sw}}^{abc} + \boldsymbol{u}_{\mathrm{d}}^{abc}\big).$$

Outline

High-performance control: Inverter nonlinearity compensation

Average model

Assuming **constant voltages** $\boldsymbol{u}_{\mathrm{sw}}^{abc}$, $\boldsymbol{u}_{\mathrm{d}}^{abc}$ and u_{dc} and **identical signs** $\mathrm{sgn}(\boldsymbol{i}_{\mathrm{vsi}}^{abc})$ **of the currents** over one switching period $T_{\mathrm{sw}} = \frac{1}{f_{\mathrm{sw}}}$, the **average mid-point voltages** at sampling instant k (i.e., $t = kT_{\mathrm{sw}}$) are given by

$$\begin{aligned}
\overline{\boldsymbol{u}}_{\mathrm{M}}^{abc}[k] \;&:=\; \frac{1}{T_{\mathrm{sw}}}\int_{(k-1)T_{\mathrm{sw}}}^{kT_{\mathrm{sw}}} \boldsymbol{u}_{\mathrm{M}}^{abc}(\tau)\,\mathrm{d}\tau \\
&=\; \mathrm{diag}\Big[u_{\mathrm{dc}}[k]\mathbf{1}_3 - \boldsymbol{u}_{\mathrm{sw}}^{abc}[k] + \boldsymbol{u}_{\mathrm{d}}^{abc}[k]\Big]\Big(\boldsymbol{d}_{\mathrm{vsi}}^{abc}[k] - \tfrac{1}{2}\mathbf{1}_3\Big) \\
&\quad -\tfrac{1}{2}\,\mathrm{diag}\Big[\mathrm{sgn}(\boldsymbol{i}_{\mathrm{vsi}}^{abc}[k])\Big]\Big(\boldsymbol{u}_{\mathrm{sw}}^{abc}[k] + \boldsymbol{u}_{\mathrm{d}}^{abc}[k]\Big)
\end{aligned} \tag{7}$$

with the duty cycle vector

$$\boldsymbol{d}_{\mathrm{vsi}}^{abc}[k] := \frac{1}{T_{\mathrm{sw}}}\int_{(k-1)T_{\mathrm{sw}}}^{kT_{\mathrm{sw}}} \boldsymbol{s}_{\mathrm{vsi}}^{abc}(\tau)\,\mathrm{d}\tau = \frac{\boldsymbol{t}_{\mathrm{on}}^{abc}[k]}{T_{\mathrm{sw}}}, \tag{8}$$

which depends on the on-time vector $\boldsymbol{t}_{\mathrm{on}}^{abc}[k] := (T_{\mathrm{on}}^{a}[k], T_{\mathrm{on}}^{b}[k], T_{\mathrm{on}}^{c}[k])^\top$ (e.g., as consequence of modulation).

Outline

High-performance control: Inverter nonlinearity compensation

Dead-time effects in a half-bridge

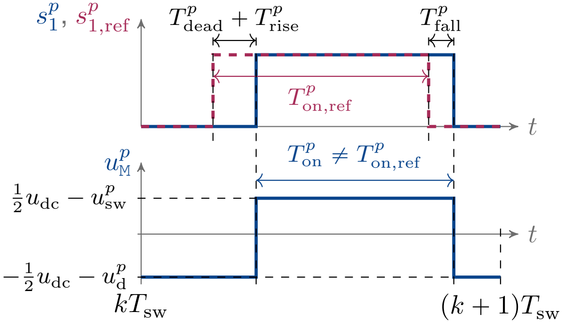

positive current (i.e., $i_{\mathrm{hb}^p} \geqslant 0$)

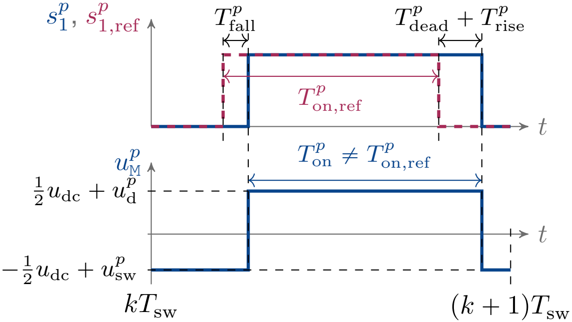

negative current (i.e., $i_{\mathrm{hb}}^p < 0$)

Hence, for each half-bridge / each phase $p \in \{a, b, c\}$, one obtains

$$T_{\mathrm{on}}^p = T_{\mathrm{on,ref}}^p - \left(T_{\mathrm{dead}}^p + T_{\mathrm{rise}}^p - T_{\mathrm{fall}}^p\right)\mathrm{sgn}\left(i_{\mathrm{hb}}^p\right).$$

High-performance control: Inverter nonlinearity compensation

Dead-time effects in a three-phase 2L-VSI

For $\boldsymbol{i}_{\mathrm{vsi}}^{abc} := (i_{\mathrm{hb}}^{a}, i_{\mathrm{hb}}^{b}, i_{\mathrm{hb}}^{c})^\top$, $\boldsymbol{t}_{\mathrm{on}}^{abc} := (T_{\mathrm{on}}^{a}, T_{\mathrm{on}}^{b}, T_{\mathrm{on}}^{c})^\top$, $\boldsymbol{t}_{\mathrm{dead}}^{abc} := (T_{\mathrm{dead}}^{a}, T_{\mathrm{dead}}^{b}, T_{\mathrm{dead}}^{c})^\top$, $\boldsymbol{t}_{\mathrm{rise}}^{abc} := (T_{\mathrm{rise}}^{a}, T_{\mathrm{rise}}^{b}, T_{\mathrm{rise}}^{c})^\top$ and $\boldsymbol{t}_{\mathrm{fall}}^{abc} := (T_{\mathrm{fall}}, T_{\mathrm{fall}}^{b}, T_{\mathrm{fall}}^{c})^\top$, the three-phase 2L-VSI result is

$$\boldsymbol{t}_{\mathrm{on}}^{abc} = \boldsymbol{t}_{\mathrm{on,ref}}^{abc} - \mathrm{diag}\Big[\mathrm{sgn}\big(\boldsymbol{i}_{\mathrm{vsi}}^{abc}\big)\Big]\Big(\boldsymbol{t}_{\mathrm{dead}}^{abc} + \boldsymbol{t}_{\mathrm{rise}}^{abc} - \boldsymbol{t}_{\mathrm{fall}}^{abc}\Big). \tag{9}$$

Inserting $\boldsymbol{d}_{\mathrm{vsi}}^{abc}[k] = \frac{\boldsymbol{t}_{\mathrm{on}}^{abc}[k]}{T_{\mathrm{sw}}}$ (i.e., (8)) with (9) into (7) and recalling that

$$\overline{\boldsymbol{u}}_{\mathrm{M,ref}}^{abc}[k] = \left(\frac{\boldsymbol{t}_{\mathrm{on,ref}}^{abc}[k]}{T_{\mathrm{sw}}} - \frac{1}{2}\mathbf{1}_3\right) u_{\mathrm{dc}}[k] \quad \Longleftrightarrow \quad \frac{\boldsymbol{t}_{\mathrm{on,ref}}^{abc}[k]}{T_{\mathrm{sw}}} = \frac{\overline{\boldsymbol{u}}_{\mathrm{M,ref}}^{abc}[k]}{u_{\mathrm{dc}}[k]} + \frac{1}{2}\mathbf{1}_3$$

yields (details omitted and argument $[k]$ neglected)

$$\begin{aligned}\overline{\boldsymbol{u}}_{\mathrm{M}}^{abc} \overset{(7),(8),(9)}{=} & \underbrace{\mathrm{diag}\Big[\mathbf{1}_3 - \frac{1}{u_{\mathrm{dc}}}\big(\boldsymbol{u}_{\mathrm{sw}}^{abc} - \boldsymbol{u}_{\mathrm{d}}^{abc}\big)\Big]}_{=:[\boldsymbol{C}_{\mathrm{vsi}}^{abc}]^{-1}} \overline{\boldsymbol{u}}_{\mathrm{M,ref}}^{abc} \\ & \underbrace{- \mathrm{diag}\Big[\mathrm{sgn}\big(\boldsymbol{i}_{\mathrm{vsi}}^{abc}\big)\Big]\Big(\mathrm{diag}\Big[u_{\mathrm{dc}}\mathbf{1}_3 - \boldsymbol{u}_{\mathrm{sw}}^{abc} + \boldsymbol{u}_{\mathrm{d}}^{abc}\Big]\frac{\boldsymbol{t}_{\mathrm{dead}}^{abc} + \boldsymbol{t}_{\mathrm{rise}}^{abc} - \boldsymbol{t}_{\mathrm{fall}}^{abc}}{T_{\mathrm{sw}}} + \frac{1}{2}\big(\boldsymbol{u}_{\mathrm{sw}}^{abc} + \boldsymbol{u}_{\mathrm{d}}^{abc}\big)\Big)}_{=:\boldsymbol{c}_{\mathrm{vsi}}^{abc}}\end{aligned} \tag{10}$$

Outline

High-performance control: Inverter nonlinearity compensation

Transformation to (d, q)-reference frame (# 1)

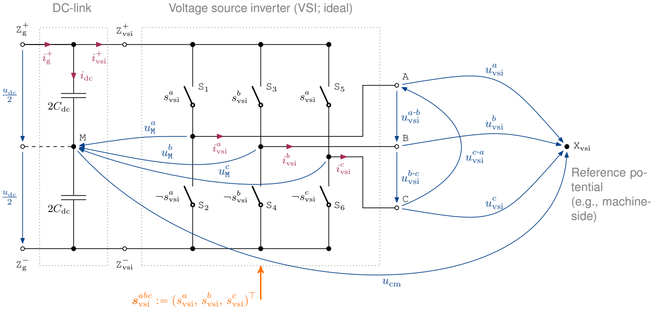

Clearly, the following holds

$$\boldsymbol{u}_{\mathrm{vsi}}^{abc} = \boldsymbol{u}_{\mathtt{M}}^{abc} + u_{\mathrm{cm}}\mathbf{1}_3 \quad \text{or} \quad \boldsymbol{u}_{\mathrm{ref}}^{abc} = \boldsymbol{u}_{\mathtt{M},\mathrm{ref}}^{abc} + u_{\mathrm{cm,ref}}\mathbf{1}_3,$$

which implies

$$\boldsymbol{u}_{\mathrm{vsi}}^{\alpha\beta} = \boldsymbol{T}_{\mathrm{c}}\boldsymbol{u}_{\mathrm{vsi}}^{abc} = \underbrace{\boldsymbol{T}_{\mathrm{c}}\boldsymbol{u}_{\mathtt{M}}^{abc}}_{=\boldsymbol{u}_{\mathtt{M}}^{\alpha\beta}} + \underbrace{\boldsymbol{T}_{\mathrm{c}}u_{\mathrm{cm}}\mathbf{1}_3}_{=\mathbf{0}_2} \quad \text{or} \quad \boldsymbol{u}_{\mathrm{ref}}^{\alpha\beta} = \boldsymbol{T}_{\mathrm{c}}\boldsymbol{u}_{\mathrm{ref}}^{abc} = \underbrace{\boldsymbol{T}_{\mathrm{c}}\boldsymbol{u}_{\mathtt{M},\mathrm{ref}}^{abc}}_{=\boldsymbol{u}_{\mathtt{M},\mathrm{ref}}^{\alpha\beta}} + \underbrace{\boldsymbol{T}_{\mathrm{c}}u_{\mathrm{cm,ref}}\mathbf{1}_3}_{=\mathbf{0}_2},$$

High-performance control: Inverter nonlinearity compensation

Transformation to (d, q)-reference frame (# 2)

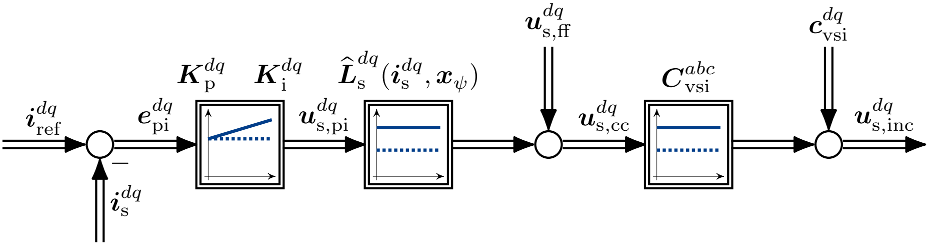

$$\boldsymbol{u}^{dq}_{\mathrm{s,cc}} \overset{!}{=} \boldsymbol{u}^{dq}_{\mathrm{vsi}} = \boldsymbol{T}_{\mathrm{p}}(\phi_{\mathrm{p}})^{-1}\boldsymbol{T}_{\mathrm{c}}\boldsymbol{u}^{abc}_{\mathrm{vsi}} = \boldsymbol{T}_{\mathrm{p}}(\phi_{\mathrm{p}})^{-1}\boldsymbol{T}_{\mathrm{c}}\boldsymbol{u}^{abc}_{\mathtt{M}} + \boldsymbol{T}_{\mathrm{p}}(\phi_{\mathrm{p}})^{-1}\underbrace{\boldsymbol{T}_{\mathrm{c}}u_{\mathrm{cm}}\boldsymbol{1}_3}_{=\boldsymbol{0}_2}$$

$$\overset{(10)}{=} \underbrace{\boldsymbol{T}_{\mathrm{p}}(\phi_{\mathrm{p}})^{-1}\boldsymbol{T}_{\mathrm{c}}[\boldsymbol{C}^{abc}_{\mathrm{vsi}}]^{-1}\boldsymbol{T}_{\mathrm{c}}^{-1}\boldsymbol{T}_{\mathrm{p}}(\phi_{\mathrm{p}})}_{=:[\boldsymbol{C}^{dq}_{\mathrm{vsi}}]^{-1}}\boldsymbol{u}^{dq}_{\mathrm{ref}} - \underbrace{\boldsymbol{T}_{\mathrm{p}}(\phi_{\mathrm{p}})^{-1}\boldsymbol{T}_{\mathrm{c}}\boldsymbol{c}^{abc}_{\mathrm{vsi}}}_{=:\boldsymbol{c}^{dq}_{\mathrm{vsi}}}$$

$$\Longrightarrow \quad \boxed{\boldsymbol{u}^{dq}_{\mathrm{s,inc}} := \boldsymbol{u}^{dq}_{\mathrm{ref}} = \boldsymbol{C}^{abc}_{\mathrm{vsi}}\boldsymbol{u}^{dq}_{\mathrm{s,cc}} + \boldsymbol{c}^{dq}_{\mathrm{vsi}}} \tag{11}$$

Outline

High-performance control: Inverter nonlinearity compensation

Validation: Measured voltage response of SEMIKRON SKiiP 83 AC 12 in SEW MDX61B0220 at ± 10 A

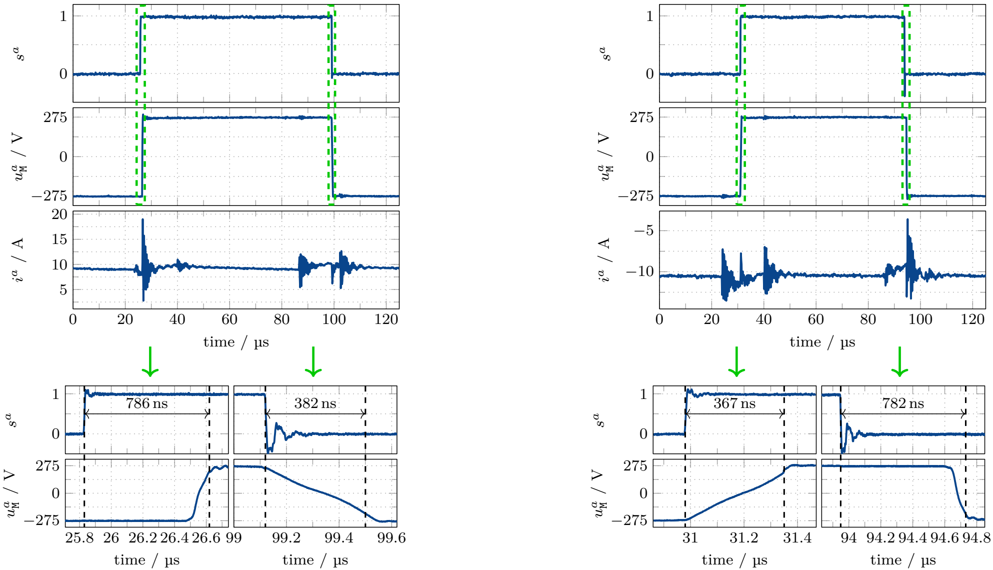

High-performance control: Inverter nonlinearity compensation

Validation: Measured voltage response of SEMIKRON SKiiP 83 AC 12 in SEW MDX61B0220 at ± 20 A

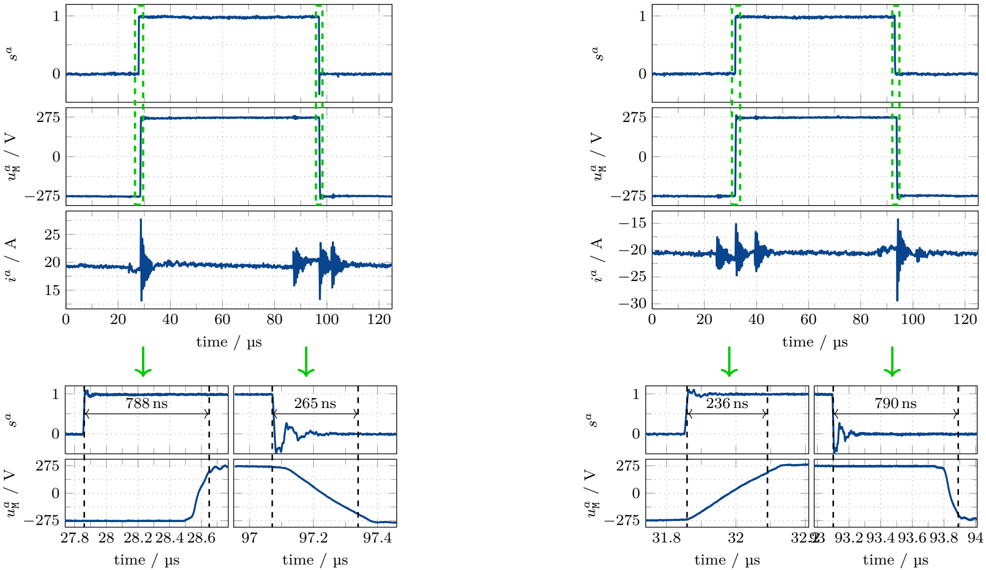

High-performance control: Inverter nonlinearity compensation

Validation: Measurement results [——] without INC and [——] with INC

Low-voltage measurements

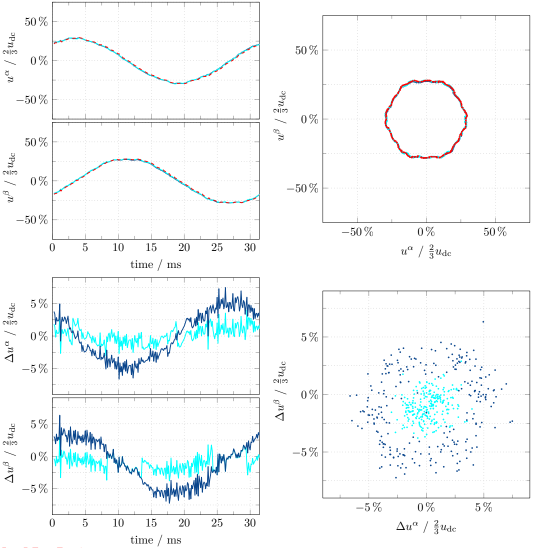

High-voltage measurements

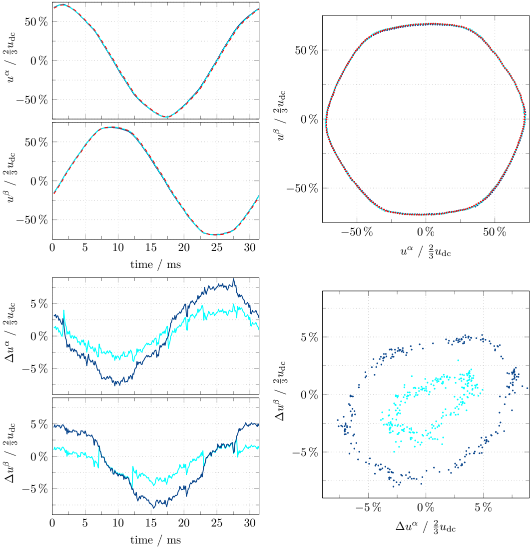

Outline

6 High-performance control

Outline

High-performance control

Optimal reference voltage saturation: Overview

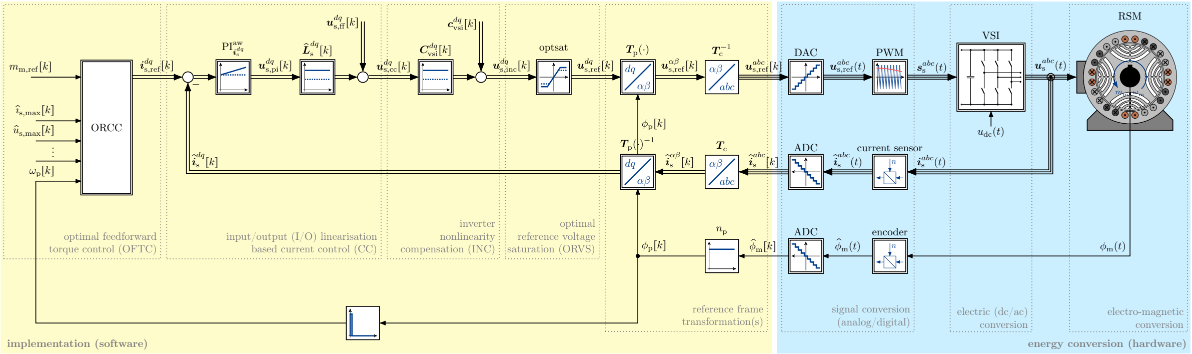

High-performance control: Optimal reference voltage saturation

Problem statement: Drawbacks of converters

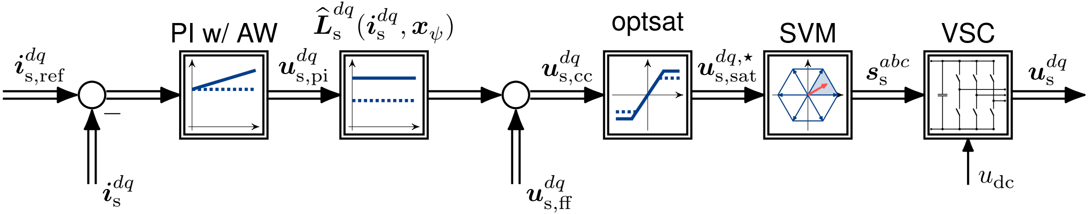

Any voltage source converter (VSC) suffers from *four* inevitable drawbacks (D_i):

(D_1) voltage deterioration due to nonlinear current-dependent voltage drops over semiconductors [167],

(D_2) voltage ripples due to the switching behavior of the power electronic devices [168],

(D_3) delayed voltage response due to modulation [169], and

(D_4) output voltage constraints due to a limited dc-link voltage.

$\Longrightarrow$ Now we will discuss and solve the last problem in an optimal way ("optsat") in order to reduce its impact, in particular, on proportional-integral (PI) based control methods which still represent the vast majority in industrial applications. For more advanced control methods like model predictive control, the voltage constraints can directly be considered during controller design and/or the optimization stage [135, 170, 171].

Outline

High-performance control: Optimal reference voltage saturation

Proposed solution Optimal Reference Voltage Saturation (ORVS)

Goal of ORVS:
Minimization of the deviation between the desired current dynamics $\frac{\mathrm{d}}{\mathrm{d}t}\boldsymbol{i}_\mathrm{s}^{dq}(\boldsymbol{u}_\mathrm{s,pi}^{dq})$ (time derivative of the currents) obtained for the control action $\boldsymbol{u}_\mathrm{s,pi}^{dq}$ computed by the PI control system if the voltage constraints were not present and the feasible current dynamics $\frac{\mathrm{d}}{\mathrm{d}t}\boldsymbol{i}_\mathrm{s}^{dq}(\boldsymbol{u}_\mathrm{s,sat}^{dq,\star}, \widehat{u}_\mathrm{s,max})$ due to the active voltage constraint $\widehat{u}_\mathrm{s,max}$, i.e.

$$\boldsymbol{u}_\mathrm{s,sat}^{dq,\star} = \arg\min_{\boldsymbol{u}_\mathrm{s}^{dq}} \left\| \frac{\mathrm{d}}{\mathrm{d}t}\boldsymbol{i}_\mathrm{s}^{dq}(\boldsymbol{u}_\mathrm{s,pi}^{dq}) - \frac{\mathrm{d}}{\mathrm{d}t}\boldsymbol{i}_\mathrm{s}^{dq}(\boldsymbol{u}_\mathrm{s}^{dq}, \widehat{u}_\mathrm{s,max}) \right\| = \begin{cases} \boldsymbol{u}_\mathrm{s,cc}^{dq} \frac{\widehat{u}_\mathrm{s,max}}{\|\boldsymbol{u}_\mathrm{s,cc}^{dq}\|}, & \text{if } \|\boldsymbol{u}_\mathrm{s,ff}^{dq}\| \geqslant \widehat{u}_\mathrm{s,max}, \\ \boldsymbol{u}_\mathrm{s,ff}^{dq} + (1-\zeta^\star)\,\widehat{\boldsymbol{L}}_\mathrm{s}^{dq} \boldsymbol{u}_\mathrm{s,pi}^{dq}, & \text{if } \|\boldsymbol{u}_\mathrm{s,cc}^{dq}\| \geqslant \widehat{u}_\mathrm{s,max}, \\ \boldsymbol{u}_\mathrm{s,cc}^{dq}, & \text{else} \end{cases}$$

In contrast to **no saturation** or **conventional saturation**

$$\boldsymbol{u}_\mathrm{s,sat}^{dq} := \begin{cases} \boldsymbol{u}_\mathrm{s,cc}^{dq} \frac{\widehat{u}_\mathrm{s,max}}{||\boldsymbol{u}_\mathrm{s,cc}^{dq}||}, & \text{if } ||\boldsymbol{u}_\mathrm{s,cc}^{dq}|| \geqslant \widehat{u}_\mathrm{s,max}, \\ \boldsymbol{u}_\mathrm{s,cc}^{dq}, & \text{else}, \end{cases}$$

High-performance control: Optimal reference voltage saturation

Proposed solution Illustration of the idea of **Optimal Reference Voltage Saturation (ORVS)**

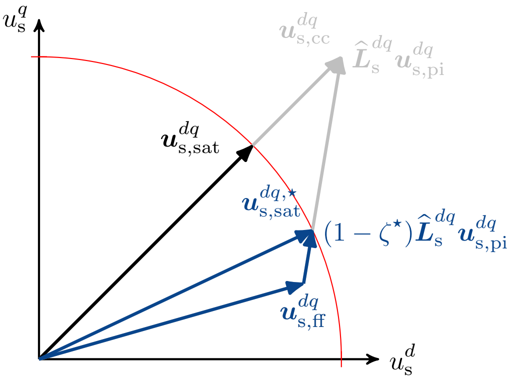

☞ Consideration of **voltage hexagon** as constraint is possible! (another paper in preparation)

$$\widehat{u}_{\mathrm{s,max}}(u_{\mathrm{dc}}) := \begin{cases} \frac{u_{\mathrm{dc}}}{2}, & \text{for PWM,} \\ \frac{u_{\mathrm{dc}}}{\sqrt{3}}, & \text{for SVM.} \end{cases}$$

Outline

High-performance control: Optimal reference voltage saturation

Block diagram of nonlinear current dynamics with current/angle-dependent differential inductances and flux linkages

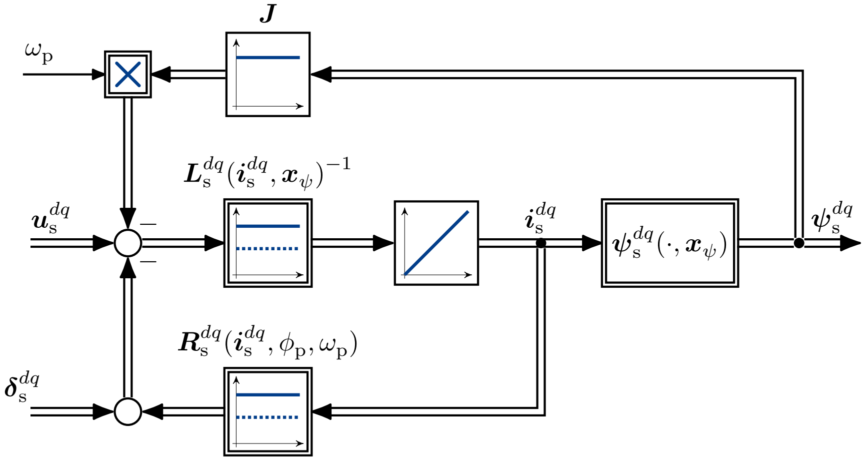

High-performance control: Optimal reference voltage saturation

Block diagram: Nonlinear flux linkage maps ($\phi_m = 0^\circ$) of synchronous machine

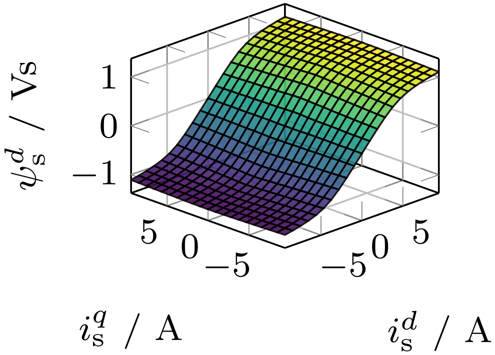

(**a**) d-axis flux linkage map.

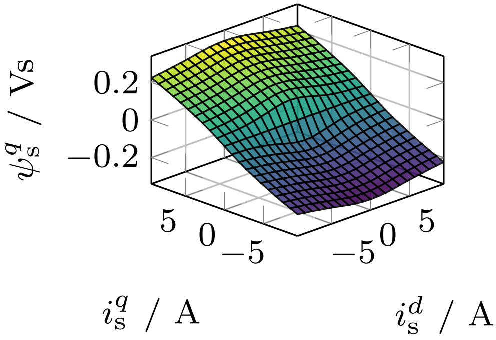

(**b**) q-axis flux linkage map.

Outline

High-performance control: Optimal reference voltage saturation

Input/ouput (I/O) linearization (recap)

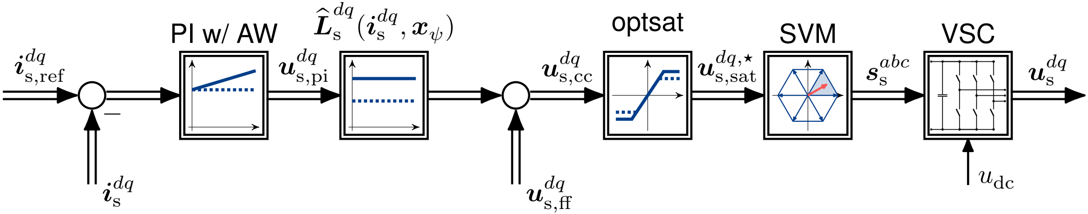

I/O linearization approach

$$\boldsymbol{u}_{\mathrm{s}}^{dq} \approx \boldsymbol{u}_{\mathrm{s,cc}}^{dq} := \widehat{\boldsymbol{L}}_{\mathrm{s}}^{dq} \boldsymbol{u}_{\mathrm{s,pi}}^{dq} + \underbrace{\boldsymbol{R}_{\mathrm{s}}^{dq} \boldsymbol{i}_{\mathrm{s}}^{dq} + \omega_{\mathrm{p}} \boldsymbol{J} \boldsymbol{\psi}_{\mathrm{s}}^{dq} + \boldsymbol{\delta}_{\mathrm{s}}^{dq}}_{=:\boldsymbol{u}_{\mathrm{ff}}^{dq}}, \tag{12}$$

gives simple **integral current dynamics** $\frac{\mathrm{d}}{\mathrm{d}t} \boldsymbol{i}_{\mathrm{s}}^{dq} = \boldsymbol{u}_{\mathrm{s,pi}}^{dq}$ and allows for simple PLL-like **tuning by pole placement** (recall last slides).

Outline

High-performance control: Optimal reference voltage saturation

PI controller design with anti-windup (recap)

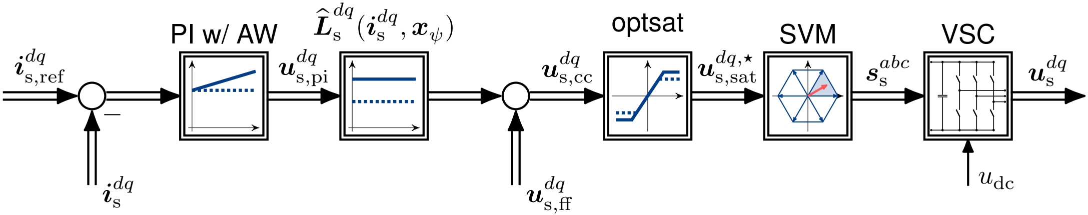

Current control system

$$\left.\begin{aligned} \boldsymbol{u}_{\mathrm{s,pi}}^{dq} &= \boldsymbol{K}_{\mathrm{p}}^{dq}\left(\boldsymbol{i}_{\mathrm{s,ref}}^{dq} - \boldsymbol{i}_{\mathrm{s}}^{dq}\right) + \boldsymbol{K}_{\mathrm{i}}^{dq}\boldsymbol{x}_{\mathrm{i}}^{dq}, \\ \frac{\mathrm{d}}{\mathrm{d}t}\boldsymbol{x}_{\mathrm{i}}^{dq} &= f_{\mathrm{aw}}\left(\widehat{u}_{\mathrm{s,max}}, \boldsymbol{u}_{\mathrm{s,cc}}^{dq}\right)\left(\boldsymbol{i}_{\mathrm{s,ref}}^{dq} - \boldsymbol{i}_{\mathrm{s}}^{dq}\right) \end{aligned}\right\} \tag{13}$$

with integral state $\boldsymbol{x}_{\mathrm{i}}^{dq}$, gain matrices $\boldsymbol{K}_{\mathrm{p}}^{dq}$ & $\boldsymbol{K}_{\mathrm{i}}^{dq}$ and anti-windup (“conditional integration”) with

$$f_{\mathrm{aw}}\left(\widehat{u}_{\mathrm{s,max}}, \boldsymbol{u}_{\mathrm{s,cc}}^{dq}\right) = \begin{cases} 0, & \text{if } \|\boldsymbol{u}_{\mathrm{s,cc}}^{dq}\| > \widehat{u}_{\mathrm{s,max}}, \\ 1, & \text{else.} \end{cases}$$

Outline

High-performance control: Optimal reference voltage saturation

Reference voltage saturation: Comparison of different approaches

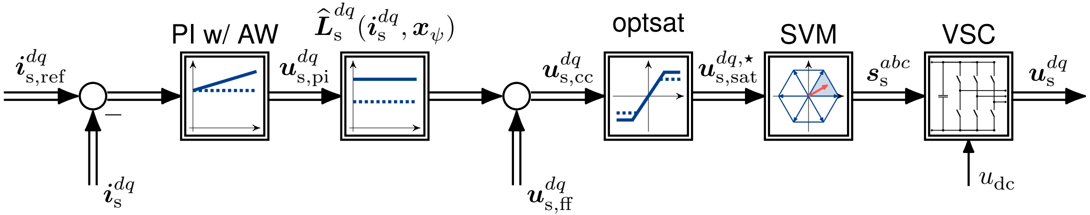

- **optimal reference voltage saturation** [——] with

$$\boldsymbol{u}_{\rm s,sat}^{dq,\star} := \arg\min_{\boldsymbol{u}_{\rm s}^{dq}} \left\| \tfrac{\rm d}{{\rm d}t}\boldsymbol{i}_{\rm s}^{dq}(\boldsymbol{u}_{\rm s,pi}^{dq}) - \tfrac{\rm d}{{\rm d}t}\boldsymbol{i}_{\rm s}^{dq}(\boldsymbol{u}_{\rm s}^{dq}, \widehat{u}_{\rm s,max}) \right\| = \begin{cases} \boldsymbol{u}_{\rm s,cc}^{dq} \dfrac{\widehat{u}_{\rm s,max}}{\|\boldsymbol{u}_{\rm s,cc}^{dq}\|}, & \text{if } \|\boldsymbol{u}_{\rm s,ff}^{dq}\| \geqslant \widehat{u}_{\rm s,max}, \\ \boldsymbol{u}_{\rm s,ff}^{dq} + (1-\zeta^\star)\,\widehat{\boldsymbol{L}}_{\rm s}^{dq}\boldsymbol{u}_{\rm s,pi}^{dq}, & \text{if } \|\boldsymbol{u}_{\rm s,cc}^{dq}\| \geqslant \widehat{u}_{\rm s,max}, \\ \boldsymbol{u}_{\rm s,cc}^{dq}, & \text{else} \end{cases}$$

- **conventional saturation** [——] with $\boldsymbol{u}_{\rm s,sat}^{dq} := \begin{cases} \boldsymbol{u}_{\rm s,cc}^{dq} \dfrac{\widehat{u}_{\rm s,max}}{||\boldsymbol{u}_{\rm s,cc}^{dq}||}, & \text{if } ||\boldsymbol{u}_{\rm s,cc}^{dq}|| \geqslant \widehat{u}_{\rm s,max}, \\ \boldsymbol{u}_{\rm s,cc}^{dq}, & \text{else}, \end{cases}$

- **no saturation (and no anti-windup)** [——]

Outline

High-performance control: Optimal reference voltage saturation

Validation: Simulation results at standstill ($\omega_{\mathrm{m}} = 0$): Control system *with* ORVS [——], *with* conventional saturation [——] and *without* saturation and anti-windup [——]

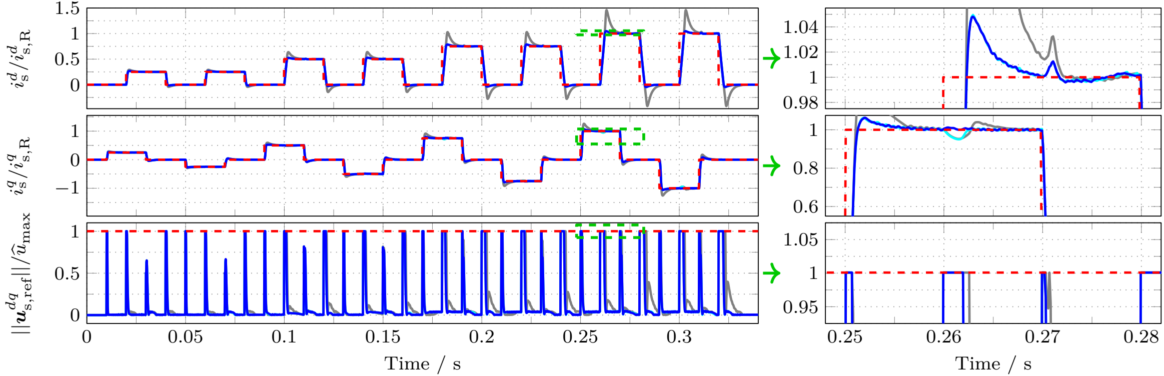

High-performance control: Optimal reference voltage saturation

Validation: Simulation results at rated speed ($\omega_{\mathrm{m}} = \omega_{\mathrm{m,R}}$): Control system *with* ORVS [——], *with* conventional saturation [——] and *without* saturation and anti-windup [——]

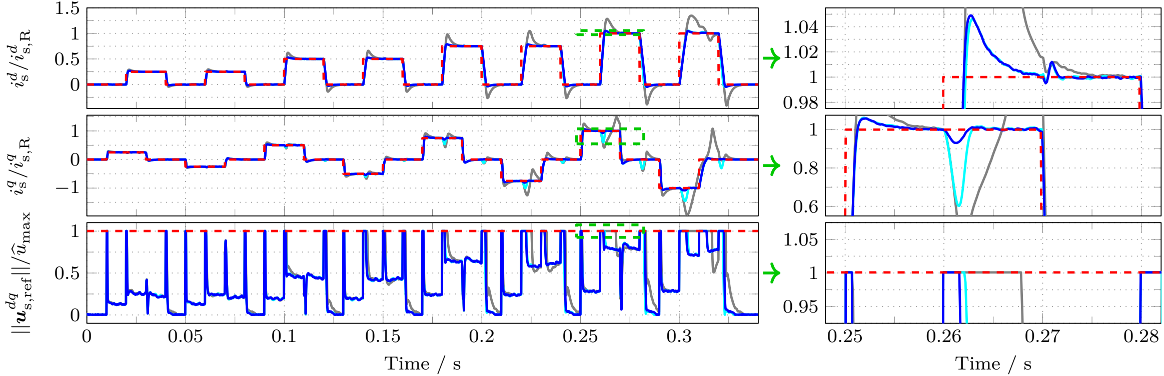

Outline

Outline

Optimal operation: Motivation

Examples of anisotropic synchronous machines [172] with "saliency ratio" $L_{\mathrm{s}}^{d}/L_{\mathrm{s}}^{q} \neq 1$ ($\Leftrightarrow L_{\mathrm{s,app}}^{d}/L_{\mathrm{s,app}}^{q} \neq 1$)

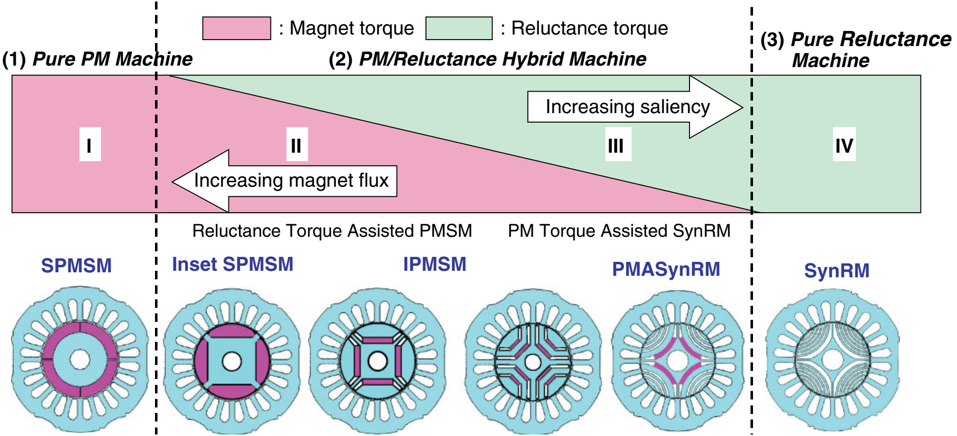

$$m_{\mathrm{m}}\left(i_{\mathrm{s}}^{d},\, i_{\mathrm{s}}^{q}\right) = \frac{2n_{\mathrm{p}}}{3\kappa^2}\left(\boldsymbol{i}_{\mathrm{s}}^{dq}\right)^{\top}\boldsymbol{J}\boldsymbol{\psi}_{\mathrm{s}}^{dq} = \frac{2n_{\mathrm{p}}}{3\kappa^2}\left[\underbrace{\psi_{\mathrm{pm}}^{d} i_{\mathrm{s}}^{q} - \psi_{\mathrm{pm}}^{q} i_{\mathrm{s}}^{d}}_{\text{magnetic torque}} + \underbrace{\left(L_{\mathrm{s,app}}^{d} - L_{\mathrm{s,app}}^{q}\right) i_{\mathrm{s}}^{d} i_{\mathrm{s}}^{q}}_{\text{reluctance torque}} + \underbrace{L_{\mathrm{s,app}}^{dq}\left(\left(i_{\mathrm{s}}^{q}\right)^2 - \left(i_{\mathrm{s}}^{d}\right)^2\right)}_{\text{cross-coupling torque}}\right]$$

Optimal operation: Motivation

Optimal Feedforward Torque Control (**OFTC**) problem: **Isotropic, linear PMSM** (without iron losses)

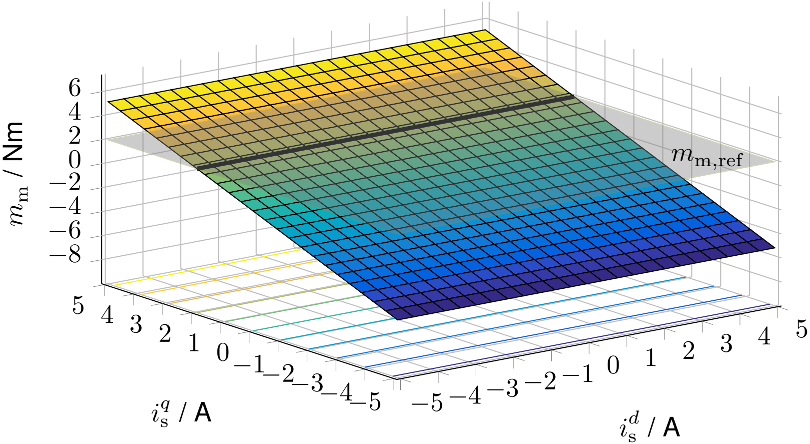

$$m_{\mathrm{m,ref}} \stackrel{!}{=} m_{\mathrm{m}}\left(i_{\mathrm{s}}^{d},\, i_{\mathrm{s}}^{q}\right) = \frac{2n_{\mathrm{p}}}{3\kappa^2}\,\psi_{\mathrm{pm}} i_{\mathrm{s}}^{q} \Longrightarrow \boxed{\boldsymbol{i}_{\mathrm{s,ref}}^{dq} := \left(i_{\mathrm{s,ref}}^{d},\, i_{\mathrm{s,ref}}^{q}\right)^{\top} = \left(0,\ \frac{3\kappa^2\, m_{\mathrm{m,ref}}}{2n_{\mathrm{p}}\psi_{\mathrm{pm}}}\right)^{\top}}$$

Optimal operation: Motivation

Optimal Feedforward Torque Control (**OFTC**) problem: **Anisotropic, affine PMSM** (without iron losses)

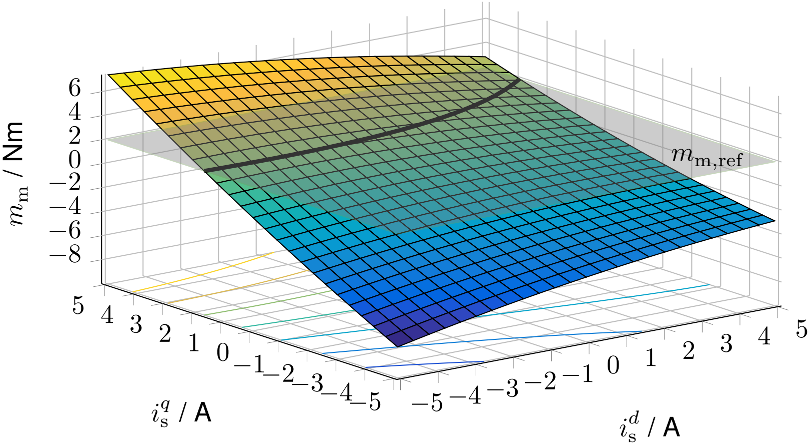

$$m_{\mathrm{m,ref}} \overset{!}{=} \underbrace{\frac{2n_{\mathrm{p}}}{3\kappa^2}\Big[\psi_{\mathrm{pm}}^{d} i_{\mathrm{s}}^{q} - \psi_{\mathrm{pm}}^{q} i_{\mathrm{s}}^{d} + \big(L_{\mathrm{s,app}}^{d} - L_{\mathrm{s,app}}^{q}\big) i_{\mathrm{s}}^{d} i_{\mathrm{s}}^{q} + L_{\mathrm{s,app}}^{dq}\big((i_{\mathrm{s}}^{q})^2 - (i_{\mathrm{s}}^{d})^2\big)\Big]}_{m_{\mathrm{m}}(i_{\mathrm{s}}^{d}, i_{\mathrm{s}}^{q})} \Longrightarrow \boxed{\boldsymbol{i}_{\mathrm{s,ref}}^{dq} := (?,?)^{\top}}$$

Optimal operation: Motivation

Optimal Feedforward Torque Control (**OFTC**) problem: **Identical for all nonlinear machines**

Nonlinear IPMSM $(3.9\,\mathrm{kW@5\,500\,rpm})$

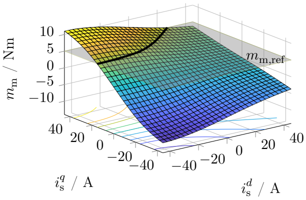

Nonlinear IM $(3\,\mathrm{kW@1\,445\,rpm})$

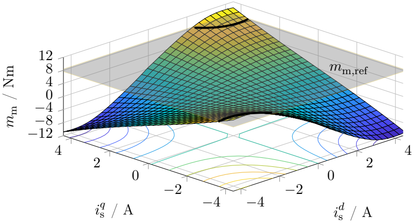

Nonlinear DFIM $(10\,\mathrm{kW@1\,500\,rpm})$

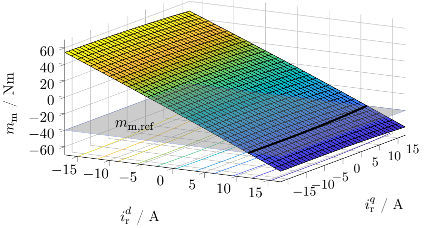

Nonlinear RSM $(9.6\,\mathrm{kW@1\,500\,rpm})$

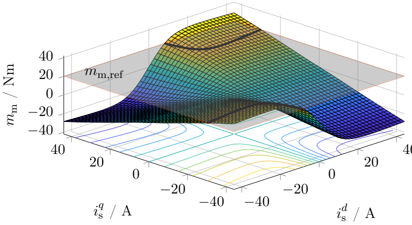

Outline

Optimal operation: Problem statement and proposed solution

Optimal Feedforward Torque Control (**OFTC**) within the control system

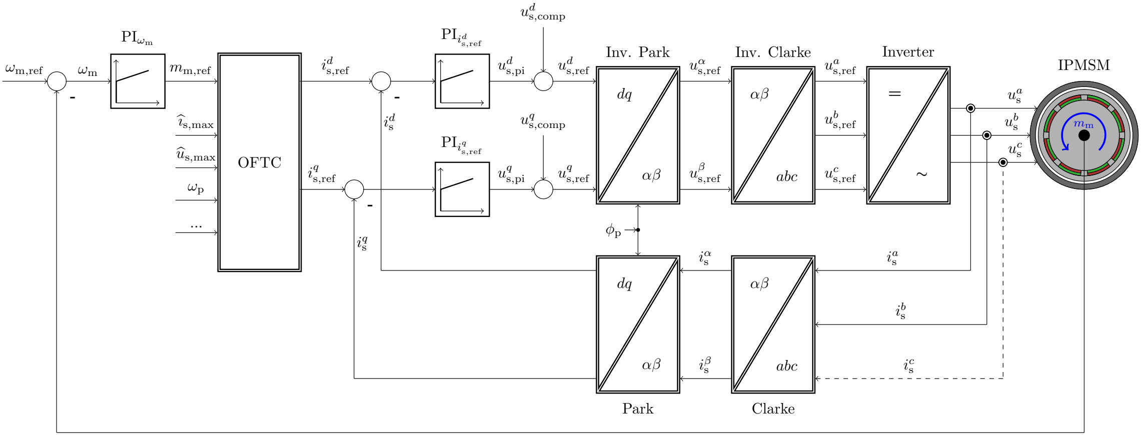

Optimal operation: Problem statement and proposed solution

Optimal Feedforward Torque Control (**OFTC**) problem: Optimal reference current computation (ORCC)

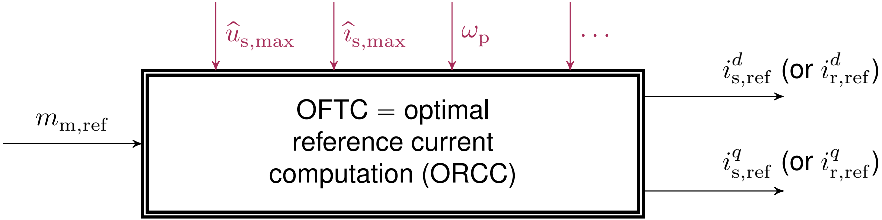

$$\boldsymbol{i}^{dq}_{\mathrm{s,ref}}(m_{\mathrm{m,ref}}, \widehat{u}_{\mathrm{s,max}}, \widehat{\imath}_{\mathrm{s,max}}, \omega_{\mathrm{p}}, \ldots) = \begin{pmatrix} i^{d}_{\mathrm{s,ref}}(m_{\mathrm{m,ref}}, \widehat{u}_{\mathrm{s,max}}, \widehat{\imath}_{\mathrm{s,max}}, \omega_{\mathrm{p}}, \ldots) \\ i^{q}_{\mathrm{s,ref}}(m_{\mathrm{m,ref}}, \widehat{u}_{\mathrm{s,max}}, \widehat{\imath}_{\mathrm{s,max}}, \omega_{\mathrm{p}}, \ldots) \end{pmatrix}$$

✓ Numerical solutions and/or look-up tables
(but: limited storage, accuracy, real-time applicability)

? Analytical solutions

(some do exist but impose simplifying assumptions such as ~~$R_{\mathrm{s}} = 0$, $R_{\mathrm{s,Fe}} = 0$ and/or $L_{\mathrm{s,m}} = 0$, etc.~~)

Optimal operation: Problem statement and proposed solution

Considered anisotropic synchronous machines with iron losses: **Nonlinear transformer model**

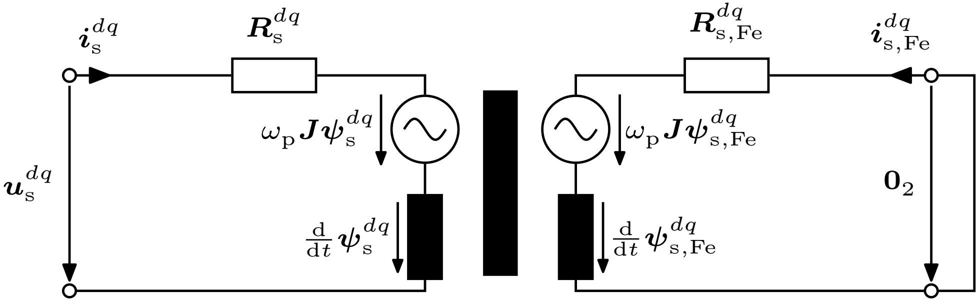

with $\psi_{\mathrm{s}}^{dq} = \psi_{\mathrm{s,Fe}}^{dq}$ (single assumption!) and (possibly) *nonlinear*

- *current, angle, speed* and *temperature* dependent stator resistance, i.e. $\boldsymbol{R}_{\mathrm{s}}^{dq} := \boldsymbol{R}_{\mathrm{s}}^{dq}(\boldsymbol{i}_{\mathrm{s}}^{dq}, \phi_{\mathrm{p}}, \omega_{\mathrm{p}}, \vartheta_{\mathrm{s}})$
- *current, angle, speed* and *temperature* dependent iron resistance, i.e. $\boldsymbol{R}_{\mathrm{s,Fe}}^{dq} := \boldsymbol{R}_{\mathrm{s,Fe}}^{dq}(\boldsymbol{i}_{\mathrm{s}}^{dq}, \phi_{\mathrm{p}}, \omega_{\mathrm{p}}, \vartheta_{\mathrm{s}})$
- *current, angle, speed* and *temperature* dependent flux linkages, i.e. $\boldsymbol{\psi}_{\mathrm{s}}^{dq} := \boldsymbol{\psi}_{\mathrm{s}}^{dq}(\boldsymbol{i}_{\mathrm{s}}^{dq}, \phi_{\mathrm{p}}, \omega_{\mathrm{p}}, \vartheta_{\mathrm{s}})$

Optimal operation: Problem statement and proposed solution

Considered anisotropic synchronous machines with iron losses: **Nonlinear machine dynamics** ($\Longrightarrow$ steady-state model)

Stator:
$$\overbrace{\begin{pmatrix} u_\mathrm{s}^d \\ u_\mathrm{s}^q \end{pmatrix}}^{=:\boldsymbol{u}_\mathrm{s}^{dq}} = \overbrace{\begin{bmatrix} R_\mathrm{s}^d & R_\mathrm{s}^{dq} \\ R_\mathrm{s}^{qd} & R_\mathrm{s}^q \end{bmatrix}}^{=:\boldsymbol{R}_\mathrm{s}^{dq}} \overbrace{\begin{pmatrix} i_\mathrm{s}^d \\ i_\mathrm{s}^q \end{pmatrix}}^{=:\boldsymbol{i}_\mathrm{s}^{dq}} + \omega_\mathrm{p} \overbrace{\begin{bmatrix} 0 & -1 \\ 1 & 0 \end{bmatrix}}^{=:\boldsymbol{J}} \overbrace{\begin{pmatrix} \psi_\mathrm{s}^d \\ \psi_\mathrm{s}^q \end{pmatrix}}^{=:\boldsymbol{\psi}_\mathrm{s}^{dq}} + \cancel{\frac{\mathrm{d}}{\mathrm{d}t}\boldsymbol{\psi}_\mathrm{s}^{dq}}$$

Iron:
$$\underbrace{\begin{pmatrix} 0 \\ 0 \end{pmatrix}}_{=:\boldsymbol{0}_2} = \underbrace{\begin{bmatrix} R_\mathrm{s,Fe}^d & R_\mathrm{s,Fe}^{dq} \\ R_\mathrm{s,Fe}^{qd} & R_\mathrm{s,Fe}^q \end{bmatrix}}_{=:\boldsymbol{R}_\mathrm{s,Fe}^{dq}} \underbrace{\begin{pmatrix} i_\mathrm{s,Fe}^d \\ i_\mathrm{s,Fe}^q \end{pmatrix}}_{=:\boldsymbol{i}_\mathrm{s,Fe}^{dq}} + \omega_\mathrm{p} \boldsymbol{J} \boldsymbol{\psi}_\mathrm{s}^{dq} + \cancel{\frac{\mathrm{d}}{\mathrm{d}t}\boldsymbol{\psi}_\mathrm{s}^{dq}}$$

$$\boldsymbol{i}_\mathrm{s,Fe}^{dq} = -\left(\boldsymbol{R}_\mathrm{s,Fe}^{dq}\right)^{-1} \left[\omega_\mathrm{p} \boldsymbol{J} \boldsymbol{\psi}_\mathrm{s}^{dq} + \cancel{\frac{\mathrm{d}}{\mathrm{d}t}\boldsymbol{\psi}_\mathrm{s}^{dq}} \right]$$

Mech.:
$$\frac{\mathrm{d}}{\mathrm{d}t}\omega_\mathrm{m} = \frac{1}{\Theta_\mathrm{m}} \left(m_\mathrm{m} + m_\mathrm{l} \right)$$ with $\omega_\mathrm{p} = n_\mathrm{p} \omega_\mathrm{m}$

$$m_\mathrm{m} = \frac{2}{3\kappa^2} \left(\boldsymbol{i}_\mathrm{s}^{dq} + \boldsymbol{i}_\mathrm{s,Fe}^{dq} \right)^\top \boldsymbol{J} \boldsymbol{\psi}_\mathrm{s}^{dq}$$

Losses:
$$p_\mathrm{s,loss} = \underbrace{\frac{2}{3\kappa^2} \left(\boldsymbol{i}_\mathrm{s}^{dq}\right)^\top \boldsymbol{R}_\mathrm{s}^{dq} \boldsymbol{i}_\mathrm{s}^{dq}}_{=:p_\mathrm{s,Cu}} + \underbrace{\frac{2}{3\kappa^2} \left(\boldsymbol{i}_\mathrm{s,Fe}^{dq}\right)^\top \boldsymbol{R}_\mathrm{s,Fe}^{dq} \boldsymbol{i}_\mathrm{s,Fe}^{dq}}_{=:p_\mathrm{s,Fe}}$$

Optimal operation: Problem statement and proposed solution

Optimal Reference Current Computation (**ORCC**): Optimization problem(s) with multiple constraints

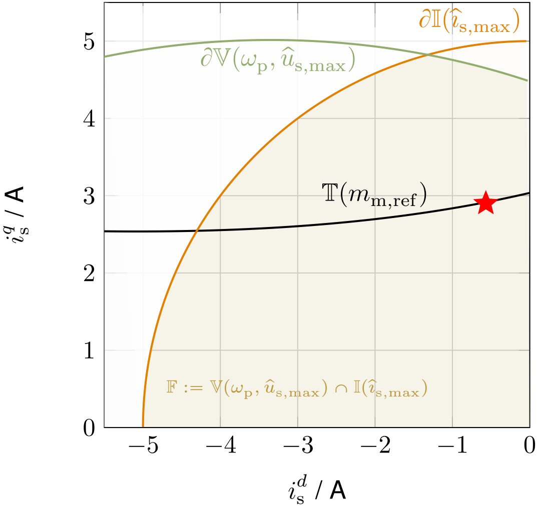

$$\max_{\boldsymbol{i}_s^{dq} \in \mathbb{F}} \; -f(\boldsymbol{i}_s^{dq}) \quad \text{subject to}$$

$$\begin{cases} \|\boldsymbol{i}_s^{dq}\|^2 \leqslant \hat{\imath}_{s,\max}^2, \\ \text{(current circular area)} \\ \|\boldsymbol{u}_s^{dq}(\boldsymbol{i}_s^{dq}, \omega_p, \dots)\|^2 \leqslant \hat{u}_{s,\max}^2, \\ \text{(voltage elliptical area)} \\ |m_m(\boldsymbol{i}_s^{dq}, \omega_p, \dots)| \leqslant |m_{m,ref}|, \\ \text{and } \operatorname{sign}(m_{m,ref}) = \\ \operatorname{sign}(m_m(\boldsymbol{i}_s^{dq})). \end{cases}$$

$\Longrightarrow$ e.g. minimize copper losses, i.e., $-f(\boldsymbol{i}_s^{dq}) = -\|\boldsymbol{i}_s^{dq}\|^2$.

$\Longrightarrow$ $\boldsymbol{i}_{s,ref}^{dq} = \boldsymbol{i}_{s,MTPC}^{dq}$ at ★, i.e., MTPC with $m_{m,ref} = m_m(\boldsymbol{i}_{s,ref}^{dq})$ feasible.

Outline

Outline

Optimal operation: OFTC with analytical ORCC

Sequential Quadratic Programming (SQP): Linearization, implicit formulation, optimization & intersection points

Step 1: Online linearization of flux linkages, machine torque, iron resistance, etc.: for example:

- **flux linkages** (first-order Taylor approximation around operating point $\bar{\boldsymbol{i}}_{\mathrm{s}}^{dq}$ [■])
- **machine torque** (second-order Taylor approximation around operating point $\bar{\boldsymbol{i}}_{\mathrm{s}}^{dq}$ [■])

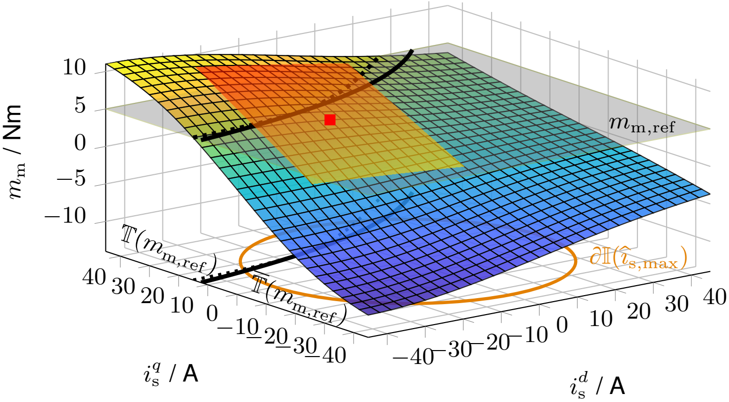

- ...

Optimal operation: OFTC with analytical ORCC

Sequential Quadratic Programming (SQP): Linearization, implicit formulation, optimization & intersection points

Step 2: Derivation of quadrics $Q_A(\boldsymbol{i}_\mathrm{s}^{dq}) := (\boldsymbol{i}_\mathrm{s}^{dq})^\top \boldsymbol{A}\, \boldsymbol{i}_\mathrm{s}^{dq} + 2\boldsymbol{a}^\top \boldsymbol{i}_\mathrm{s}^{dq} + \alpha$:

- Current circular area: $(i_\mathrm{s}^d)^2 + (i_\mathrm{s}^q)^2 \leqslant \widehat{\imath}_{\mathrm{s,max}}^2 \iff \|\boldsymbol{i}_\mathrm{s}^{dq}\|^2 = (\boldsymbol{i}_\mathrm{s}^{dq})^\top \boldsymbol{I}_2 \boldsymbol{i}_\mathrm{s}^{dq} \leqslant \widehat{\imath}_{\mathrm{s,max}}^2$

$$\implies \quad \mathbb{I}(\widehat{\imath}_{\mathrm{s,max}}) := \left\{\, \boldsymbol{i}_\mathrm{s}^{dq} \in \mathbb{R}^2 \;\middle|\; (\boldsymbol{i}_\mathrm{s}^{dq})^\top \boldsymbol{I}_2 \boldsymbol{i}_\mathrm{s}^{dq} - \widehat{\imath}_{\mathrm{s,max}}^2 \leqslant 0 \,\right\}$$

- (Linearized) Voltage elliptical area: $(u_\mathrm{s}^d)^2 + (u_\mathrm{s}^q)^2 \leqslant \widehat{u}_{\mathrm{s,max}}^2 \iff \|\boldsymbol{u}_\mathrm{s}^{dq}(\boldsymbol{i}_\mathrm{s}^{dq}, \omega_\mathrm{p}, \dots)\|^2 = \dots \leqslant \widehat{u}_{\mathrm{s,max}}^2$

$$\implies \quad \overline{\mathbb{V}}(\widehat{u}_{\mathrm{s,max}}) := \left\{\, \boldsymbol{i}_\mathrm{s}^{dq} \in \mathbb{R}^2 \;\middle|\; (\boldsymbol{i}_\mathrm{s}^{dq})^\top \overline{\boldsymbol{V}}(\overline{\omega}_\mathrm{p})\, \boldsymbol{i}_\mathrm{s}^{dq} + 2\,\overline{\boldsymbol{v}}(\overline{\omega}_\mathrm{p})^\top \boldsymbol{i}_\mathrm{s}^{dq} + \overline{\nu}(\overline{\omega}_\mathrm{p}, \widehat{u}_{\mathrm{s,max}}) \leqslant 0 \right\}$$

- (Linearized) Reference torque hyperbola: $m_\mathrm{m}(\boldsymbol{i}_\mathrm{s}^{dq}, \omega_\mathrm{p}, \dots) = \frac{3}{2} n_\mathrm{p} (\boldsymbol{i}_\mathrm{s}^{dq} + \boldsymbol{i}_{\mathrm{s,Fe}}^{dq})^\top \boldsymbol{J} \boldsymbol{\psi}_\mathrm{s}^{dq} \overset{!}{=} m_{\mathrm{m,ref}} \iff \dots$

$$\implies \quad \overline{\mathbb{T}}(m_{\mathrm{m,ref}}) := \left\{\, \boldsymbol{i}_\mathrm{s}^{dq} \in \mathbb{R}^2 \;\middle|\; (\boldsymbol{i}_\mathrm{s}^{dq})^\top \overline{\boldsymbol{T}} \boldsymbol{i}_\mathrm{s}^{dq} + 2\,\overline{\boldsymbol{t}}^\top \boldsymbol{i}_\mathrm{s}^{dq} - m_{\mathrm{m,ref}} = 0 \,\right\}$$

- ...

Optimal operation: OFTC with analytical ORCC

Sequential Quadratic Programming (SQP): Linearization, implicit formulation, optimization & intersection points

Step 3: Optimization problem with equality constraint

$$\max_{\boldsymbol{i}_{\mathrm{s}}^{dq}} -\Big(\underbrace{(\boldsymbol{i}_{\mathrm{s}}^{dq})^\top \boldsymbol{A}\boldsymbol{i}_{\mathrm{s}}^{dq} + 2\boldsymbol{a}^\top \boldsymbol{i}_{\mathrm{s}}^{dq} + \alpha}_{=:Q_A(\boldsymbol{i}_{\mathrm{s}}^{dq})}\Big) \text{ s.t. } \underbrace{(\boldsymbol{i}_{\mathrm{s}}^{dq})^\top \boldsymbol{B}\boldsymbol{i}_{\mathrm{s}}^{dq} + 2\boldsymbol{b}^\top \boldsymbol{i}_{\mathrm{s}}^{dq} + \beta}_{=:Q_B(\boldsymbol{i}_{\mathrm{s}}^{dq})} = 0$$

$\Longrightarrow$ Hyperbolas for e.g. MTPC, MTPL or MTPV (with $R_{\mathrm{s}}, R_{\mathrm{s,Fe}} \neq 0$ & $L_{\mathrm{s,m}} \neq 0$, etc.)

Step 4: Intersection of two quadrics (e.g. voltage ellipse and current circle)

$$\boldsymbol{i}_{\mathrm{s,ref}}^{dq} := \arg\min_{\|\boldsymbol{i}_{\mathrm{s}}^{dq}\|} \left\{ \boldsymbol{i}_{\mathrm{s}}^{dq} \in \mathbb{R}^2 \;\middle|\; Q_A(\boldsymbol{i}_{\mathrm{s}}^{dq}) = 0 \;\wedge\; Q_B(\boldsymbol{i}_{\mathrm{s}}^{dq}) = 0 \right\}$$

$\Longrightarrow$ Optimal operation point ★ (reference current; iteration possibly necessary)

Both lead to subproblem of solving a fourth-order (quartic) polynomial

$$\chi(\lambda) := c_4\,\lambda^4 + c_3\,\lambda^3 + c_2\,\lambda^2 + c_1\,\lambda + c_0 \overset{!}{=} 0$$

$\Longrightarrow$ Analytical solutions exist (e.g. Euler's solution, see [173])

Outline

Optimal operation: OFTC with analytical ORCC

Operation strategies: Overview

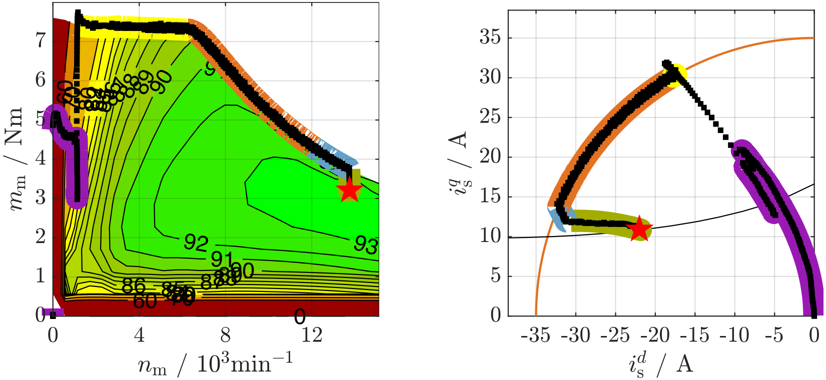

- Maximum Torque per Losses (MTPL) [ ] (or Maximum Torque per Current (MTPC) [ ])
- Maximum Current (MC) [ ] and Maximum Current extended (MC_ext) [ ]
- Maximum Torque per Voltage (MTPV) [ ] (or Maximum Torque per Flux (MTPF)))
- Field Weakening (FW) [ ]

Optimal operation: OFTC with analytical ORCC

Operation strategies: Maximum Torque per Current (**MTPC** @ $0 \cdot \omega_{\mathrm{m,R}}$; $m_{\mathrm{m,ref}}$ **feasible**)

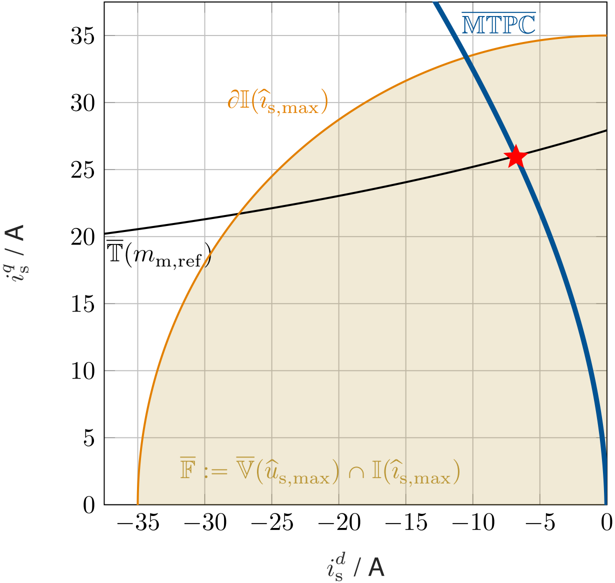

Optimization problem

$$\max_{\boldsymbol{i}_{\mathrm{s}}^{dq} \in \overline{\mathbb{F}}} -p_{\mathrm{s,Cu}}(\boldsymbol{i}_{\mathrm{s}}^{dq}) \quad \text{s.t.}$$

$$\underbrace{(\boldsymbol{i}_{\mathrm{s}}^{dq})^\top \overline{\boldsymbol{T}} \boldsymbol{i}_{\mathrm{s}}^{dq} + 2\,\overline{\boldsymbol{t}}^\top \boldsymbol{i}_{\mathrm{s}}^{dq}}_{\approx m_{\mathrm{m}}(\boldsymbol{i}_{\mathrm{s}}^{dq})} - m_{\mathrm{m,ref}} = 0$$

Solution set

$$\overline{\mathbb{MTPC}}(\overline{\boldsymbol{i}}_{\mathrm{s}}^{dq}, \overline{\omega}_{\mathrm{p}}, \dots) := \Big\{ \boldsymbol{i}_{\mathrm{s}}^{dq} \in \mathbb{R}^2 \;\Big|\; (\boldsymbol{i}_{\mathrm{s}}^{dq})^\top \overline{\boldsymbol{M}}_{\mathrm{C}}\, \boldsymbol{i}_{\mathrm{s}}^{dq} + 2\,\overline{\boldsymbol{m}}_{\mathrm{C}}^\top \boldsymbol{i}_{\mathrm{s}}^{dq} = 0 \Big\}$$

Optimal reference currents (★)

$$\boldsymbol{i}_{\mathrm{s,MTPC}}^{dq} = \overline{\mathbb{MTPC}} \cap \overline{\mathbb{T}}(m_{\mathrm{m,ref}})$$

Optimal operation: OFTC with analytical ORCC

Operation strategies: Maximum Torque per Losses (**MTPL** @ $1 \cdot \omega_{\mathrm{m,R}}$; $m_{\mathrm{m,ref}}$ **feasible**)

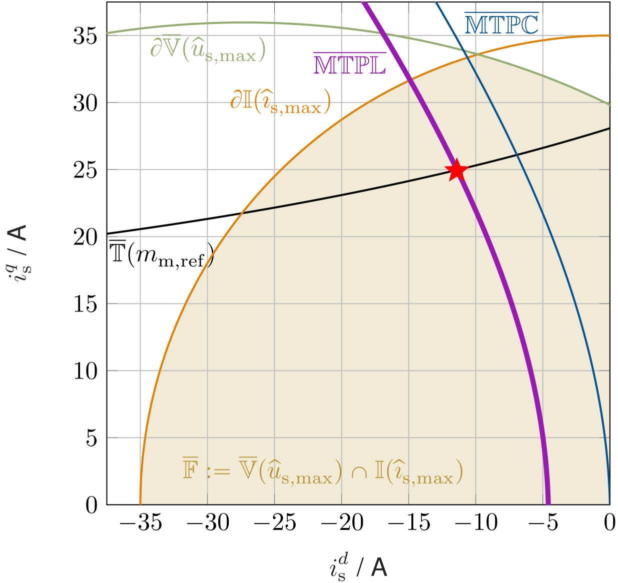

Optimization problem

$$\max_{\boldsymbol{i}_{\mathrm{s}}^{dq} \in \overline{\mathbb{F}}} -p_{\mathrm{s,Cu}}(\boldsymbol{i}_{\mathrm{s}}^{dq}) - p_{\mathrm{s,Fe}}(\boldsymbol{i}_{\mathrm{s}}^{dq}) \quad \text{s.t.}$$

$$\underbrace{(\boldsymbol{i}_{\mathrm{s}}^{dq})^\top \overline{\boldsymbol{T}} \boldsymbol{i}_{\mathrm{s}}^{dq} + 2\,\overline{\boldsymbol{t}}^\top \boldsymbol{i}_{\mathrm{s}}^{dq}}_{\approx m_{\mathrm{m}}(\boldsymbol{i}_{\mathrm{s}}^{dq})} - m_{\mathrm{m,ref}} = 0$$

Solution set

$$\overline{\mathrm{MTPL}}(\overline{\boldsymbol{i}}_{\mathrm{s}}^{dq}, \overline{\omega}_{\mathrm{p}}, \ldots) := \Big\{ \boldsymbol{i}_{\mathrm{s}}^{dq} \in \mathbb{R}^2 \;\Big|\; (\boldsymbol{i}_{\mathrm{s}}^{dq})^\top \overline{\boldsymbol{M}}_{\mathrm{L}}\, \boldsymbol{i}_{\mathrm{s}}^{dq} + 2\,\overline{\boldsymbol{m}}_{\mathrm{L}}^\top \boldsymbol{i}_{\mathrm{s}}^{dq} + \overline{\mu}_{\mathrm{L}} = 0 \Big\}$$

Optimal reference currents (★)

$$\boldsymbol{i}_{\mathrm{s,MTPL}}^{dq} = \overline{\mathrm{MTPL}} \cap \overline{\mathbb{T}}(m_{\mathrm{m,ref}})$$

Optimal operation: OFTC with analytical ORCC

Operation strategies: Maximum Current (**MC** @ $2 \cdot \omega_{\mathrm{m,R}}$; $m_{\mathrm{m,ref}}$ **not feasible**)

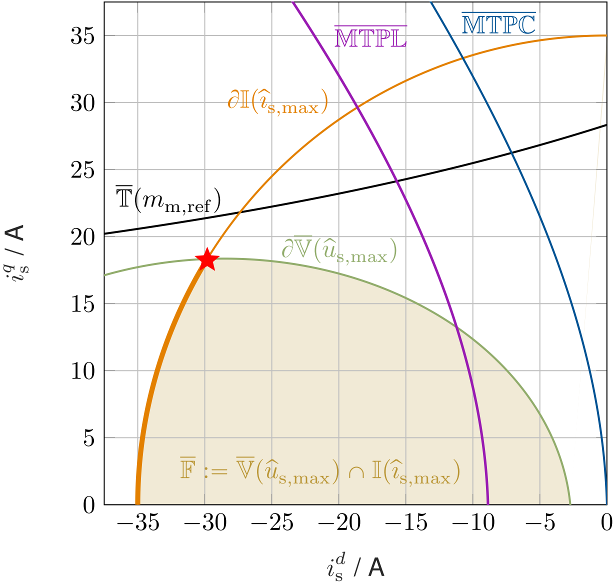

Optimization problem

$$\max_{\boldsymbol{i}_s^{dq} \in \overline{\mathbb{F}}} |(m_m(\boldsymbol{i}_s^{dq}))| \quad \text{s.t.}$$

$$\operatorname{sign}(m_m) = \operatorname{sign}(m_{m,\mathrm{ref}})$$

Feasible set

$$\overline{\mathbb{MC}}(\overline{\boldsymbol{i}}_s^{dq}, \overline{\omega}_p, \ldots, \widehat{u}_{s,\max}, \widehat{\imath}_{s,\max}) := \overline{\mathbb{V}}(\widehat{u}_{s,\max}) \cap \partial\mathbb{I}(\widehat{\imath}_{s,\max})$$

Optimal current reference (★)

$$\boldsymbol{i}_{s,\mathrm{MC}}^{dq} = \partial\overline{\mathbb{V}}(\widehat{u}_{s,\max}) \cap \partial\mathbb{I}(\widehat{\imath}_{s,\max})$$

Optimal operation: OFTC with analytical ORCC

Operation strategies: Maximum Current extended (**MC**$_{\mathrm{ext}}$ @ $1 \cdot \omega_{\mathrm{m,R}}$; $m_{\mathrm{m,ref}}$ **feasible**)

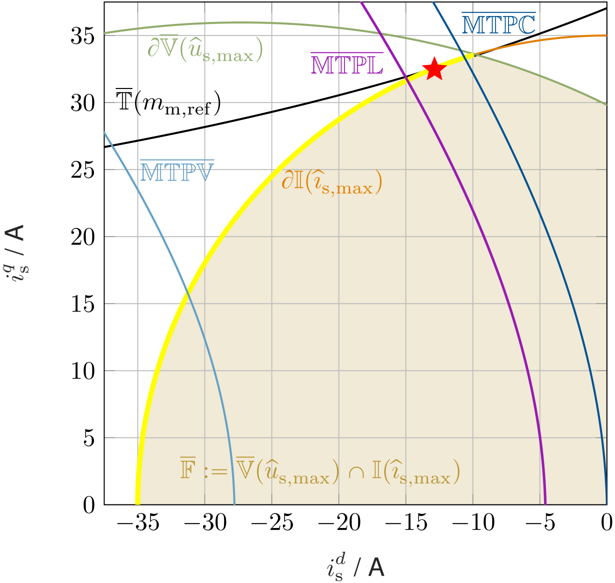

Optimization problem

$$\max_{\boldsymbol{i}_{\mathrm{s}}^{dq} \in \overline{\mathbb{F}}} |(m_{\mathrm{m}}(\boldsymbol{i}_{\mathrm{s}}^{dq}))| \quad \text{s.t.}$$
$$\mathrm{sign}(m_{\mathrm{m}}) = \mathrm{sign}(m_{\mathrm{m,ref}})$$

Solution set

$$\overline{\mathbb{MC}}_{\mathrm{ext}}(\overline{\boldsymbol{i}}_{\mathrm{s}}^{dq}, \overline{\omega}_{\mathrm{p}}, \ldots, \widehat{u}_{\mathrm{s,max}}, \widehat{\imath}_{\mathrm{s,max}}) := \overline{\mathbb{V}}(\widehat{u}_{\mathrm{s,max}}) \cap \partial\mathbb{I}(\widehat{\imath}_{\mathrm{s,max}})$$

Optimal current reference (★)

$$\boldsymbol{i}_{\mathrm{s,MC_{ext}}}^{dq} = \overline{\mathbb{T}}(m_{\mathrm{m,ref}}) \cap \partial\mathbb{I}(\widehat{\imath}_{\mathrm{s,max}})$$

with $i_{\mathrm{s,MTPL}}^{d} < i_{\mathrm{s,MC_{ext}}}^{d}$

Optimal operation: OFTC with analytical ORCC

Operation strategies: Field Weakening (**FW** @ $1.40 \cdot \omega_{\mathrm{m,R}}$; $m_{\mathrm{m,ref}}$ **feasible**)

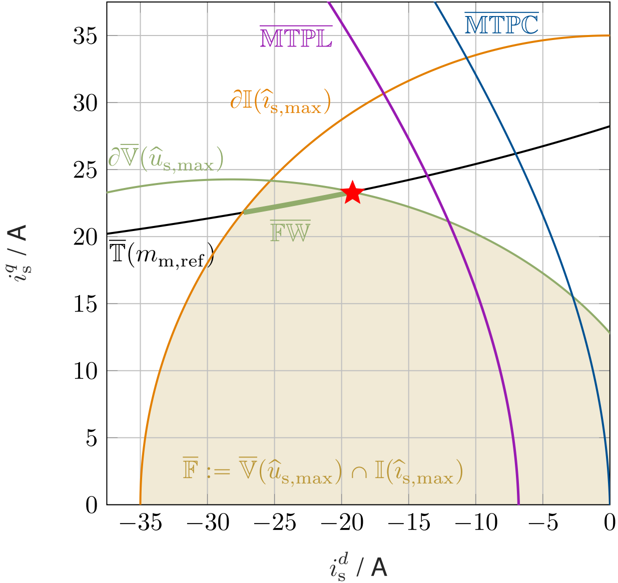

Optimization problem

$$\max_{\boldsymbol{i}_{\mathrm{s}}^{dq} \in \overline{\mathbb{F}}} -p_{\mathrm{s,Cu}}(\boldsymbol{i}_{\mathrm{s}}^{dq}) - p_{\mathrm{s,Fe}}(\boldsymbol{i}_{\mathrm{s}}^{dq}) \quad \text{s.t.}$$

$$\underbrace{(\boldsymbol{i}_{\mathrm{s}}^{dq})^{\top} \boldsymbol{T} \boldsymbol{i}_{\mathrm{s}}^{dq} + 2\,\boldsymbol{t}^{\top} \boldsymbol{i}_{\mathrm{s}}^{dq}}_{=m_{\mathrm{m}}(\boldsymbol{i}_{\mathrm{s}}^{dq})} - m_{\mathrm{m,ref}} = 0$$

Feasible set

$$\overline{\mathrm{FW}}(\overline{\boldsymbol{i}}_{\mathrm{s}}^{dq}, \overline{\omega}_{\mathrm{p}}, \ldots, m_{\mathrm{m,ref}}, \widehat{u}_{\mathrm{s,max}}, \widehat{\imath}_{\mathrm{s,max}}) := \overline{\mathbb{F}}(\widehat{u}_{\mathrm{s,max}}, \widehat{\imath}_{\mathrm{s,max}}) \cap \overline{\mathbb{T}}(m_{\mathrm{m,ref}})$$

Optimal reference currents (★)

$$\boldsymbol{i}_{\mathrm{s,FW}}^{dq} = \partial\overline{\mathbb{V}}(\widehat{u}_{\mathrm{s,max}}) \cap \overline{\mathbb{T}}(m_{\mathrm{m,ref}})$$

Optimal operation: OFTC with analytical ORCC

Operation strategies: Maximum Torque per Voltage (**MTPV** @ $3.50 \cdot \omega_{\mathrm{m,R}}$; $m_{\mathrm{m,ref}}$ **not feasible**)

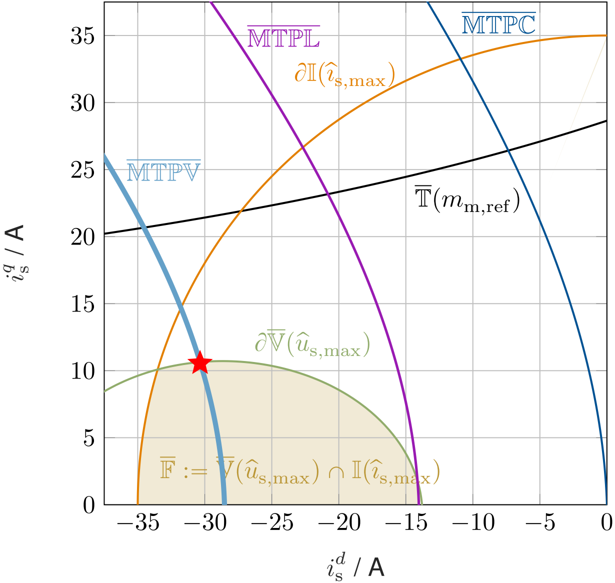

Optimization problem

$$\max_{\boldsymbol{i}_{\mathrm{s}}^{dq} \in \overline{\mathbb{F}}} -\left\|\boldsymbol{u}_{\mathrm{s}}^{dq}(\boldsymbol{i}_{\mathrm{s}}^{dq})\right\|^2 \quad \text{s.t.}$$

$$\underbrace{(\boldsymbol{i}_{\mathrm{s}}^{dq})^\top \overline{\boldsymbol{T}} \boldsymbol{i}_{\mathrm{s}}^{dq} + 2\,\overline{\boldsymbol{t}}^\top \boldsymbol{i}_{\mathrm{s}}^{dq}}_{=m_{\mathrm{m}}(\boldsymbol{i}_{\mathrm{s}}^{dq})} - m_{\mathrm{m,ref}} = 0$$

Solution set

$$\overline{\mathbb{MTPV}}(\overline{\boldsymbol{i}}_{\mathrm{s}}^{dq}, \overline{\omega}_{\mathrm{p}}, \cdots) := \left\{ \boldsymbol{i}_{\mathrm{s}}^{dq} \in \mathbb{R}^2 \;\middle|\; (\boldsymbol{i}_{\mathrm{s}}^{dq})^\top \overline{\boldsymbol{M}}_{\mathrm{V}}\, \boldsymbol{i}_{\mathrm{s}}^{dq} + 2\,\overline{\boldsymbol{m}}_{\mathrm{V}}^\top \boldsymbol{i}_{\mathrm{s}}^{dq} + \overline{\mu}_{\mathrm{V}} = 0 \right\}$$

Optimal reference currents (★)

$$\boldsymbol{i}_{\mathrm{s,MTPV}}^{dq} = \overline{\mathbb{MTPV}} \cap \partial\overline{\mathbb{V}}(\widehat{u}_{\mathrm{s,max}})$$

Outline

Optimal operation: OFTC with analytical ORCC

Operation management: Decision tree

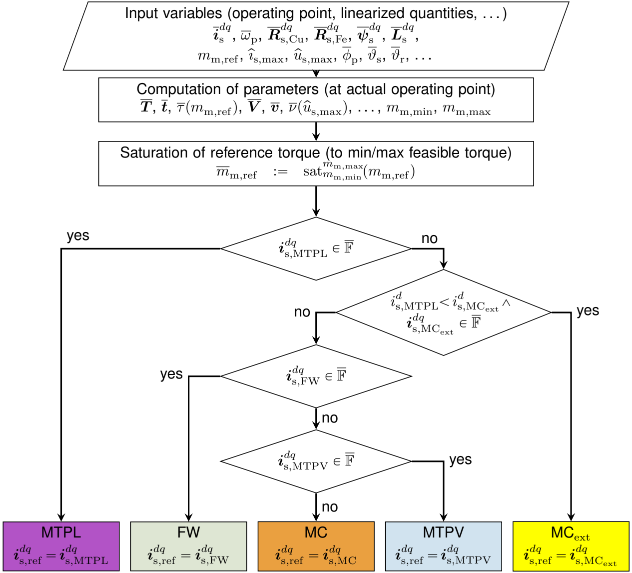

Outline

Optimal operation: OFTC with analytical ORCC

Implementation results: Exemplary laboratory setup

Reluctance SM (RSM) and Permanent-magnet SM

Host PC (rapid prototyping)

Real-time system and VSIs

Optimal operation: OFTC with analytical ORCC

Implementation results: Nonlinear maps of torque, flux linkages and differential inductances of RSM ($9.6\,\mathrm{kW}@1\,500\,\mathrm{rpm}$)

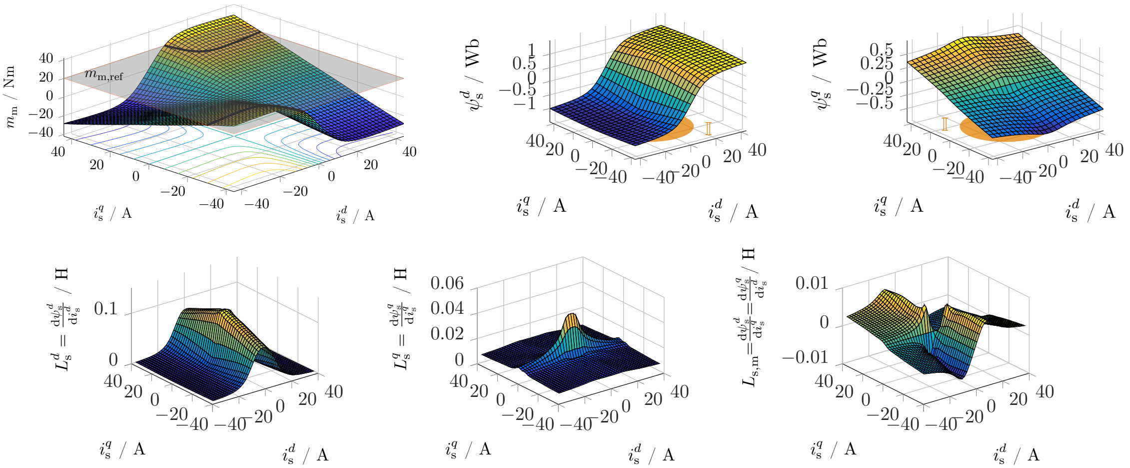

Optimal operation: OFTC with analytical ORCC

Implementation results: Comparison of numerical and analytical solutions for MTPC of RSM ($9.6\,\mathrm{kW}@1\,500\,\mathrm{rpm}$)

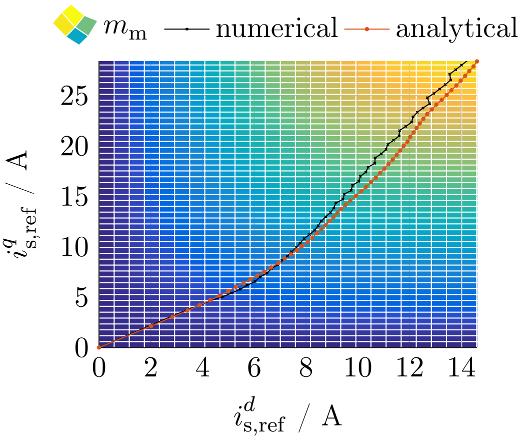

Cartesian coordinates

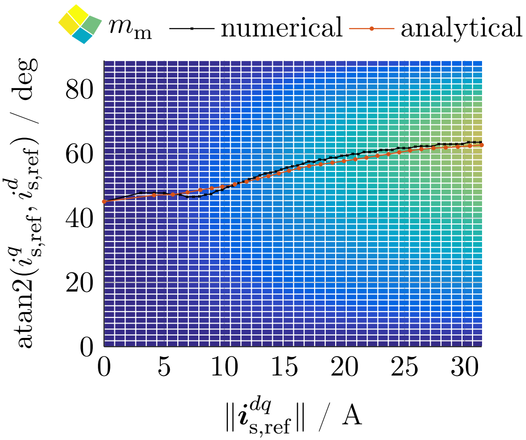

polar coordinates

Optimal operation: OFTC with analytical ORCC

Implementation results: Comparison of computational load (Euler's solution for fourth-order polynomials)

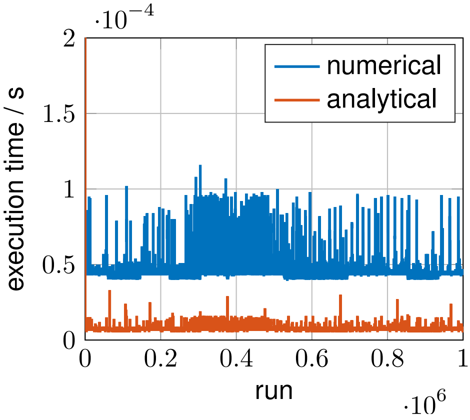

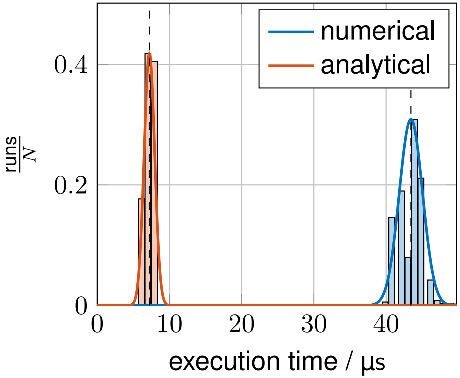

- Execution times for $N = 10^6$ runs (downsampled by factor 100)
- Standard deviations $\sigma_n = 1.61 \cdot 10^{-6}$ s and $\sigma_a = 0.73 \cdot 10^{-6}$ s
- Average execution times $\mu_n = 43.4 \cdot 10^{-6}$ s and $\mu_a = 7.23 \cdot 10^{-6}$ s ($>$**6x faster**)

Optimal operation: OFTC with analytical ORCC

Implementation results: Implementation by colleagues for PME-RSM $(4.5\,\mathrm{kW@1\,500\,rpm})$

$[\max\left(L_\mathrm{s}^d(\boldsymbol{i}_\mathrm{s}^{dq})/L_\mathrm{s}^q(\boldsymbol{i}_\mathrm{s}^{dq})\right) = 1.43]$ [174]

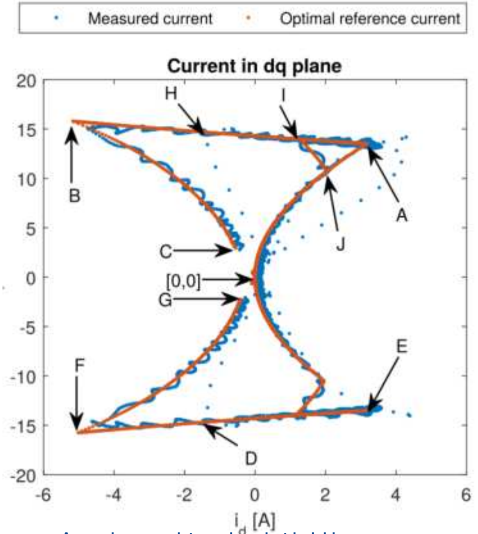

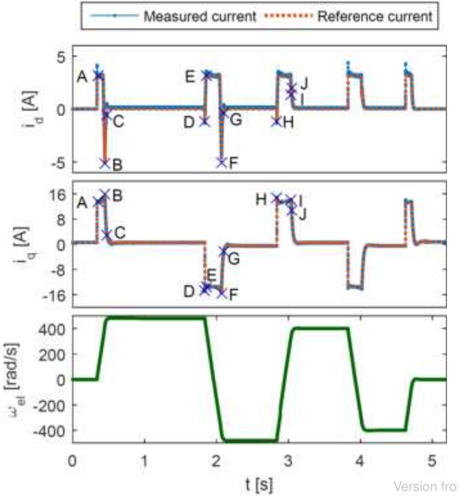

Optimal operation: OFTC with analytical ORCC

Implementation results: Efficiency enhancements considering iron losses for IPMSM (generator mode) [15]

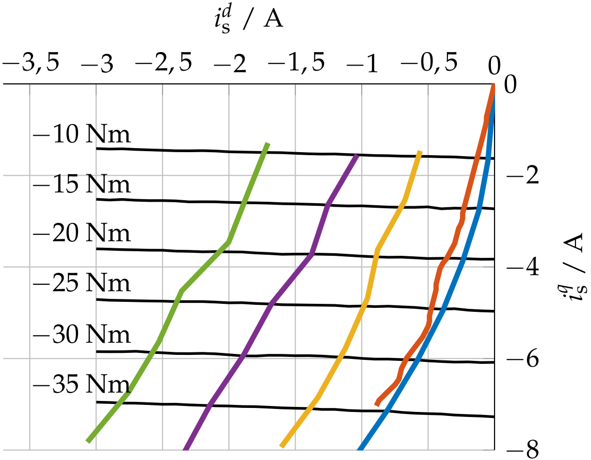

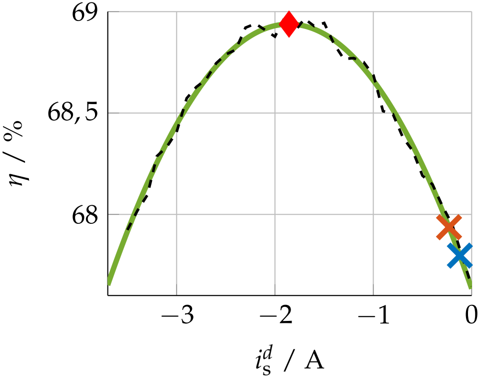

Optimal operation: OFTC with analytical ORCC

Implementation results: Nonlinear maps of torque, flux linkages, differential inductances and iron resistance of IPMSM ($3.9\,$kW@$5\,500\,$rpm)

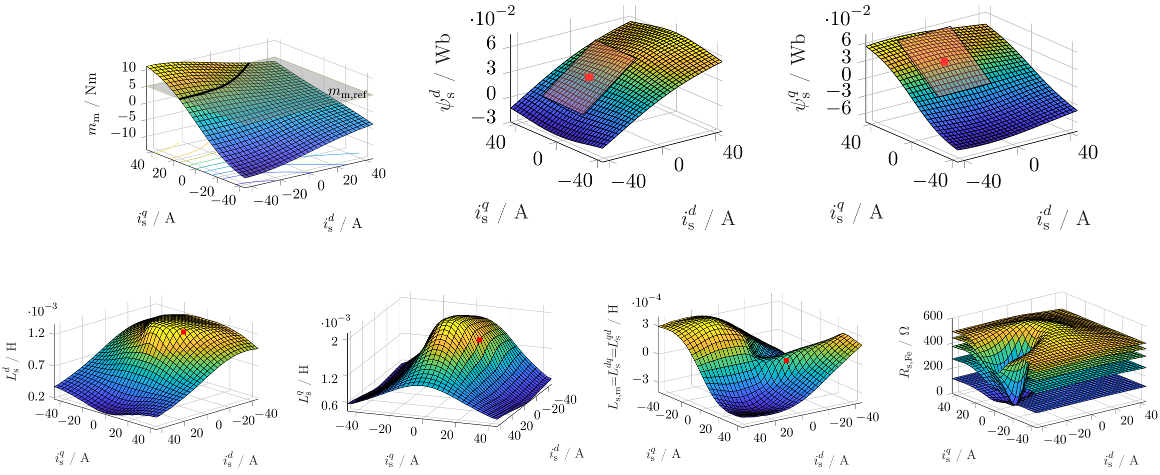

Optimal operation: OFTC with analytical ORCC

Implementation results: Animation of optimal operation of IPMSM ($3.9\,\mathrm{kW}@5\,500\,\mathrm{rpm}$)

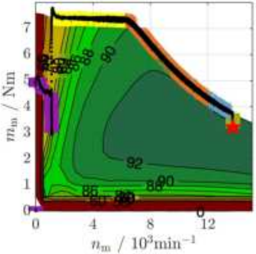

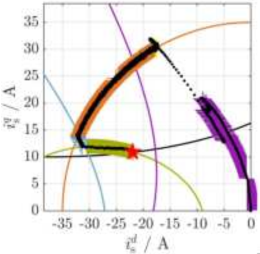

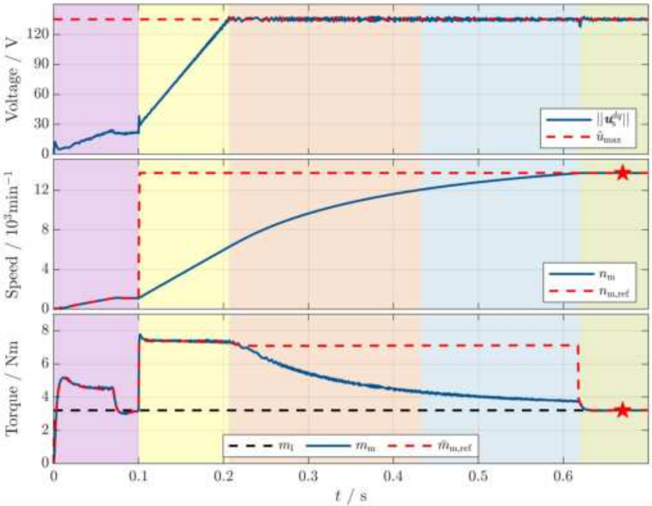

MTPL [ ]

MC$_{\mathrm{ext}}$ [ ]

MC [ ]

MTPV [ ]

FW [ ]

Optimal operation: OFTC with analytical ORCC

Implementation results: Comparison of MTPL [ ] & MTPC [ ] for **four** operating points (OPs) of IPMSM (3.9 kW@$5\,500$ rpm)

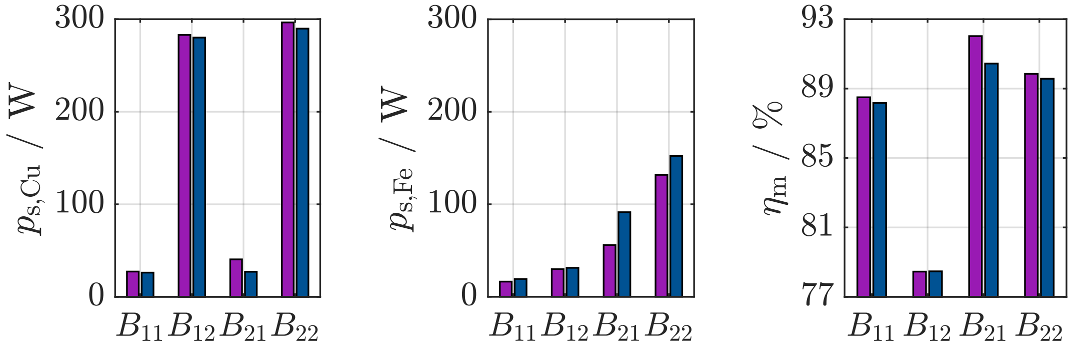

OP	Speed	Torque
B_{11}	$30\%\, n_{\mathrm{m,R}}$	$30\%\, m_{\mathrm{m,R}}$
B_{12}	$30\%\, n_{\mathrm{m,R}}$	$100\%\, m_{\mathrm{m,R}}$
B_{21}	$100\%\, n_{\mathrm{m,R}}$	$30\%\, m_{\mathrm{m,R}}$
B_{22}	$100\%\, n_{\mathrm{m,R}}$	$100\%\, m_{\mathrm{m,R}}$

- Copper losses increase with torque
- Iron losses increase with speed *and* torque
- MTPL outperforms MTPC for three OPs (equal for B_{12})
- highest efficiency enhancement for high speeds and low(er) torque (i.e., B_{21} with $\Delta\eta_{\mathrm{m}} > 2\%$)

Outline

Outline

Optimal operation: OFTC with ANN-based ORCC

Overview: OFTC with Artificial Neural Network (ANN)-based ORCC within the control system

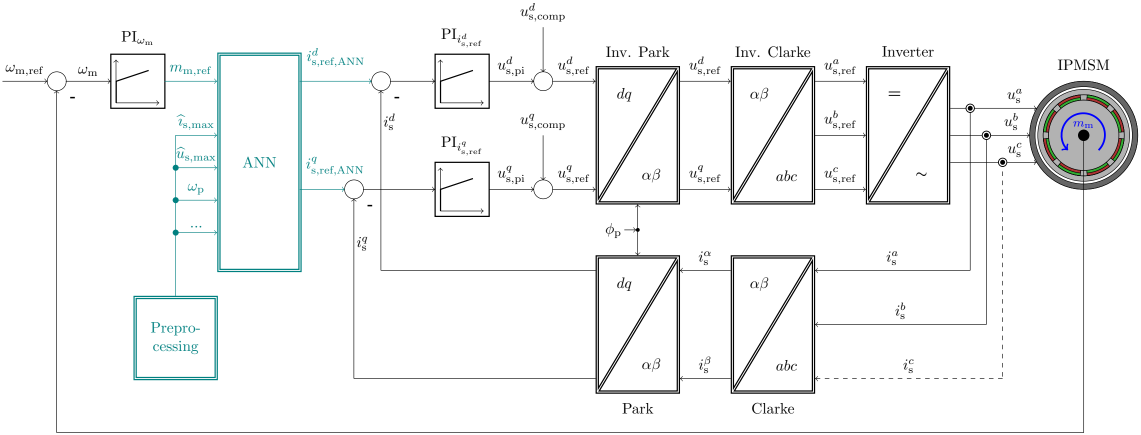

Outline

Optimal operation: OFTC with ANN-based ORCC

Artificial Neural Network Design: Used ANN topology

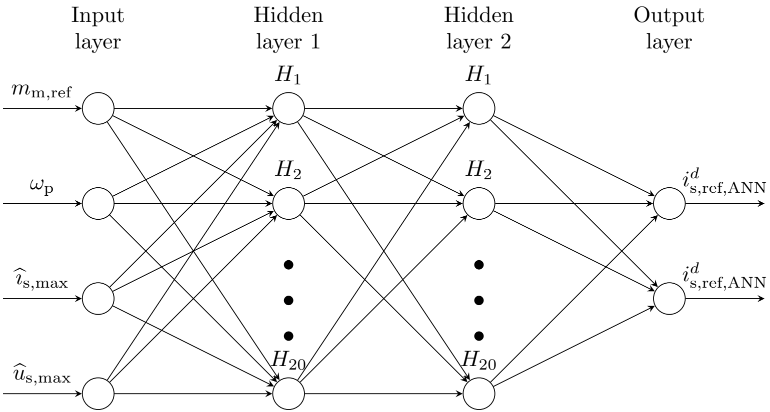

$$\hat{\boldsymbol{y}} = \begin{pmatrix} i^{d}_{\mathrm{ref,ANN}} \\ i^{q}_{\mathrm{ref,ANN}} \end{pmatrix} = \boldsymbol{\Phi}_4\Bigg(\boldsymbol{W}_4\boldsymbol{\Phi}_3\Bigg(\boldsymbol{W}_3\boldsymbol{\Phi}_2\Bigg(\boldsymbol{W}_2\boldsymbol{\Phi}_1\Bigg(\boldsymbol{W}_1 \underbrace{\begin{pmatrix} m_{\mathrm{m,ref}} \\ \omega_{\mathrm{p}} \\ \widehat{\imath}_{\mathrm{s,max}} \\ \widehat{u}_{\mathrm{s,max}} \end{pmatrix}}_{=:\boldsymbol{x}} + \boldsymbol{b}_1\Bigg) + \boldsymbol{b}_2\Bigg)\Bigg) + \boldsymbol{b}_3\Bigg) + \boldsymbol{b}_4\Bigg).$$

Optimal operation: OFTC with ANN-based ORCC

Artificial Neural Network Design: Possible and used ANN activation function(s)

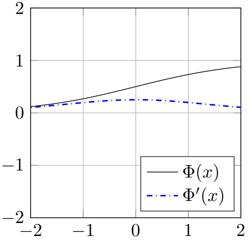

(a) Sigmoid.

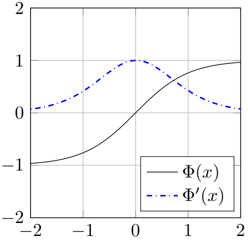

(b) Tangens hyperbolicus.

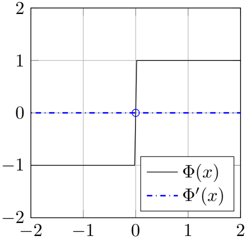

(c) Signum (sign).

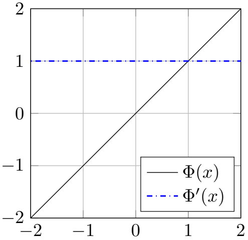

(d) **Identity**.

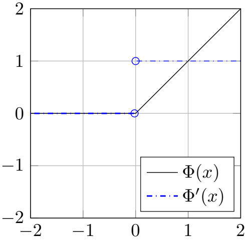

(e) **Rectified Linear Unit (ReLU)**.

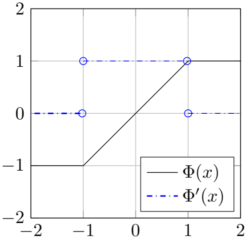

(f) Saturation.

Optimal operation: OFTC with ANN-based ORCC

Artificial Neural Network Design: ANN training and validation

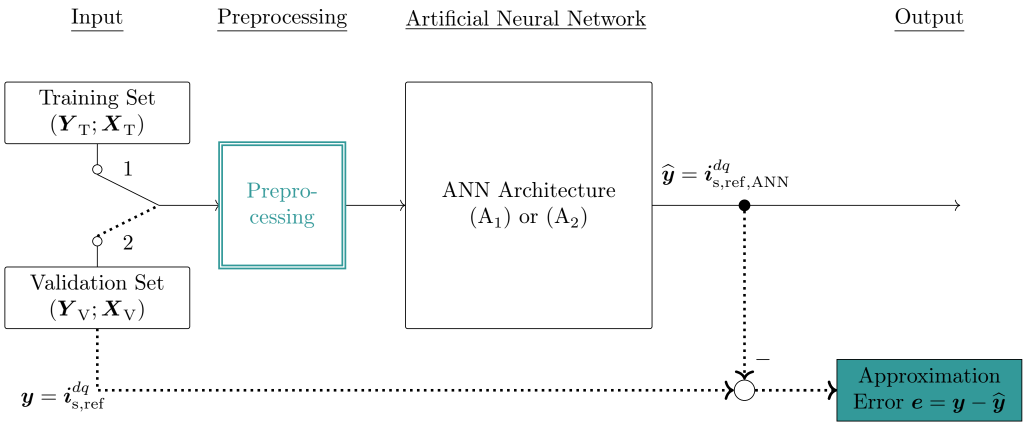

Optimal operation: OFTC with ANN-based ORCC

Artificial Neural Network Design: Estimation accuracy (norm of estimation error) versus floating point operations

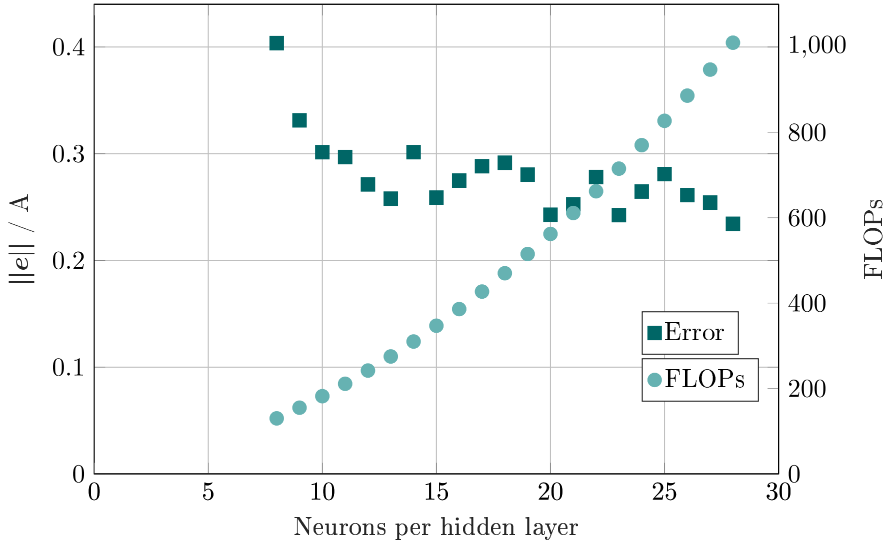

Outline

Optimal operation: OFTC with ANN-based ORCC

Implementation results: Time series

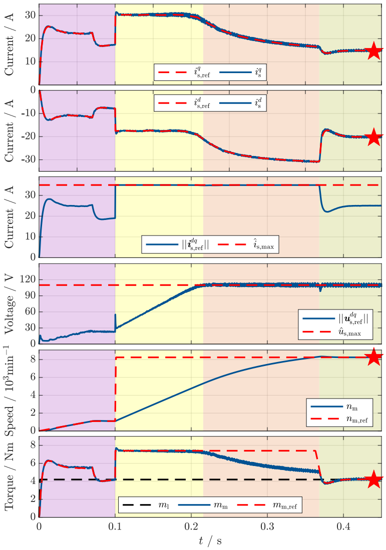

(a) OFTC with analytical ORCC (OFTC$_{\mathrm{ANA}}$).

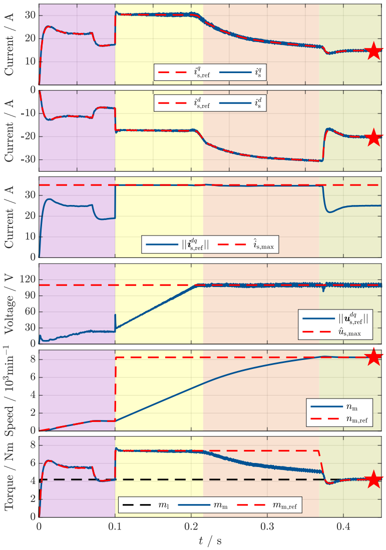

(b) ANN-based OFTC (OFTC$_{\mathrm{ANN}}$).

Optimal operation: OFTC with ANN-based ORCC

Implementation results: Speed-torque map

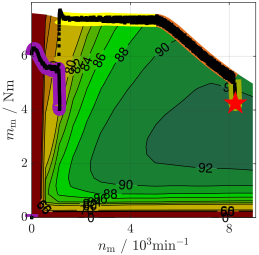

(a) Speed-torque map ($\mathrm{OFTC}_{\mathrm{ANA}}$).

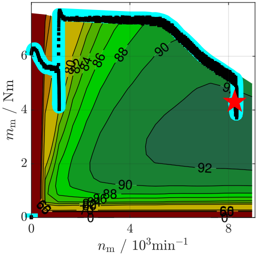

(b) Speed-torque map ($\mathrm{OFTC}_{\mathrm{ANN}}$).

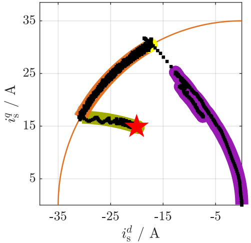

(c) Current locus ($\mathrm{OFTC}_{\mathrm{ANA}}$).

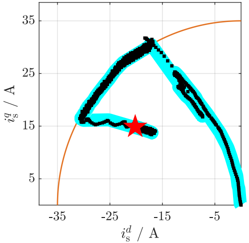

(d) Current locus ($\mathrm{OFTC}_{\mathrm{ANN}}$).

Optimal operation: OFTC with ANN-based ORCC

Implementation results: Performance comparison and execution times

Performance measure	**X=OFTC$_{\mathrm{LUT}}$**	**X=OFTC$_{\mathrm{NUM}}$**	**X=OFTC$_{\mathrm{ANA}}$**	**X=OFTC$_{\mathrm{ANN}}$**
$\int \lvert i^d_{\mathrm{s,ref,OFTC_{NLP}}} - i^d_{\mathrm{s,ref,X}} \rvert \mathrm{d}t$	$0.176\,\mathrm{As}$	$0.186\,\mathrm{As}$	$0.384\,\mathrm{As}$	$0.227\,\mathrm{As}$
$\int \lvert i^q_{\mathrm{s,ref,OFTC_{NLP}}} - i^q_{\mathrm{s,ref,X}} \rvert \mathrm{d}t$	$0.195\,\mathrm{As}$	$0.207\,\mathrm{As}$	$0.256\,\mathrm{As}$	$0.213\,\mathrm{As}$
$\int \lvert m_{\mathrm{ref,X}} - m_{\mathrm{m}} \rvert \mathrm{d}t$	$0.018\,\mathrm{Nms}$	$0.017\,\mathrm{Nms}$	$0.026\,\mathrm{Nms}$	$0.020\,\mathrm{Nms}$
$\int \lvert \widehat{u}_{\mathrm{s,max}} - \lVert \boldsymbol{u}^{dq}_{\mathrm{s,ref,X}} \rVert \rvert \mathrm{d}t$	$0.445\,\mathrm{Vs}$	$0.446\,\mathrm{Vs}$	$0.454\,\mathrm{Vs}$	$0.459\,\mathrm{Vs}$
$\int \lvert \widehat{\imath}_{\mathrm{s,max}} - \lVert \boldsymbol{i}^{dq}_{\mathrm{s,ref,X}} \rVert \rvert \mathrm{d}t$	$0.010\,\mathrm{As}$	$0.000\,\mathrm{As}$	$0.000\,\mathrm{As}$	$0.059\,\mathrm{As}$
$\int \lvert n_{\mathrm{m,ref}} - n_{\mathrm{m,X}} \rvert \mathrm{d}t$	$752.4\,\frac{\mathrm{s}}{\mathrm{min}}$	$750.9\,\frac{\mathrm{s}}{\mathrm{min}}$	$752.6\,\frac{\mathrm{s}}{\mathrm{min}}$	$757.8\,\frac{\mathrm{s}}{\mathrm{min}}$
$\bar{t}_{\mathrm{exec,X}}$	$2\,734.782\,\mathrm{\mu s}$	$448.745\,\mathrm{\mu s}$	$439.671\,\mathrm{\mu s}$	$5.855\,\mathrm{\mu s}$

Outline

Conclusion

Summary and future work

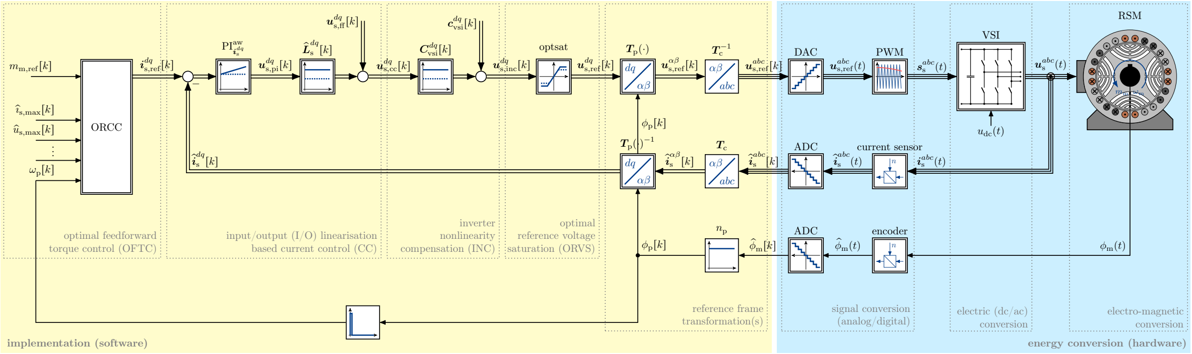

To take home

- **Generic** approach to modern electrical drive systems
  - **Nonlinear modelling**
  - **Dynamic simulation**
  - **High-performance control**
  - **Optimal operation**

Future work

- more extensive experimental validation
- impact of (parameter/modelling/alignment) uncertainties
- new book series “**Moderne elektrische Antriebe” with Springer** in preparation (first volume to appear in 2025)

References

Journal article (published 2022; see doi: 10.3390/en15051838)

energies

MDPI

Article

Artificial Neural Network Based Optimal Feedforward Torque Control of Interior Permanent Magnet Synchronous Machines: A Feasibility Study and Comparison with the State-of-the-Art

Max A. Buettner †, Niklas Monzen † and Christoph M. Hackl *

Department of Electrical Engineering and Information Technology, Hochschule München (HM) University of Applied Sciences, Lothstr. 64, 80335 München, Germany; max.buettner@hm.edu (M.A.B.); niklas.monzen@hm.edu (N.M.)

* Correspondence: christoph.hackl@hm.edu

† These authors contributed equally to this work.

Citation: Buettner, M.A.; Monzen, N.;

Abstract: A novel Artificial Neural Network (ANN) Based Optimal Feedforward Torque Control (OFTC) strategy is proposed which, after proper ANN design, training and validation, allows to analytically compute the optimal reference currents (minimizing copper and iron losses) for Interior Permanent Magnet Synchronous Machines (IPMSMs) with highly operating point dependent nonlinear electric and magnetic characteristics. In contrast to conventional OFTC, which either utilizes large look-up tables (LUTs; with more than three input parameters) or computes the optimal reference currents numerically or analytically but iteratively (due to the necessary online linearization), the proposed ANN-based OFTC strategy does not require iterations nor a decision tree to find the optimal operation strategy such as e.g., Maximum Torque per Losses (MTPL), Maximum Current (MC) or Field Weakening (FW). Therefore, it is (much) faster and easier to implement while (i) still

References

Journal article [105] (published 2017; doi: 10.1080/00207179.2017.1338359)

INTERNATIONAL JOURNAL OF CONTROL, 2017
https://doi.org/10.1080/00207179.2017.1338359

Taylor & Francis
Taylor & Francis Group

OPEN ACCESS Check for updates

A unified theory for optimal feedforward torque control of anisotropic synchronous machines

Hisham Eldeeb[a], Christoph M. Hackl[a,*], Lorenz Horlbeck[b] and Julian Kullick[a]

[a]Research Group 'Control of Renewable Energy Systems (CRES)', Munich School of Engineering (MSE), Technical University of Munich (TUM), Munich, Germany; [b]Institute of Automotive Technology (FTM), Technical University of Munich (TUM), Munich, Germany

ABSTRACT

A unified theory for optimal feedforward torque control of anisotropic synchronous machines with *non-negligible stator resistance* and *mutual inductance* is presented which allows to *analytically* compute (1) the optimal direct and quadrature reference currents for all operating strategies, such as maximum torque per current (MTPC), maximum current, field weakening, maximum torque per voltage (MTPV) or maximum torque per flux (MTPF), and (2) the transition points indicating when to switch between the operating strategies due to speed, voltage or current constraints. The analytical solutions allow for an (almost) instantaneous selection and computation of actual operation strategy and corresponding reference currents. Numerical methods (approximating these solutions only) are *no longer* required. The unified theory is based on one simple idea: all optimisation problems, their respective constraints and the computation of the intersection point(s) of voltage ellipse, current circle or torque, MTPC, MTPV, MTPF hyperbolas are reformulated implicitly as *quadrics* which allows to invoke the Lagrangian formalism and to find the roots of fourth-order polynomials analytically. The proposed theory is suitable for any anisotropic synchronous machine. Implementation and measurement results illustrate effectiveness and applicability of the theoretical findings in real world.

ARTICLE HISTORY
Received 18 March 2017
Accepted 31 May 2017

KEYWORDS
Maximum torque per ampere (MTPA); maximum torque per current (MTPC); maximum torque per voltage (MTPV); maximum torque per flux (MTPF); maximum current (MC); field weakening (FW); analytical solution; optimal feedforward torque control; efficiency; copper losses; anisotropy; synchronous machine; interior

References

Conference publication (published in ICIT 2021 proceedings; see doi: 10.1109/icit46573.2021.9453497)

Generic loss minimization for nonlinear synchronous machines by analytical computation of optimal reference currents considering copper and iron losses

Christoph Hackl, Julian Kullick and Niklas Monzen

Laboratory for Mechatronic and Renewable Energy Systems (LMRES)

Munich University of Applied Sciences (MUAS)

Munich, Germany

{christoph.hackl, julian.kullick, niklas.monzen}@hm.edu

***Abstract*—The unified theory introduced in [1] allows to solve *analytically* the optimal feedforward torque control (OFTC) problem of anisotropic synchronous machines (SMs). In this paper, the theory is extended by considering relevant machine nonlinearities and incorporating copper *and* iron losses, thus minimizing the overall (steady-state) losses in the machine. Instead of the well known maximum torque per current (MTPC) operation strategy, *maximum torque per losses (MTPL)* is realized. The unified theory for the derivation of the analytical solution is briefly recapitulated. Moreover, current *and* speed dependent iron losses, as well as magnetic saturation and cross-coupling effects are considered. The resulting nonlinear optimization problem is solved via online linearization of the relevant expressions**

for synchronous machines (SMs) with anisotropic rotor designs, e.g. interior permanent magnet synchronous machines (IPMSMs), reluctance synchronous machines (RSMs) or PM-assisted RMSs (PMA-RSMs), efficiency can be increased by optimal feedforward torque control (OFTC) [3, 4].

The main idea of OFTC is to exploit the ambiguity in the selection of the stator current's *direct* and *quadrature* components (producing the same amount of torque), such that losses are minimized while physical constraints are satisfied (e.g. current or voltage limits). Depending on the actual operating conditions, different optimization problems may be formulated

References

Conference publication (published in ISIE 2021 proceedings; see doi: 10.1109/ISIE45552.2021.9576186)

Optimal feedforward torque control for nonlinear induction machines considering stator & rotor copper losses and current & voltage limits

Andre Thommessen, Christoph Hackl
Laboratory for Mechatronic and Renewable Energy Systems (LMRES)
Munich University of Applied Sciences (MUAS)
Munich, Germany
{andre.thommessen, christoph.hackl}@hm.edu

***Abstract*—In order to *analytically* solve the optimal feed-forward torque control (OFTC) problem of induction machines (IMs), the unified theory for synchronous machine introduced in [1] is extended by considering relevant IM *nonlinearities* and incorporating stator *and* rotor copper losses. Instead of the well known *Maximum Torque per (stator) Current* (MTPC) operation strategy, *Maximum Torque per (copper) Losses* (MTPL$_{\mathrm{Cu}}$) is realized and extended by the *Maximum (rotor) Current* (MC$_{\mathrm{r,\,ext}}$) strategy due to stator *and* rotor current limitations. Modeling magnetic saturation and cross-coupling effects leads to a constrained *nonlinear* optimization problem which is solved based on the idea of *sequential quadratic programming* (SQP). The**

generic approach can also be applied to other types of inverter-fed IMs, such as squirrel-cage induction machines (SCIMs).

The highest priority of the OFTC is to provide the reference torque while minimizing losses. In a wide operating range, there usually exist (infinitely many) different combinations of reference currents resulting in the same torque. Thus, an optimal reference current computation (ORCC) is desirable which minimizes the current-dependent IM losses while reaching the reference torque and taking into account operating (e.g. current & voltage) limits. To do so, this paper proposes a physics-

References

Chapter 6.9 in [175] (published in 2020 in Schröder “Elektrische Antriebssysteme”; doi: 10.1007/978-3-662-62700-6)

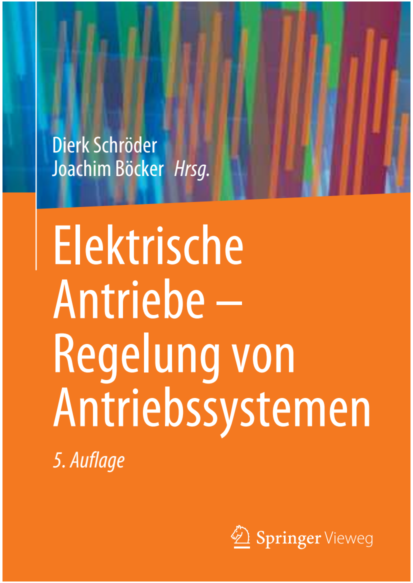

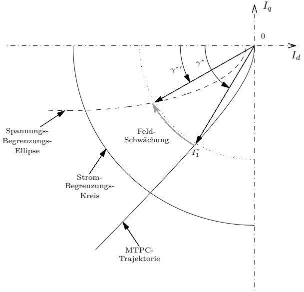

Abb. 6.101 Wirkungsweise der Feldschwächregelung mit Spannungsrückkopplung

6.9 Optimale Betriebsführung von nichtlinearen Synchronmaschinen

C. M. Hackl, J. Kullick, N. Monzen

Der folgende Abschnitt basiert auf den Publikationen [HH16; Eld+16; EHK16; Eld+17b; Hac+17; Eld+17a]. Darin wurde die erste allgemeine Theorie zur analytischen Berechnung der optimalen (verlustminimierenden) Sollströme für anisotrope Synchronmaschinen mit konstanter Erregung vorgestellt. Die weithin verbreiteten und vereinfachenden Annahmen wie z. B. die Vernachlässigung des Statorwiderstandes oder der magnetischen Kreuzkopplung konnten aufgehoben werden. Zusätzlich erlaubt die Theorie die Berücksichtigung von Eisenverlusten und Nicht-

References

Monograph [46] (published May 2017; doi: 10.1007/978-3-319-55036-7)

References I

[1] Christoph M. Hackl. A physics-based model of electro-active polymer actuators as the bases for a Gopinath-style motion state observer. Bachelorthesis, Lehrstuhl für Elektrische Antriebssysteme, Technische Universität München, Germany & Department of Mechanical Engineering and Department of Electrical & Computer Engineering, University of Wisconsin-Madison, USA, 2003.

[2] Christoph Hackl, H.-Y. Tang, R.D. Lorenz, L.-S. Turng, and Dierk Schröder. A multiphysics model of planar electro-active polymer actuators. In *Conference Record of the 39th IEEE Industrial Application Society Annual Meeting*, volume 3, pages 2125–2130. Institute of Electrical and Electronics Engineers (IEEE), 2004.

[3] Christoph Hackl, H.-Y. Tang, R.D. Lorenz, L.-S. Turng, and Dierk Schröder. A multidomain model of planar electro-active polymer actuators. *IEEE Transactions on Industry Applications*, 41(5):1142–1148, sep 2005.

[4] Christoph M. Hackl and Beatrix Mair. Optimale Bahnzugregelung am Beispiel einer Papierstreichanlage. In *Konferenzband des 9. Bahnlaufseminar*, TU Chemnitz, Deutschland, 2007.

[5] Christoph M. Hackl and Beatrix Mair. Optimierung der Bahnspannungsregelung durch dezentrale Regelsysteme auf der Basis von moderner Mikroelektronik und intelligenter Software zur Steigerung der Produktionssicherheit und der Produktivität von Papierstreichanlagen. Abschlussbericht zum Forschungsvorhaben AiF/IGF 14140N, Arbeitsgemeinschaft industrieller Forschungsvereinigungen “Otto von Guerick” (AiF), 2007.

[6] Beatrix Mair and Christoph M. Hackl. Optimierung der Bahnspannungsregelung durch dezentrale Regelsysteme auf der Basis von moderner Mikroelektronik und intelligenter Software zur Steigerung der Produktionssicherheit und der Produktivität von Papierstreichanlagen. PTS Forschungsbericht, The Paper Technology Specialists, Hessstr. 134, 80797 München, Germany, 2007.

[7] Christoph M. Hackl and Beatrix Mair. Besser Bahnen ziehen – Optimale Bahnzugregelung mit dSPACE-Prototyping-System. *dSPACE Magazine*, 2:40–45, 2008.

[8] Christoph M. Hackl and Beatrix Mair. Smoothing the tension - optimal web tension control with a dSPACE prototyping system. *dSPACE Magazine*, 2:40–45, 2008.

[9] Christian Endisch, Christoph Hackl, and Dierk Schröder. Optimal brain surgeon for general dynamic neural networks. In José Neves, Manuel Filipe Santos, and José Manuel Machado, editors, *Progress in Artificial Intelligence*, volume 4974/2007 of *Lecture Notes in Artificial Intelligence*, pages 15–28. Springer-Verlag, Berlin, 2007.

References II

[10] Christian Endisch, Christoph Hackl, and Dierk Schröder. System identification with general dynamic neural networks and network pruning. *International Journal of Computational Intelligence*, 4(3):187–195, 2007.

[11] Christian. Endisch, Peter Stolze, Peter Endisch, Christoph M.. Hackl, and Ralph M. Kennel. Levenberg-Marquardt-based OBS algorithm using adaptive pruning interval for system identification with dynamic neural networks. In *Proceedings of the IEEE International Conference on Systems, Man and Cybernetics*, pages 3402–3408, San Antonio, TX, USA, oct 2009. Institute of Electrical and Electronics Engineers (IEEE).

[12] C. Endisch, P. Stolze, C. Hackl, and D. Schröder. Comments on “Backpropagation algorithms for a broad class of dynamic networks”. *IEEE Transactions on Neural Networks*, 20(3):540–541, mar 2009.

[13] Mohamed Abdelrahem, Christoph Hackl, and Ralph Kennel. Application of extended kalman filter to parameter estimation of doubly-fed induction generators in variable-speed wind turbine systems. In *2015 International Conference on Clean Electrical Power (ICCEP)*. IEEE.

[14] Christoph M. Hackl. Speed funnel control with disturbance observer for wind turbine systems with elastic shaft. In *Proceedings of the 54th IEEE Conference on Decision and Control (CDC 2015)*, pages 2005–2012, Osaka, Japan, 2015.

[15] Simon Krüner and Christoph M. Hackl. Experimental identification of the optimal current vectors for a permanent-magnet synchronous machine in wave energy converters. *Energies*, 12(862), 2019.

[16] Christoph M. Hackl and Markus Landerer. A unified method for online detection of phase variables and symmetrical components of unbalanced three-phase systems with harmonic distortion. *Energies*, 12(17), 2019.

[17] Mohamed Abdelrahem, Ralph Kennel, Christoph Hackl, Mehmet Dal, and José Rodríguez. Efficient finite-position-set mras observer for encoder-less control of dfigs. In *2019 IEEE International Symposium on Predictive Control of Electrical Drives and Power Electronics (PRECEDE)*, pages 1–6, May 2019.

[18] Christoph M. Hackl and Markus Landerer. A unified method for generic signal parameter estimation of arbitrarily distorted single-phase grids with dc-offset. *IEEE Open Journal of the Industrial Electronics Society*, 1:235–246, 2020.

References III

[19] T. Kreppel, F. Rojas, C. M. Hackl, O. Kalmbach, M. Díaz, and G. Gatica. Extended Model of Chopper Cells for Open Circuit Fault Detection in Modular Multilevel Cascade Converters using Sliding Mode Observers. In *2020 IEEE 11th International Symposium on Power Electronics for Distributed Generation Systems (PEDG)*, pages 487–493, 2020. ISSN: 2329-5767.

[20] Mostafa Ahmed, Mohamed Abdelrahem, Ralph Kennel, and Christoph M. Hackl. A robust maximum power point tracking based model predictive control and extended kalman filter for pv systems. In *2020 International Symposium on Power Electronics, Electrical Drives, Automation and Motion (SPEEDAM)*, pages 514–519, 2020.

[21] Mostafa Ahmed, Mohamed Abdelrahem, Ralph Kennel, and Christoph M. Hackl. Maximum power point tracking based model predictive control and extended kalman filter using single voltage sensor for pv systems. In *2020 IEEE 29th International Symposium on Industrial Electronics (ISIE)*, pages 1039–1044, 2020.

[22] Christoph M. Hackl and Markus Landerer. Modified second-order generalized integrators with modified frequency locked loop for fast harmonics estimation of distorted single-phase signals. *IEEE Transactions on Power Electronics*, 2020.

[23] Julian Kullick and Christoph M Hackl. Nonlinear modeling, identification and optimal feedforward torque control of induction machines using steady-state machine maps. *IEEE Transactions on Industrial Electronics*, pages 1–1, 2022.

[24] Max A. Buettner, Niklas Monzen, and Christoph M. Hackl. Artificial neural network based optimal feedforward torque control of interior permanent magnet synchronous machines: A feasibility study and comparison with the state-of-the-art. *Energies*, 15(5):1838, 2022.

[25] Shih-Wei Su, Christoph M. Hackl, and Ralph Kennel. Analytical prototype functions for flux linkage approximation in synchronous machines. *IEEE Open Journal of the Industrial Electronics Society*, 3:265–282, 2022.

[26] Shih-Wei Su, Hannes Börngen, Christoph M. Hackl, and Ralph Kennel. Nonlinear current control of reluctance synchronous machines with analytical flux linkage prototype functions. *IEEE Open Journal of the Industrial Electronics Society*, pages 1–12, 2022.

[27] Christoph M. Hackl. *Contributions to High-gain Adaptive Control in Mechatronics*. PhD thesis, Lehrstuhl für Elektrische Antriebssysteme und Leistungselektronik, Technische Universität München (TUM), Germany, 2012.

References IV

[28] Christoph M. Hackl. Dynamische Reibungsmodellierung: Das Lund-Grenoble (LuGre) Reibmodell. In Dierk Schröder, editor, *Elektrische Antriebe – Regelung von Antriebssystemen*, chapter 25, pages 1615–1657. Springer-Verlag, 2015.

[29] Christoph M. Hackl. Dynamische Reibungsmodellierung: Das Lund-Grenoble (LuGre) Reibmodell. In Dierk Schröder, editor, *Elektrische Antriebe – Regelung von Antriebssystemen*, chapter 9.4, pages 1315–1357. Springer-Verlag, 2020.

[30] Hans Schuster, Christoph Michael Hackl, Christian Westermaier, and Dierk Schröder. Funnel-control for electrical drives with uncertain parameters. In *Proceedings of the 7th International Power Engineering Conference*, Singapore, 2005.

[31] Christoph M. Hackl and Dierk Schröder. Extension of high-gain controllable systems for improved accuracy. In *Proceedings of the 2006 IEEE International Conference on Control Applications (CCA 2006)*, pages 2231–2236, Munich, Germany, oct 2006. Institute of Electrical and Electronics Engineers (IEEE).

[32] Christoph Michael Hackl and Dierk Schröder. Funnel-control for nonlinear multi-mass flexible systems. In *Proceedings of the 32nd Annual Conference on IEEE Industrial Electronics*, pages 4707–4712, Paris, France, 2006.

[33] Christoph M. Hackl, Hans Schuster, Christian Westermaier, and Dierk Schröder. Funnel-control with integrating prefilter for nonlinear, time-varying two-mass flexible servo systems. In *Proceedings of the 9th International Workshop on Advanced Motion Control*, pages 456–461, Istanbul, Turkey, 2006. Institute of Electrical and Electronics Engineers (IEEE).

[34] Christoph M. Hackl, Yang Ji, and Dierk Schröder. Enhanced funnel-control with improved performance. In *Proceedings of the 15th Mediterranean Conference on Control and Automation*, pages Paper T01–016, Athens, Greece, jun 2007. Institute of Electrical and Electronics Engineers (IEEE).

[35] Christoph M. Hackl, Yang Ji, and Dierk Schröder. Funnel-control with constrained control input compensation. In *Proceedings of the 9th IASTED International Conference CONTROL AND APPLICATIONS*, pages 147–152, Montreal, Quebec, Canada, 2007.

[36] Christoph M. Hackl, Yang Ji, and Dierk Schröder. Nonidentifier-based adaptive control with saturated control input compensation. In *Proceedings of the 15th Mediterranean Conference on Control and Automation*, pages Paper T01–15, Athens, Greece, jun 2007. Institute of Electrical and Electronics Engineers (IEEE).

References V

[37] Christoph M. Hackl and Dierk Schröder. Funnel-control with online foresight. In *Proceedings of the 26th IASTED International Conference MODELLING, IDENTIFICATION AND CONTROL*, pages 171–176, Innsbruck, Austria, 2007.

[38] Christoph M. Hackl and Dierk Schröder. Non-identifier based adaptive control in robotics: An introduction. *International Journal of Factory Automation, Robotics and Soft Computing*, 4:90–99, 2008.

[39] Christoph M. Hackl, Christian Endisch, and Dierk Schröder. Specially designed funnel-control in mechatronics. In *Proceedings of the 5th International Conference on Computational Intelligence, Robotics and Autonomous Systems*, pages 59–64, 2008.

[40] Christoph M. Hackl, Christian Endisch, and Dierk Schröder. Contributions to non-identifier based adaptive control in mechatronics. *Robotics and Autonomous Systems, Elsevier*, 57(10):996–1005, 2009.

[41] Christoph M. Hackl. Funnel Control: Implementierung, Erweiterung und Anwendung. In Dierk Schröder, editor, *Intelligente Verfahren: Systemidentifikation und Regelung nichtlinearer Systeme*, pages 697–760. Springer-Verlag, Berlin, 2010.

[42] Christoph M. Hackl and Stephan Trenn. The bang-bang funnel controller: An experimental verification. *PAMM*, 12(1):735–736, dec 2012.

[43] Christoph M. Hackl, Norman Hopfe, Achim Ilchmann, Markus Mueller, and Stephan Trenn. Funnel control for systems with relative degree two. *SIAM Journal on Control and Optimization*, 51(2):965–995, jan 2013.

[44] Christoph M. Hackl. Funnel control for wind turbine systems. In *Proceedings of the 2014 IEEE International Conference on Control Applications (CCA 2014)*, pages 1377–1382, Antibes, France, oct 2014. Institute of Electrical and Electronics Engineers (IEEE).

[45] Christoph M. Hackl. Current PI-funnel control with anti-windup for synchronous machines. In *Proceedings of the 54th IEEE Conference on Decision and Control (CDC 2015)*, pages 1997–2004, Osaka, Japan, dec 2015. Institute of Electrical and Electronics Engineers (IEEE).

[46] Christoph M. Hackl. *Non-identifier based adaptive control in mechatronics: Theory and Application*. Number 466 in Lecture Notes in Control and Information Sciences. Springer International Publishing, Berlin, 2017.

[47] Christoph M. Hackl, Christian Endisch, and Dierk Schröder. Applicability of funnel-control in robotics. In *Proceedings of the 5th International Conference on Computational Intelligence, Robotics and Autonomous Systems*, pages 65–70, Linz, Austria, 2008.

References VI

[48] Christoph M. Hackl, Christian Endisch, and Dierk Schröder. Funnel-control in robotics: An introduction. In *Proceedings of the 16th Mediterranean Conference on Control and Automation*, pages 913–919, Ajaccio, France, jun 2008. Institute of Electrical and Electronics Engineers (IEEE).

[49] Christoph M. Hackl and Dierk Schröder. Non-identifier based adaptive control in robotics: An introduction. In Salvatore Pennacchio, editor, *Recent adavances in Control Systems, Robotics and Automation*, volume 1. INTERNATIONALSAR International Society for Advanced Research, Palermo, Italy, third edition, 2009.

[50] Christoph M. Hackl. High-gain adaptive position control. *International Journal of Control*, 84(10):1695–1716, oct 2011.

[51] Christoph M. Hackl, Andreas G. Hofmann, Rik W. De Doncker, and Ralph M. Kennel. Funnel control for speed & position control of electrical drives: A survey. In *Proceedings of the 19th Mediterranean Conference on Control & Automation (MED)*, pages 181–188, Corfu Island, Greece, jun 2011. Institute of Electrical and Electronics Engineers (IEEE).

[52] Christoph M. Hackl, Andreas G. Hofmann, and Ralph M. Kennel. Funnel control in mechatronics: An overview. In *Proceedings of the 50th IEEE Conference on Decision and Control (CDC) and European Control Conference (ECC)*, pages 8000–8007, Orlando, FL, USA, dec 2011. Institute of Electrical and Electronics Engineers (IEEE).

[53] Christoph M. Hackl. 'Funnel control' zur Positionsregelung von starren Drehgelenkrobotern mit grob bekannter Trägheitsmatrix. In *Tagungsband des GMA-Fachausschuss 1.40*, pages 302–310, Anif, Austria, 2012.

[54] Christoph M. Hackl and Ralph M. Kennel. Position funnel control for rigid revolute joint robotic manipulators with known inertia matrix. In *Proceedings of the 20th Mediterranean Conference on Control and Automation*, pages 615–620, Barcelona, Spain, jul 2012. Institute of Electrical and Electronics Engineers (IEEE).

[55] Christoph M. Hackl and Ralph M. Kennel. Position funnel control with linear internal model. In *Proceedings of 2012 IEEE International Conference on Control Applications (CCA 2012)*, pages 1334–1339, Dubrovnik, Croatia, oct 2012. Institute of Electrical and Electronics Engineers (IEEE).

[56] Timm Faulwasser and Christoph M. Hackl. Path-following funnel control for rigid-link revolute-joint robotic systems. In *Proceedings of the 21st International Symposium on Mathematical Theory of Networks and Systems*, pages 1044–1051, Groningen, Netherlands, 2014.

References VII

[57] Julian Kullick and Christoph Hackl. Dynamic Modeling and Simulation of Deep Geothermal Electric Submersible Pumping Systems. *Energies*, 10(10):1659, October 2017.

[58] Florian Bauer, Christoph M. Hackl, Keyue Ma Smedley, and Ralph M. Kennel. Multicopter with series connected propeller drives. *IEEE Transactions on Control Systems Technology*, pages 1–12, 2017.

[59] Christoph M. Hackl, Florian Larcher, Alexander Dötlinger, and Ralph. M. Kennel. Is multiple-objective model-predictive control "optimal"? In *Proceedings of the 2013 IEEE International Symposium on Predictive Control of Electrical Drives and Power Electronics (PRECEDE 2013)*, pages 1–8, Munich, Germany, oct 2013. Institute of Electrical and Electronics Engineers (IEEE).

[60] Z. Zhang, C. Hackl, F. Wang, Z. Chen, and R. Kennel. Encoderless model predictive control of back-to-back converter direct-drive permanent-magnet synchronous generator wind turbine systems. In *Proceedings of 15th European Conference on Power Electronics and Applications*, pages 1–10. Institute of Electrical and Electronics Engineers (IEEE), sep 2013.

[61] Mohamed Abdelrahem, Christoph M. Hackl, and Ralph Kennel. Sensorless control of doubly-fed induction generators in variable-speed wind turbine systems. In *Proceedings of the 5th International Conference on Clean Electrical Power (ICCEP)*, pages 423–430, Taormina, Italy, jun 2015. Institute of Electrical and Electronics Engineers (IEEE).

[62] Christian Dirscherl, Josef Fessler, Christoph Hackl, and Hanko Ipach. State-feedback control and observer design of grid-connected power inverters with LCL-filter. In *Proceedings of the 5th Colloquium of the Munich School of Engineering*, Garching, Germany, 2015.

[63] Christian Dirscherl, Josef Fessler, Christoph M. Hackl, and Hanko Ipach. State-feedback controller and observer design for grid-connected voltage source power converters with LCL-filter. In *Proceedings of the 2015 IEEE International Conference on Control Applications (CCA 2015)*, pages 215–222, Sydney, Australia, sep 2015. Institute of Electrical and Electronics Engineers (IEEE).

[64] Christian Dirscherl, Christoph Hackl, and Korbinian Schechner. Explicit model predictive control with disturbance observer for grid-connected voltage source power converters. In *Proceedings of the 2015 IEEE International Conference on Industrial Technology (ICIT 2015)*, pages 999–1006. Institute of Electrical and Electronics Engineers (IEEE), mar 2015.

References VIII

[65] Christian Dirscherl, Christoph M. Hackl, and Korbinian Schechner. Pole-placement based nonlinear state-feedback control of the DC-link voltage in grid-connected voltage source power converters: A preliminary study. In *Proceedings of the 2015 IEEE International Conference on Control Applications (CCA 2015)*, pages 207–214, Sydney, Australia, sep 2015. Institute of Electrical and Electronics Engineers (IEEE).

[66] Christoph M. Hackl. MPC with analytical solution and integral error feedback for LTI MIMO systems and its application to current control of grid-connected power converters with LCL-filter. In *Proceedings of the 2015 IEEE International Symposium on Predictive Control of Electrical Drives and Power Electronics (PRECEDE 2015)*, pages 61–66, Valparaiso, Chile, oct 2015. Institute of Electrical and Electronics Engineers (IEEE).

[67] Zhenbin Zhang, Hue Xu, M. Xue, Z. Chen, T. Sun, Ralph Kennel, and Christoph Hackl. Predictive control with novel virtual flux estimation for back-to-back power converters. *IEEE Transactions on Industrial Electronics*, 62(5):2823–2834, may 2015.

[68] Ayman Ayad, Mohamed Hashem, Christoph Hackl, and Ralph Kennel. Proportional-resonant controller design for quasi-Z-source inverters with LC filters. In *Proceedings of the 42nd IEEE Industrial Electronics Conference (IECON 2016)*, Firenze, Italy, 2016.

[69] Christoph M. Hackl. On the equivalence of proportional-integral and proportional-resonant controllers with anti-windup. *arXiv:1610.07133*, 2016.

[70] Josh C. Mitchell, Maarten J. Kamper, and Christoph M. Hackl. Small-scale reluctance synchronous generator variable speed wind turbine system with DC transmission linked inverters. In *Proceedings of the IEEE Energy Conversion Congress & Exposition (ECCE)*, Milwaukee, WI, USA, 2016.

[71] Zhenbin Zhang, Christoph Hackl, Mohamed Abdelrahem, and Ralph Kennel. Voltage sensorless direct model predictive control of 3L-NPC back-to-back power converter PMSG wind turbine systems with fast dynamics. In *Proceedings of the Power Electronics Student Summit (PESS 2016)*, Aachen, Germany, 2016.

[72] Zhenbin Zhang, Christoph Hackl, and Ralph Kennel. Computationally efficient DMPC for three-level NPC back-to-back converters in wind turbine systems with PMSG. *IEEE Transactions on Power Electronics*, 32:8018–8034, 2017.

[73] Zhenbin Zhang, Christoph Hackl, and Ralph Kennel. FPGA based direct model predictive current control of PMSM drives with 3L-NPC power converters. In *Proceedings of the PCIM Europe 2016*, 2016.

References IX

[74] Zhenbin Zhang, Ralph Kennel, and Christoph Hackl. Computationally efficient direct model predictive control for three-level NPC back-to-back converter PMSG wind turbine systems. In *Proceedings of the 2016 International Symposium on Power Electronics, Electrical Drives, Automation and Motion (SPEEDAM 2016)*, pages 1045–1050, Anacapri, Italy, jun 2016. Institute of Electrical and Electronics Engineers (IEEE).

[75] Zhenbin Zhang, Ralph Kennel, and Christoph M. Hackl. Performance-enhanced direct multiple-vector model predictive power control for grid-tied AFEs. In *Proceedings of the 2016 IEEE 8th International Power Electronics and Motion Control Conference (IPEMC-ECCE Asia)*, pages 2904–2909, Hefei, China, may 2016. Institute of Electrical and Electronics Engineers (IEEE).

[76] Mohamed Abdelrahem, Christoph Michael Hackl, and Ralph Kennel. Finite set model predictive control with on-line parameter estimation for active frond-end converters. *Electrical Engineering*, 100(3):1497–1507, Sep 2018.

[77] M. Espinoza, R. Cardenas, J. C. Clare, D. Soto, M. Diaz, E. Espina, and C. M. Hackl. An integrated converter and machine control system for mmc-based high power drives. *IEEE Transactions on Industrial Electronics*, PP(99):1–1, 2018.

[78] Christoph M. Hackl, Urs Pecha, and Korbinian Schechner. Modeling and control of permanent-magnet synchronous generators under open-switch converter faults. *IEEE Transactions on Power Electronics*, 2018.

[79] Korbinian Schechner, Florian Bauer, and Christoph M. Hackl. Nonlinear DC-link PI control for airborne wind energy systems during pumping mode. In Roland Schmehl, editor, *Airborne Wind Energy: Advances in Technology Development and Research*. Springer Singapore, 2019.

[80] M. Diaz, R. Cardenas, M. Espinoza, C. M. Hackl, F. Rojas, J. C. Clare, and P. Wheeler. Vector control of a modular multilevel matrix converter operating in the full output-frequency range. *IEEE Transactions on Industrial Electronics*, 66(7):5102–5114, July 2019.

[81] Michael Saegmueller, Christoph Hackl, Rolf Witzmann, and Rene Richter. Analytic solutions for minimum conduction loss modulation of dual active bridge converters including frequency variation. In *IECON 2020 The 46th Annual Conference of the IEEE Industrial Electronics Society*. IEEE, oct 2020.

[82] O. Kalmbach, C. M. Hackl, and F. Rojas. A Generic Switching State-Space Model for Modular Multilevel Cascade Converters. In *2020 IEEE 11th International Symposium on Power Electronics for Distributed Generation Systems (PEDG)*, pages 447–454, 2020. ISSN: 2329-5767.

References X

[83] Oliver Kalmbach, Christian Dirscherl, and Christoph M. Hackl. Discrete-Time DC-Link Voltage and Current Control of a Grid-Connected Inverter with LCL-Filter and Very Small DC-Link Capacitance. *Energies*, 13(21):5613, 2020.

[84] Mostafa Ahmed, Mohamed Abdelrahem, Ralph Kennel, and Christoph M. Hackl. An enhanced maximum power point tracking based finite-control-set model predictive control for pv systems. In *2020 11th Power Electronics, Drive Systems, and Technologies Conference (PEDSTC)*, pages 1–6, 2020.

[85] Christoph Hackl, Christian Dirscherl, and Korbinian Schechner. Modellierung und Regelung von Windkraftanlagen (see https://arxiv.org/abs/1703.08661 for the english translation). In Dierk Schröder, editor, *Elektrische Antriebe – Regelung von Antriebssystemen*, chapter 10.3, pages 1504–1585. Springer-Verlag, 2020.

[86] Michael Saegmueller, Christoph Hackl, Rolf Witzmann, and René Richter. Analytic solutions for full operating range single-side zvs modulation of dual active bridge converters. In *Proceedings of the IEEE International Symposium on Industrial Electronics (ISIE) 2021*. IEEE, 2021.

[87] Christoph Hackl, Simon Krüner, and Zhao Song. 3d-modulation and pi state-feedback control for voltage source inverters with split dc-link. In *Proceedings of the IEEE International Symposium on Industrial Electronics (ISIE) 2021*. IEEE, 2021.

[88] Ibrahim Harbi, Mostafa Ahmed, Christoph M. Hackl, Ralph Kennel, and Mohamed Abdelrahem. A nine-level split-capacitor active-neutral-point-clamped inverter and its optimal modulation technique. *IEEE Transactions on Power Electronics*, 37(7):8045–8064, 2022.

[89] Christoph M. Hackl, Christian Endisch, and Dierk Schröder. Error reference control of nonlinear two-mass flexible servo systems. In *Proceedings of the 16th Mediterranean Conference on Control and Automation*, pages 1047–1053, Ajaccio, France, jun 2008. Institute of Electrical and Electronics Engineers (IEEE).

[90] Peter Landsmann, Christoph M. Hackl, and Ralph M. Kennel. Eliminating all machine parameters in encodersless predictive torque control without signal injection. In *Proceedings of the 2011 IEEE International Electric Machines and Drives Conference*, pages 1259–1264. Institute of Electrical and Electronics Engineers (IEEE), may 2011.

References XI

[91] Christoph M. Hackl. Funnel control with disturbance observer for two-mass systems. In *Proceedings of the 52nd IEEE Conference on Decision and Control (CDC)*, pages 6244–6249, Florence, Italy, dec 2013. Institute of Electrical and Electronics Engineers (IEEE).

[92] Christoph M. Hackl. PI-funnel control with Anti-windup and its application for speed control of electrical drives. In *Proceedings of the 52nd IEEE Conference on Decision and Control (CDC)*, pages 6250–6255, Florence, Italy, dec 2013. Institute of Electrical and Electronics Engineers (IEEE).

[93] Christian Dirscherl, Christoph M. Hackl, and Korbinian Schechner. Modeling and control of wind turbine systems with permanent-magnet synchronous generators (PMSG) and doubly fed induction generators (DFIG). In *Proceedings of the 4th Colloquium of the Munich School of Engineering*, Garching, Germany, 2014.

[94] Christoph M. Hackl. Klein-Windkraftanlagen mit effizienter und kostengünstiger Generatortopologie für Micro-Grids: Eine Voruntersuchung. In *Poster auf der Jahresversammlung des Bundes der Freunde der Technischen Universität München e.V.*, Munich, Germany, 2014.

[95] Christoph Hackl and Korbinian Schechner. Non-ideal torque control in wind turbine systems: Causes and impacts. In *Proceedings of the 5th Colloquium of the Munich School of Engineering*, Garching, Germany, 2015.

[96] Christoph M. Hackl, Maarten J. Kamper, Julian Kullick, and Joshua Mitchell. Nonlinear PI current control of reluctance synchronous machines. 2015.

[97] Christoph M. Hackl and Korbinian Schechner. Non-ideal torque control in wind turbine systems: Causes and impacts. In *Proceedings of the* 5^{th} *MSE-Kolloquium on "Innovations for Energy Systems, Mobility, Buildings and Materials"*, Munich, Germany, 2015.

[98] Mohamed Abdelrahem, Christoph M. Hackl, and Ralph Kennel. Encoderless model predictive control of doubly-fed induction generators in variable-speed wind turbine systems. In *Proceedings of the 6th edition of the conference "The Science of Making Torque from Wind" (TORQUE 2016)*, Open access Journal of Physics: Conference Series 753 (2016) 112005, Munich, Germany, 2016.

References XII

[99] Hisham Eldeeb, Christoph M. Hackl, Lorenz Horlbeck, and Julian Kullick. On the optimal feedforward torque control problem of anisotropic synchronous machines: Quadrics, quartics and analytical solutions. 2016.

[100] Hisham Eldeeb, Christoph M. Hackl, and Julian Kullick. Efficient operation of anisotropic synchronous machines for wind energy systems. In *Proceedings of the 6th edition of the conference "The Science of Making Torque from Wind" (TORQUE 2016)*, Open access Journal of Physics: Conference Series 753 (2016) 112005, Munich, Germany, 2016.

[101] Christoph M. Hackl, Maarten J. Kamper, Julian Kullick, and Joshua Mitchell. Current control of reluctance synchronous machines with online adjustment of the controller parameters. In *Proceedings of the 2016 IEEE International Symposium on Industrial Electronics (ISIE 2016)*, pages 153–160. Institute of Electrical and Electronics Engineers (IEEE).

[102] Lorenz Horlbeck and Christoph M. Hackl. Analytical solution for the MTPV hyperbola including the stator resistance. In *Proceedings of the IEEE International Conference on Industrial Technology (ICIT 2016)*, pages 1060–1067, Taipei, Taiwan, mar 2016. Institute of Electrical and Electronics Engineers (IEEE).

[103] Zhenbin Zhang, Ralph Kennel, and Christoph M. Hackl. Two direct torque and power control methods for back-to-back power converter PMSG wind turbine systems. In *Proceedings of the 2016 IEEE 8th International Power Electronics and Motion Control Conference (IPEMC-ECCE Asia)*, pages 1515–1520, Hefei, China, may 2016. Institute of Electrical and Electronics Engineers (IEEE).

[104] Mohamed. Abdelrahem, Christoph Hackl, and Ralph Kennel. Finite Position Set-Phase Locked Loop for Sensorless Control of Direct-Driven Permanent-Magnet Synchronous Generators. *IEEE Transactions on Power Electronics*, PP(99):1–1, 2017.

[105] Hisham Eldeeb, Christoph M. Hackl, Lorenz Horlbeck, and Julian Kullick. A unified theory for optimal feedforward torque control of anisotropic synchronous machines. *International Journal of Control*, 2017.

[106] Hisham Eldeeb, Christoph M. Hackl, Lorenz Horlbeck, and Julian Kullick. Analytical solutions for the optimal reference currents for MTPC/MTPA, MTPV and MTPF control of anisotropic synchronous machines. In *Proceedings of the IEEE International Electric Machines & Drives Conference (IEMDC 2017)*, pages 1–6, Miami, FL, USA, 2017.

[107] Mohamed Abdelrahem, Christoph Michael Hackl, and Ralph Kennel. Implementation and experimental investigation of a sensorless field-oriented control scheme for permanent-magnet synchronous generators. *Electrical Engineering*, may 2017.

References XIII

[108] A. D. Birda, J. Reuss, and C. Hackl. Synchronous optimal pulse-width modulation with differently modulated waveform symmetry properties for feeding synchronous motor with high magnetic anisotropy. In *2017 19th European Conference on Power Electronics and Applications (EPE'17 ECCE Europe)*, pages P.1–P.10, Sept 2017.

[109] H. Eldeeb, C. Hackl, M. Abdelrahem, and A. S. Abdel-Khalik. A unified SVPWM realization for minimizing circulating currents of dual three phase machines. In *2017 IEEE 12th International Conference on Power Electronics and Drive Systems (PEDS)*, pages 925–931, Dec 2017.

[110] Mauricio Espinoza, Matias Díaz, Enrique Espina, Christoph M. Hackl, and Roberto Cardénas. Control strategies for modular multilevel converters driving cage machines. In *Proceedings of the 3rd IEEE Southern Power Electronics Conference (SPEC 2017)*, pages 1–6, Dec 2017.

[111] Mohamed Abdelrahem, Christoph M. Hackl, Zhenbin Zhang, and Ralph Kennel. Robust predictive control for direct-driven surface-mounted permanent-magnet synchronous generators without mechanical sensors. *IEEE Transactions on Energy Conversion*, 33(1):179–189, 2018.

[112] Korbinian Schechner and Christoph M. Hackl. Scaling of the drive train dynamics of large-scale wind turbine systems for real-time emulation in small-scale laboratory setups. *IEEE Transactions on Industrial Electronics*, 66(9):6779–6788, 2018.

[113] H. Eldeeb, A. S. Abdel-Khalik, and C. Hackl. Dynamic modelling of dual three-phase IPMSM drives with different neutral configurations. *IEEE Transactions on Industrial Electronics*, PP(99):1–1, 2018.

[114] H. Eldeeb, M. Abdelrahem, C. Hackl, and A. S. Abdel-Khalik. Enhanced electromechanical modeling of asymmetrical dual three-phase IPMSM drives. In *2018 IEEE 27th International Symposium on Industrial Electronics (ISIE)*, pages 126–132, June 2018.

[115] H. Eldeeb, A. S. Abdel-Khalik, and C. Hackl. Post-fault full torque-speed exploitation of dual three-phase IPMSM drives. *IEEE Transactions on Industrial Electronics*, 2018.

[116] Hisham Magdy Eldeeb, Ayman Samy Abdel-Khalik, Julian Kullick, and Christoph M. Hackl. Pre and post-fault current control of dual three-phase reluctance synchronous drives. *IEEE Transactions on Industrial Electronics*, pages 1–1, 2019.

References XIV

[117] Athina Birda, Jörg Reuss, and Christoph M. Hackl. Simple fundamental current estimation and smooth transition between synchronous optimal pwm and asynchronous svm. *IEEE Transactions on Industrial Electronics*, pages 1–1, 2019.

[118] Xiaonan Gao, Mohamed Abdelrahem, Christoph M. Hackl, Zhenbin Zhang, and Ralph Kennel. Direct predictive speed control with a sliding manifold term for pmsm drives. *IEEE Journal of Emerging and Selected Topics in Power Electronics*, pages 1–1, 2019.

[119] Mohamed Abdelrahem, Christoph Michael Hackl, Ralph Kennel, and José Rodríguez. Efficient direct-model predictive control with discrete-time integral action for pmsgs. *IEEE Transactions on Energy Conversion*, 34(2):1063–1072, 2019.

[120] Mohamed Abdelrahem, Christoph Hackl, Ralph Kennel, and Jose Rodriguez. Sensorless predictive speed control of permanent-magnet synchronous generators in wind turbine applications. In *PCIM Europe 2019; International Exhibition and Conference for Power Electronics, Intelligent Motion, Renewable Energy and Energy Management*, pages 1–8, May 2019.

[121] Shih-Wei Su, Ralph Kennel, and Christoph M. Hackl. Analytical flux linkage approximation prototypes for reluctance synchronous machines. In *2020 International Symposium on Power Electronics, Electrical Drives, Automation and Motion (SPEEDAM)*. IEEE, jun 2020.

[122] Mohamed Abdelrahem, Christoph M. Hackl, José Rodríguez, and Ralph Kennel. Model reference adaptive system with finite-set for encoderless control of PMSGs in micro-grid systems. *Energies*, 13(18):4844, sep 2020.

[123] Christoph Hackl, Julian Kullick, and Niklas Monzen. Optimale Betriebsführung für nichtlineare Synchronmaschinen. In Joachim Böcker and Gerd Griepentrog, editors, *Elektrische Antriebe – Regelung von Antriebssystemen*. Springer-Verlag, 2020.

[124] Antonin Glac, Vaclav Smidl, Zdenek Peroutka, and Christoph M. Hackl. Comparison of IPMSM parameter estimation methods for motor efficiency. In *IECON 2020 The 46th Annual Conference of the IEEE Industrial Electronics Society*. IEEE, oct 2020.

[125] Christoph Hackl, Julian Kullick, and Peter Landsmann. Nichtlineare Stromregelverfahren für Reluktanz-Synchronmaschinen. In Joachim Böcker and Gerd Griepentrog, editors, *Elektrische Antriebe – Regelung von Antriebssystemen*. Springer-Verlag, 2020.

[126] Ahmed Farhan, Mohamed Abdelrahem, Christoph M. Hackl, Ralph Kennel, Adel Shaltout, and Amr Saleh. Advanced strategy of speed predictive control for nonlinear synchronous reluctance motors. *Machines*, 8(3):44, aug 2020.

References XV

[127] Mohamed Abdelrahem, Christoph Hackl, Ralph Kennel, and Jose Rodriguez. Low sensitivity predictive control for doubly-fed induction generators based wind turbine applications. *Sustainability*, 13(16):9150.

[128] Athina Birda, Joerg Reuss, and Christoph M. Hackl. Synchronous optimal pulsewidth modulation for synchronous machines with highly operating point dependent magnetic anisotropy. *IEEE Transactions on Industrial Electronics*, 68(5):3760–3769, may 2021.

[129] Athina Birda, Christoph Grabher, Joerg Reuss, and Christoph M. Hackl. Dc-link capacitor and inverter current ripples in anisotropic synchronous motor drives produced by synchronous optimal pwm. *IEEE Transactions on Industrial Electronics*, jan 2021.

[130] Andrea Zanelli, Julian Kullick, Hisham Eldeeb, Gianluca Frison, Christoph Hackl, and Moritz Diehl. Continuous control set nonlinear model predictive control of reluctance synchronous machines. *IEEE Transactions on Control Systems Technology*, pages 1–12, 2021.

[131] C. M. Hackl, J. Kullick, and N. Monzen. Generic loss minimization for nonlinear synchronous machines by analytical computation of optimal reference currents considering copper and iron losses. In *2021 IEEE International Conference on Industrial Technology (ICIT)*. IEEE, mar 2021.

[132] Mohamed Abdelrahem, Christoph M. Hackl, Ralph Kennel, and Jose Rodriguez. Computationally efficient finite-position-set-phase-locked loop for sensorless control of PMSGs in wind turbine applications. *IEEE Transactions on Power Electronics*, 36(3):3007–3016, mar 2021.

[133] Antonín Glac, Václav Šmídl, Zdeněk Peroutka, and Christoph M. Hackl. Dependence of IPMSM motor efficiency on parameter estimates. *Sustainability*, 13(16):9299.

[134] Haotian Xie, Jianming Du, Dongliang Ke, Yingjie He, Fengxiang Wang, Christoph Hackl, José Rodríguez, and Ralph Kennel. Multistep model predictive control for electrical drives—a fast quadratic programming solution. *Symmetry*, 14(3):626.

[135] Issa Hammoud, Sebastian Hentzelt, Ke Xu, Thimo Oehlschlaegel, Mohamed Abdelrahem, Christoph M. Hackl, and Ralph Kennel. On continuous set model predictive control of permanent magnet synchronous machines. *IEEE Transactions on Power Electronics*, pages 1–1, 2022.

References XVI

[136] Julian Kullick and Christoph M. Hackl. Speed-sensorless control of induction machines with LC filter for geothermal electric submersible pumping systems. *Machines*, 10(2):87.

[137] Yuebin Pang, Jovan Knezevic, Daniel Glose, and Christoph Hackl. Sensorless control of electrically excited synchronous machines considering magnetic saturation and flux linkage dynamics for automotive applications. *IEEE Transactions on Industrial Electronics*, pages 1–11.

[138] Simon Wiedemann and Christoph M. Hackl. Simultaneous identification of inverter and machine nonlinearities for self-commissioning of electrical synchronous machine drives. *IEEE Transactions on Energy Conversion*, pages 1–14, 2023.

[139] Christian Dirscherl, Christoph Hackl, and Korbinian Schechner. Modellierung und Regelung von modernen Windkraftanlagen: Eine Einführung (see https://arxiv.org/abs/1703.08661 for the english translation). In Dierk Schröder, editor, *Elektrische Antriebe – Regelung von Antriebssystemen*, chapter 24, pages 1540–1614. Springer-Verlag, 2015.

[140] Florian Bauer, Christoph M. Hackl, and Korbinian Schechner. DC-link control for airborne wind energy systems during pumping mode. In *Proceedings of the Airborne Wind Energy Conference (AWEC 2015)*, Delft, Netherlands, 2015.

[141] Mohamed Abdelrahem, Christoph M. Hackl, and Ralph Kennel. Model predictive control of permanent magnet synchronous generators in variable-speed wind turbine systems. In *Proceedings of the Power Electronics Student Summit (PESS 2016)*, Aachen, Germany, 2016.

[142] Mohamed Abdelrahem, Christoph Michael Hackl, and Ralph Kennel. Simplified model predictive current control without mechanical sensors for variable-speed wind energy conversion systems. *Electrical Engineering*, 99(1):367–377, 2016.

[143] Mohamed Abdelrahem, Christoph M. Hackl, Zhenbin Zhang, and Ralph Kennel. Sensorless control of permanent magnet synchronous generators in variable-speed wind turbine systems. In *Proceedings of the Power Electronics Student Summit (PESS 2016)*, Aachen, Germany, 2016.

[144] Florian Bauer, Christoph M. Hackl, K. Smedley, and Ralph Kennel. Virtual-power-hardware-in-the-loop simulations in crosswind kite power with ground generation. In *Proceedings of the 2016 American Control Conference (ACC)*, pages 4071–4076, Boston, FL, USA, jul 2016. Institute of Electrical and Electronics Engineers (IEEE).

References XVII

[145] Christian Dirscherl and Christoph M. Hackl. Dynamic power flow in wind turbine systems with doubly-fed induction generator. In *Proceedings of the 2016 IEEE International Energy Conference (ENERGYCON 2016)*, pages 1–6, Leuven, Beglium, apr 2016. Institute of Electrical and Electronics Engineers (IEEE).

[146] Christoph M. Hackl and Korbinian Schechner. Non-ideal feedforward torque control of wind turbines: Impacts on annual energy production & gross earnings. In *Proceedings of the 6th edition of the conference "The Science of Making Torque from Wind" (TORQUE 2016)*, volume 753 of *Open access Journal of Physics: Conference Series 753 (2016) 112005*, page 112010, Munich, Germany, sep 2016. IOP Publishing.

[147] Florian Bauer, Ralph M. Kennel, Christoph M. Hackl, Filippo Campagnolo, Michael Patt, and Roland Schmehl. Drag power kite with very high lift coefficient. *Renewable Energy*, October 2017.

[148] Christian Dirscherl and Christoph M. Hackl. Local stability analysis and controller design for speed-controlled wind turbine systems in regime ii.5. *Energies*, (5):33, 2018.

[149] Christoph M. Hackl, Pol Jané-Soneira, Martin Pfeifer, Korbinian Schechner, and Sören Hohmann. Full- and reduced-order state-space modeling of wind turbine systems with permanent magnet synchronous generator. *Energies*, (7):33, 2018.

[150] S. Hanif, K. Zhang, C. Hackl, M. Barati, H. B. Gooi, and T. Hamacher. Decomposition and equilibrium achieving distribution locational marginal prices using trust-region method. *IEEE Transactions on Smart Grid*, PP(99):1–1, 2018.

[151] Mohamed Abdelrahem, Christoph Hackl, Ahmed Farhan, and Ralph Kennel. Finite-set mras observer for encoderless control of pmsgs in wind turbine applications. In *2019 IEEE Conference on Power Electronics and Renewable Energy (CPERE)*, pages 431–436, 2019.

[152] Katharina Bär, Abdessamad Saidi, Christoph Hackl, and Wilfried Zörner. Combined operation of photovoltaic and biogas plants for optimal transformer loading. *Chemical Engineering Transactions*, 76:601–606.

[153] Kai Zhang, Sarmad Hanif, Christoph M. Hackl, and Thomas Hamacher. A framework for multi-regional real-time pricing in distribution grids. *IEEE Transactions on Smart Grid*, 10(6):6826–6838, Nov 2019.

References XVIII

[154] Florian Bauer, Christoph M. Hackl, Keyue Smedley, and Ralph Kennel. Crosswind kite power with tower. In Roland Schmehl, editor, *Airborne Wind Energy: Advances in Technology Development and Research*. Springer-Verlag, 2019.

[155] Florian Bauer, Christoph M. Hackl, Keyue Smedley, and Ralph Kennel. On multicopter-based launching and landing of lift power kites. In Roland Schmehl, editor, *Airborne Wind Energy: Advances in Technology Development and Research*. Springer-Verlag, 2019.

[156] Mohamed Abdelrahem, Christoph Hackl, and Ralph Kennel. Robust predictive control scheme for permanent-magnet synchronous generators based modern wind turbines. *Electronics*, 10(13):1596.

[157] D. Schröder and C.M. Hackl. Grundlagen der Regelungstechnik. IHK Schwaben, Mechatronik Weiterbildung, 2009.

[158] Christoph Hackl. *Bewegungssteuerung durch geregelte elektrische Antriebe (Übung)*. Lehrstuhl für Elektrische Antriebe und Leistungselektronik – Technische Universität München, 2013.

[159] Christoph M. Hackl. Regelung von regenerativen Energiesystemen (Vorlesungsskriptum und Übungsaufgaben). online, 2014. Lehrmaterialien zur Veranstaltung "Regelung von regenerativen Energiesystemen" im Wintersemester 2013/2014 an der Technischen Universität München.

[160] Christoph M. Hackl. Projektstudium Antriebstechnik: Projektbezogen Studieren – Aktives Lernen im Team. online, 2015. Kurzskriptum mit Projektbeschreibungen zur Umsetzung des Ernst-Otto Fischer Lehrpreises 2013 im Wintersemester 2014/2015 an der Technischen Universität München.

[161] Christoph Hackl, Ellen Taraba, and Anne-Marie Fleischmann. Projektbezogen Studieren – Aktives Lernen im Team: Fachliche und überfachliche Kompetenzen von Studierenden fördern. In *Tagungsband des 2. HD-MINT-Symposium Hochschuldidaktik für MINT-Fächer*, Nürnberg, Germany, 2015.

[162] Christoph M. Hackl, Anne-Marie Fleischmann, and Ellen Taraba. Projektstudium Antriebstechnik: Projektbezogen Studieren – Aktives Lernen im Team. In *Tagungsband des 5. VDI Qualitätsdialogs Lehre - Studienerfolg verbessern*, Tagungswerk Jerusalemkirche, Berlin, Germany, 2015.

References XIX

[163] Christoph Hackl, Anne-Marie Lickert, and Ellen Taraba. Projektbezogen Studieren – Aktives Lernen im Team. In *Neues Handbuch Hochschullehre*, volume 76, pages 31–44. DUZ Medienhaus, 2016.

[164] M. Fakharmanesh, C. M. Hackl, and R. Perini. Instantaneous conduction and switching losses in two-level voltage source inverters. In *2017 IEEE International Conference on Environment and Electrical Engineering and 2017 IEEE Industrial and Commercial Power Systems Europe (EEEIC / I CPS Europe)*, pages 1–6, June 2017.

[165] Johannes Rossmann, Niklas Monzen, Maarten J. Kamper, and Christoph M. Hackl. Nonlinear three-phase reluctance synchronous machine modeling with extended torque equation. In *2023 IEEE 32nd International Symposium on Industrial Electronics (ISIE)*. IEEE, 2023.

[166] Shih-Wei Su, Niklas Monzen, Ralph Kennel, and Christoph M. Hackl. Self-identification of reluctance synchronous machines with analytical flux linkage prototype functions. In *2023 11th International Conference on Power Electronics and ECCE Asia (ICPE 2023 - ECCE Asia)*. IEEE, 2023.

[167] Hag-Wone Kim, Myung-Joong Youn, Kwan-Yuhl Cho, and Hyun-Soo Kim. Nonlinearity estimation and compensation of PWM VSI for PMSM under resistance and flux linkage uncertainty. *IEEE Transactions on Control Systems Technology*, 14(4):589–601, 2006.

[168] Joachim Holtz and Xin Qi. Optimal control of medium-voltage drives—an overview. *IEEE Transactions on Industrial Electronics*, 60(12):5472–5481, 2013.

[169] V. Blasko, V. Kaura, and W. Niewiadomski. Sampling of discontinuous voltage and current signals in electrical drives: a system approach. 34(5):1123–1130.

[170] Paolo Gherardo Carlet, Fabio Tinazzi, Silverio Bolognani, and Mauro Zigliotto. An effective model-free predictive current control for synchronous reluctance motor drives. 55(4):3781–3790.

[171] I. D. De Martin, F. Tinazzi, M. Zigliotto, and C. Hackl. System parameter-free continuous control-set predictive current control of synchronous motors. In *IECON 2022 – 48th Annual Conference of the IEEE Industrial Electronics Society*. IEEE.

[172] Shigeo Morimoto. Trend of permanent magnet synchronous machines. *IEEJ Transactions on Electrical and Electronic Engineering*, 2(2):101–108, mar 2007.

References XX

[173] R.W.D Nickalls. The quartic equation: Invariants and Euler's solution revealed. *Mathematical Gazette*, 93(526):66–75, mar 2009.

[174] Antonin Glac, Vaclav Smidl, and Zdenek Peroutka. Optimal feedforward torque control of synchronous machines with time-varying parameters. In *Proceedings of the 44th Annual Conference of the IEEE Industrial Electronics Society (IECON)*. IEEE, oct 2018.

[175] Dierk Schröder and Joachim Böcker, editors. *Elektrische Antriebe – Regelung von Antriebssystemen*. Springer Berlin Heidelberg, 2020.